37

The Mobility of Metals in Acid Mine Drainage from Abandoned Coal Mines

Torsten Franz Joachim Hälbich
B.Sc. (Hons) Biochemistry (University of Stellenbosch)

Submitted in the fulfilment of the requirements for the degree of

MASTER OF SCIENCE

in the Department of Geological Sciences
Faculty of Science
University of Cape Town
January 1997

ABSTRACT

The acid mine-drainage contaminated Blesbokspruit catchment west of Witbank in Mpumalanga province, South Africa has been investigated, by analysis of its waters, sediments, precipitates and algae, to obtain an understanding of the processes which control the mobility of metals in these waters. The Blesbokspruit drains acid mine drainage originating in surrounding, abandoned coal mine workings. The upper Blesbokspruit (approximately 8 km) including the stream origin, AMD outwelling points, downstream AMD retention ponds and a small wetland were selected for this study. Water, sediment, precipitate and algae samples were collected from the Blesbokspruit. The water quality of the catchment was determined and compared to mineralogical and major and trace element analyses of sediments, precipitates and algae.

The pH and total dissolved solids of the catchment waters ranged from pH 2.6 to 7.4 and 147 to 3071 mg/ℓ, respectively. Associated precipitates consisted primarily of jarosite with minor amounts of goethite, lepidocrocite, ferrihydrite and gypsum, with ferrihydrite being the major component of only one precipitate sample. The presence of algae at one of the sampling sites appeared to act as a template for the precipitation of ferrihydrite in a low pH and high acidity environment. Speciation modelling of the Blesbokspruit waters indicated waters saturated with respect to jarosite, goethite and quartz, in equilibrium with jurbanite, alunite and gypsum, and undersaturated with respect to ferrihydrite and kaolinite. The mobility of iron in the sulphate-rich Blesbokspruit waters appeared to be controlled by pyrite oxidation and the solubility of the basic iron sulphate mineral jarosite. In contrast Al mobility appeared to be influenced by different mechanisms. Acidity of the Blesbokspruit waters correlated well (r^2 = 0.942) with Al concentrations in the waters. Dissolved Al correlated with dissolved silica (r^2 = 0.757) in the Blesbokspruit waters and exchangeable acidity correlated with exchangeable Al (r^2 = 0.761) in the associated sediments. The data suggested that Al behaved conservatively in the pH < 4 Blesbokspruit waters and that Al solubility is controlled by dissolution of clay minerals and adsorption to organic matter in the sediments.

Although precipitates contain trace elements, precipitation does not have a major effect on the concentration of trace elements in the associated low pH waters. Trace elements were, however, accumulated in the sediments of the Blesbokspruit streambed and the wetland. The wetland acts as a sink for dissolved Na, Ca, Mg, Fe, Mn, Zn, Ni, Pb U, Cu and Co. The mobility of these elements appeared to be controlled by the dissolution of minerals containing these elements and adsorption to organic matter in the wetland and streambed sediments. Not all metals were, however, completely immobilised, and toxic concentrations of Pb (1.3 mg/ℓ) and elevated concentrations of Al (40 mg/ℓ), Fe (1.6 mg/ℓ) and Mn (6.5 mg/ℓ) remained in the water downstream of the wetland.

PREFACE

The experimental work described in this thesis was carried out in the Department of Geological Sciences, University of Cape Town, Rondebosch, from August to November, 1996, under the supervision of Associate Professor J. Willis of the Department of Geological Sciences.

These studies represent original work by the author and have not been submitted for degree purposes to another University. Where use was made of the work of others it has been acknowledged in the text.

Signed by candidate

T.F.J. Hälbich

The Lord God took the man and put him in the Garden of Eden to work it and to take care of it.

(Genesis 2 verse 15)

ACKNOWLEDGEMENTS

The following people and organisations are thanked for their contributions to this study:

- My supervisors, Associate Professor James Willis and Dr. Martin Fey of the Department of Geological Sciences at UCT for positive criticism and academic as well as practical assistance in the field and laboratory. Thanks for your enthusiasm and support during this project.
- ESKOM and the FRD who funded my studies.
- Dr. Heather Jamieson for advice and helpful suggestions.
- Mr. Patrick Sieas for patient assistance with the HPIC analysis and Mr. Ernest Stout for teaching me the finer points of briquette making.
- Mr. Bruce Cairns for constructing a sediment core cutter.
- Mrs. Antoinette Upton for help with the acquisition of chemicals and labware.
- Mrs. Josh Podge from the Botany Department for help regarding the identification of algae.
- Mr. Stuart Picketh and the Schonland Research Centre for Nuclear Sciences at the University of the Witwatersrand for organising transport of the samples.
- The Zoology Department (Liz Reynolds) for their 4^{0}C and -20^{0}C storage facilities.
- The Electron Microscopy Unit at the UCT, and in particular Mr. Dane Gerneke, for enthusiastic help with the SEM analysis.
- Nico Bezuidenhout from AMCOAL and Mieke van Tienhoven for taking fresh algae samples and transporting them to Cape Town.
- Tom Nowicki and Heather Dodds for help regarding computer software and a patient ear for many questions.
- My classmates from the M.Sc. Environmental Geochemistry Class of 1996. Thanks for excellent discussions, good humour, and your advice every time I got stuck on the computer.
- My family for their support and interest during the year.
- My wife Annelotte for your love, encouragement and patience. Without you this marathon would not have been worth running.

Abundant algae growth was noted in these acidic waters. Algae appeared as algae mats overlaying AMD outwelling points and abundant algae growth appeared in the stream bed and on the fringes of the AMD retention ponds. Preliminary work on the algae at the outwelling point indicated that these organisms were adapted to the acidic, high total dissolved solid, water environment. *Mougeotia* and *Microspora* species were identified from an algae sampled at the AMD outwelling point. Both algae species contained iron, whereas *Mougeotia* sp. contained 800 mg/kg vanadium and *Microspora* sp. contained 230 mg/kg zinc and 800 mg/kg manganese. The algae at the outwelling point, therefore, may be involved in the accumulation of metals from their environment.

TABLE OF CONTENTS

LIST OF FIGURES

LIST OF TABLES

Chapter 1

INTRODUCTION

The importance of metal mobility in the environment has been noted by a multitude of authors. Elevated metal concentrations in aqueous systems result in toxicity symptoms and eventual mortality of most living organisms. Acid mine drainage (AMD) is one of the major factors influencing metal mobility world wide. South Africa is no exception, cases of pollution of rivers and streams being reported by the lay press (Hattingh, 1996). Acid mine drainage and acid soils occur when reduced sulphur compounds and minerals are oxidised, forming sulphuric acid (H_2SO_4) and resulting in low pH, high sulphate and high metal concentrations in leachates. Metal mobility can affect metal concentrations in solution. Metal mobilization by AMD increases the concentration of metals in acidic waters which can be detrimental to plants, animals and humans (Förstner and Wittmann, 1979; Nordstrom, 1982 and Filipek *et al.*, 1987)

Examples of AMD are most prevalent in inactive or abandoned coal mines. In 1969 the source of 78% of AMD in the USA was associated with inactive or abandoned coal mines (Pierzynski *et al.*, 1994). Becker *et al.* (1993), Bennet (1993), and the Department of Water Affairs and Forestry (DWAF, 1995) describe AMD in the South African context, and in the latter case with specific reference to the AMD problems related to abandoned coal mines in the Witbank area. The collapse or fracture of the hanging wall in the abandoned coal mines around Witbank, pillar robbing and underground fires facilitated the infiltration of oxygen and water. These conditions promoted the oxidation of sulphide minerals which resulted in the formation of acidic water, high in salt concentrations as well as some heavy metals, mainly iron, manganese and aluminium (DWAF, 1995). Acidity and metal mobility are also enhanced by the presence of metal sulphide oxidizing bacteria found in South African coal mine waste environments (Bosch, 1990).

Acid mine drainage seepage collected in streams next to the abandoned coal mines and has negatively impacted on the related environments (DWAF, 1995). The mobility of metals in the AMD and the AMD contaminated area would be affected by the pH, redox potential and biological activity (bioleaching, biomineralization).

One specific AMD contaminated catchment just west of Witbank was chosen as a

suitable study area. A small stream, the Blesbokspruit, drains the contaminated waters from this site. Previous work by the Department of Water Affairs and Forestry (DWAF, 1995 and DWAF, 1994) had been done on the water quality of undergound and surface AMD contaminated waters of the Blesbokspruit. However, no attempt was made to investigate the mobility of elements in the Blesbokspruit catchment.

Fluctuations in element concentrations in the Blesbokspruit would thus be of interest. This study aims to gain an understanding of the mobility of elements from the point of emergence of AMD to a specified point downstream in the system. The following hypothesis was thus put forward:

Acid mine drainage containing high dissolved metal concentrations would precipitate secondary minerals on emergence at the surface, and also dissolve or leach other minerals in the surface of the catchment. These reactions would affect the mobility of different elements in the waters draining the Blesbokspruit catchment.

The aims of this study were the following:

- To determine the water quality of the Blesbokspruit catchment.
- To identify the mineralogy and metal content of precipitates and relate this information to metal concentrations in associated waters.
- To determine the mineralogy and element content of associated sediments.
- To investigate element content in associated algae.
- To assess the potential for element dissolution, adsorption, precipitation and coprecipitation and the effects of these processes on metal mobility in the Blesbokspruit.

Chapter 2

A REVIEW OF THE PROCESSES AFFECTING METAL MOBILITY IN ACID MINE DRAINAGE

2.1 Origin of minerals producing acid mine drainage

2.1.1 Origin of coal

Coal is a sedimentary rock that forms from the compaction of plant material that has not completely decayed. Rapid plant growth and deposition in water with a low oxygen content are needed such as shallow swamps in a temperate or tropical climate. Partial decay of the abundant plant material uses up any oxygen in the swamp water, inhibiting further decay and in doing so is preserving the remaining organic matter. Burial by sediments compresses the plant material, gradually driving out any water or other volatile compounds (Plummer and McGeary, 1979).

2.1.2 Coal mineralogy

Minerals occur in several forms and are very variable in physical properties and chemical composition. The most abundant in South African coals are clays, with carbonates, sulphides, quartz and glauconite. Phosphate minerals like apatite are present as submicroscopic grains and sometimes occur together with rutile and zircon. A summary of the more common minerals present in South African coals is given in Table 2.1 (Falcon and Snyman, 1986). Generally pyrite is the most abundant sulphide mineral present. The presence of other metal sulphides can indicate the type of metals which might be of importance if these minerals were oxidized. Clay minerals associated with coal and surrounding strata and present in AMD contaminated soils can contribute metals like Al, Fe, and Mg to an acidic environment. Goethite and haematite are potential Fe ion sources in coal waste environments (DWAF, 1995; Karathanasis *et al.*, 1988).

Table 2.1 The distribution of the more common minerals in Southern African coals (Falcon and Snyman, 1986).

Group of minerals	Syngenetic Interlaminated or associated with macerals	Epigenetic in cleats or crevices
Clay minerals	kaolinite illite montmorillonite	
Carbonates	calcite dolomite ankerite siderite discrete or impregnated in fusinites	calcite dolomite ankerite siderite
Sulphides	pyrite marcasite	pyrite marcasite
Oxides	haematite	limonite-goethite
Quartz	quartz grains chalcedony	quartz

2.1.3 Pyrite formation

The two major forms of iron disulphide (Fe_2S) in geological strata are pyrite and marcasite. Both minerals have the same chemical composition, but differ crystallographically. Because of its particular structure (orthorhombic), marcasite is less stable than pyrite (isometric) although pyrite was found to be the most prevalent form present in coals. Pyrite is most commonly found associated with the geological strata adjacent to, immediately above or below the coal seam. Pyrite is formed in a reducing environment with a continuous supply of sulphates and iron in the presence of easily decomposable organic matter. The carbon-to-sulphur ratio, availability of iron and oxidation potential are the major factors that determine the rate of pyrite formation.

The processes of pyrite formation in anoxic marine sediments overlain by oxic water can be summarized in the following steps: (1) reduction of sulphate to sulphide by bacteria, (2) reaction of hydrogen sulphide with iron minerals to form iron monosulphides, and (3) reaction of iron monosulphides with elemental sulphur to form pyrite. A limited

supply of organic carbon in marine sediments results in a lower rate of sulphate reduction. In salt marshes where organic matter content is high and sulphate reduction is rapid, pyrite is believed to form rapidly, via precipitation (small single crystals) of iron with polysulphides. Pyrite and coal forming circumstances are thus closely related (Evangelou and Zhang, 1995).

2.2 Reactions producing acid mine drainage

2.2.1 Pyrite oxidation by Fe^{3+} and dissolved O_2

Although any mineral deposit which contains sulphide is a potential source of AMD, certain mining of coals and shales of marine origin tend to contain higher sulphide concentrations than strata from fresh water paleoenvironments. Chemically, the iron disulphide pyrite, is the most important mineral of the metal sulphide minerals associated with coal mining. Pyrite oxidation takes place when the mineral is exposed to air and water. This process is complex because it involves chemical, biological and electrochemical reactions and varies with environmental conditions. Factors such as pH, $^{P}O_2$, specific surface and morphology of pyrite, presence or absence of bacteria and clay minerals, as well as hydrological factors determine the rate of oxidation. The chemical reactions involved in pyrite oxidation and acid formation (Singer and Stumm, 1970; Evangelou and Zhang, 1995) are:

(1) $FeS_2 + 7/2O_2 + H_2O \rightarrow Fe^{2+} + 2SO_4^{2-} + 2H^+$

(2) $Fe^{2+} + 1/4O_2 + H^+ \rightarrow Fe^{3+} + 1/2H_2O$

(3) $Fe^{3+} + 3H_2O \rightarrow Fe(OH)_3(s) + 3H^+$

(4) $FeS_2 + Fe^{3+} + 8H_2O \rightarrow 2FeSO_4 + 16H^+$

Reactions 1 and 4 indicate that Fe^{3+} and O_2 are the major oxidants of pyrite. Evangelou and Zhang (1995) suggest that Fe^{3+} is the preferred pyrite oxidant at circumneutral pH and the major role played by O_2 is to oxidise Fe^{2+} and thereby sustain the pyrite oxidation cycle. Reaction 3 takes place at pH values as low as 3, and is a readily reversible dissolution/precipitation reaction that serves as a source as well as a sink of solution Fe^{3+}, and is a major step in the release of acid to the environment.

At low pH (< 4.5), Fe^{3+} oxidizes pyrite more rapidly than O_2 and more rapidly than O_2 oxidizes dissolved Fe^{3+} and Fe^{2+} (Figure 1). For this reason Reaction 2 is the rate-limiting step in pyrite oxidation (Singer and Stumm, 1970). However, iron-oxidising bacteria, especially *Thiobacillus ferrooxidans*, can accelerate the rate of Fe^{2+} oxidation by a factor of 10^6. *T.ferrooxidans* is an acidophillic chemolithotrophic organism that is ubiquitous in geologic environments containing pyrite. Thus in the presence of *T.ferrooxidans* and under low pH conditions, pyrite oxidation can be described by Reactions 2 and 4 (Singer and Stumm, 1970; Evangelou and Zhang, 1995).

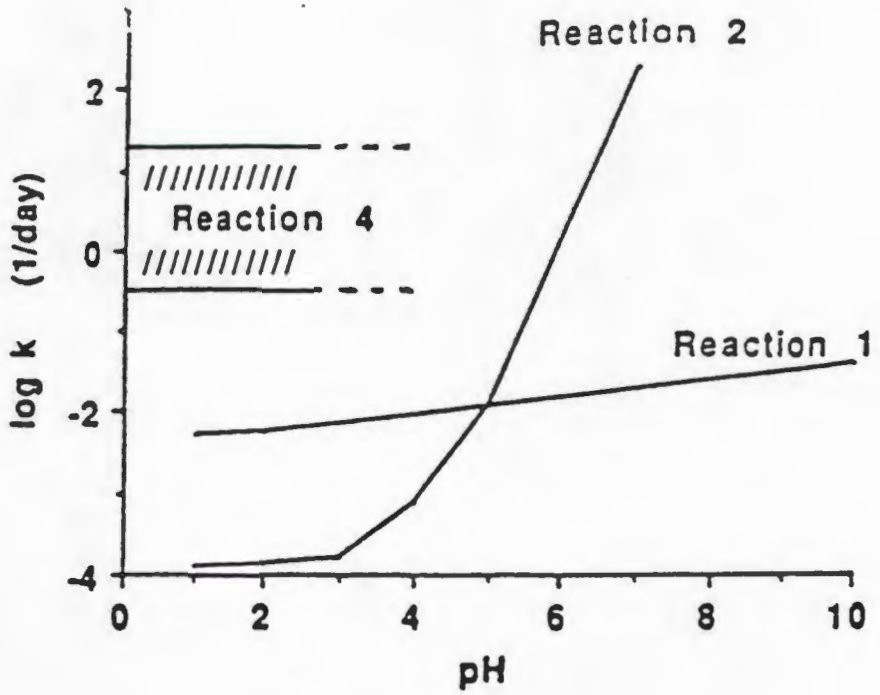

Figure 2.1 A comparison of rate constants as a function of pH for, reaction 1: oxidation of pyrite by O_2; reaction 2: oxidation of Fe^{2+} by O_2; reaction 4: oxidation of pyrite by Fe^{3+} (Evangelou and Zhang, 1995).

2.2.2 Bacterial oxidation of pyrite

The mechanisms of bacterial pyrite oxidation can be classified into direct and indirect metabolic reactions. Direct metabolic reactions require physical contact between bacteria and pyrite particles. With indirect metabolic reactions bacteria oxidize Fe^{2+} to Fe^{3+}, thereby regenerating the Fe^{3+} required for chemical oxidation of pyrite. Direct metabolic oxidation occurs when bacteria attach to the sulphate moiety of the pyrite crystal surface followed by the reactions:

(5) $FeS_2 + 7/2O_2 + H_2O \rightarrow FeSO_4 + H_2SO_4$

(6) $2FeSO_4 + 1/2O_2 + H_2SO_4 \rightarrow Fe_2(SO_4)_3 + H_2O$

(7) $FeS_2 + Fe_2(SO_4)_3 \rightarrow 3FeSO_4 + 2S$

(8) $2S + 3O_2 + 2H_2O \rightarrow 2H_2SO_4$

These reactions result in the dissolution of the sulphide surface of the crystal (Lundgren and Silver, 1980). In the case of indirect metabolic oxidation, ferric ion either alone or in combination, is the most important chemical species involved in the indirect attack on sulphide minerals. The reactions to explain this involvement with pyrite as example are:

(9) $FeS_2 + Fe_2(SO_4)_3 \rightarrow 3FeSO_4 + 2S^0$ (anaerobic)

(10) $MeS + 2Fe^{3+} + H_2 + 2O_2 \rightarrow Me^{2+} + 2Fe^{2+} + SO_4^{2-} + 2H^+$ (aerobic, Me = Metal)

In the presence of iron oxidising bacteria, the ferrous ion produced by these reactions can be oxidised to ferric ion, thereby establishing a cyclic process (Lundgren and Silver, 1980).

2.2.3 Electrochemical methods of pyrite oxidation

The overall electrochemical oxidation of pyrite is the sum of the cathodic and anodic reactions occurring at the surface. The anodic process is a complex collection of oxidation reactions in which pyrite reacts mainly with water to produce Fe^{3+}, sulphates and protons, or to produce Fe^{2+} and S^0 when the acid strength increases, as shown by reactions:

(11) $FeS_2 + 8H_2O \rightarrow Fe^{3+} + 2SO_4^{2-} + 16H^+ + 15e^-$

(12) $FeS_2(s) \rightarrow Fe^{2+} + 2S^0 + 2e^-$

The electrons are then transferred to the cathodic side (at the mineral surface or on bacteria), where the principal reaction is an oxygen reduction process shown by reaction 13 (Evangelou and Zhang, 1995).

(13) $O_2(aq) + 4H^+ + 4e^- \rightarrow 2H_2O$

2.2.4 Galvanic effect on metal-disulphide dissolution

Physical contact between two different metal-disulphide minerals in an acid/ferric sulphate-rich solution creates a galvanic cell. This galvanic cell results in a selective electrochemical dissolution of the metal-disulphide minerals. In the case of two metal-disulphide minerals with different electrical rest potentials, the mineral with the lower electrical rest potential, acting as a anode, will be dissolved. The mineral with the higher electric rest potential, acting as a cathode, will be galvanically protected. The galvanic reaction of chalcopyrite ($CuFeS_2$) / pyrite (FeS_2) can be described by an anodic oxidation reaction on the $CuFeS_2$ surface and a cathodic oxygen reduction reaction on the surface of the FeS_2. The anodic oxidation is expressed by reaction 14:

(14) $CuFeS_2 \rightarrow Cu^{2+} + Fe^{2+} + 2S^0 + 4e^-$

while the cathodic reaction can be given by:

(15) $O_2 + 4H^+ + 4e^- \rightarrow 2H_2O$

Thus the sum of the galvanic reaction can be expressed as:

(16) $CuFeS_2 + O_2 + 4H^+ \rightarrow Cu^{2+} + Fe^{2+} + 2S^0 + 2H_2O$

The elemental S and ferrous iron shown in reaction 16 will be oxidized by bacteria. The quantitative contribution of galvanic reactions in the dissolution of metal disulphides or metal sulphides in natural environments are unknown (Evangelou and Zhang, 1995).

2.3 Metal mobility in acidic waters

Waters in contact with non carbonate, pyrite-bearing rocks typically have low pH and high concentrations of iron and sulphate and are capable of mobilizing toxic concentrations of heavy metals. There are many different pathways for the release of metals from mining operations. The physical pathways applicable to the coal mines in the Witbank area are: (1) structural failures and improper design with regard to floods and other catastrophic events; (2) leaching to the surface via capillary action due to high groundwater or leaching to subsurface waters by permeation. The chemical/biological pathways are: (1) acidity, (2) oxidation/reduction, (3) precipitation/dissolution, (4) mineralogy, and (5) microbial processes. These pathways affect metal mobility and speciation in AMD, and are thus of importance to assess the hazard they present to the environment (Förstner and Wittmann, 1979).

2.3.1 The effect of pH on metal mobility

Acid mine drainage is a multi-factor pollutant, the acidity being one of these factors. pH is an intensity factor, measuring the activity of hydrogen ions, whereas, what is most important in situations with AMD is not the activity alone but the availability of hydrogen ions to neutralize bases. This quantity can be referred to as the total acidity.

The difference between AMD and other acid ecosystems such as peat drainage and acid rain affected areas is reflected in their acidity values. Acid mine drainage couples low pH to high acidity. The other acidic systems mentioned couple low pH to low acidity. Low pH will also destroy the bicarbonate buffer system, which controls the magnitude of shifts in pH. At pH values of < 4.2, all carbonate and bicarbonate is converted to carbonic acid. This readily dissociates to water and free carbon dioxide which may be lost to the atmosphere. Flocculation of silt and clay increases at low pH resulting in water of low turbidity. The rate of decomposition of clay minerals, feldspars and carbonates is also increases at low pH (Kelly, 1988).

pH affects the oxidation of Fe^{2+} and Fe^{3+}. The higher the pH of the solution the more rapidly dissolved Fe^{2+} will be oxidized and the more likely abiotic oxidation will prevail. Under very acidic conditions ($pH < 3$), oxidation and the formation of Fe^{3+} minerals must be mediated by microorganisms (Schwertmann and Fitzpatrick, 1992).

Metals in natural waters exist either as free ions or as various complexes with both

organic and inorganic ligands. Two types of soluble complexes are formed. Outer sphere complexes, are relatively weak electrostatic associations formed between a hydrated cation and a ligand in which one or both of the charged species retains a hydration shell. Inner sphere complexes are stronger associations between metal and ligand in which a covalent bond is formed. The pH of water and the availability of metal ions determine the extent of metal complexation. Many metallic cations can form inner sphere complexes with charged mineral surfaces through the process of ligand exchange. These types of complexes occur most readily on oxide and hydroxide surfaces, such as those on goethite (α-FeOOH) and gibbsite (α-$Al_2(OH)_6$). Metals that hydrolyse in water form hydroxo-metal complexes that form inner sphere complexes with the negatively charged deprotonated surface of oxides, hydroxides and oxyhydroxides of Al, Fe, and Mn. The extent of this reaction is dependant on pH (Figure 2.2). Adsorption of metals increases as pH is raised and decreases at low pH values (Förstner and Wittmann, 1979; Evans, 1989; Stumm and Morgan, 1970).

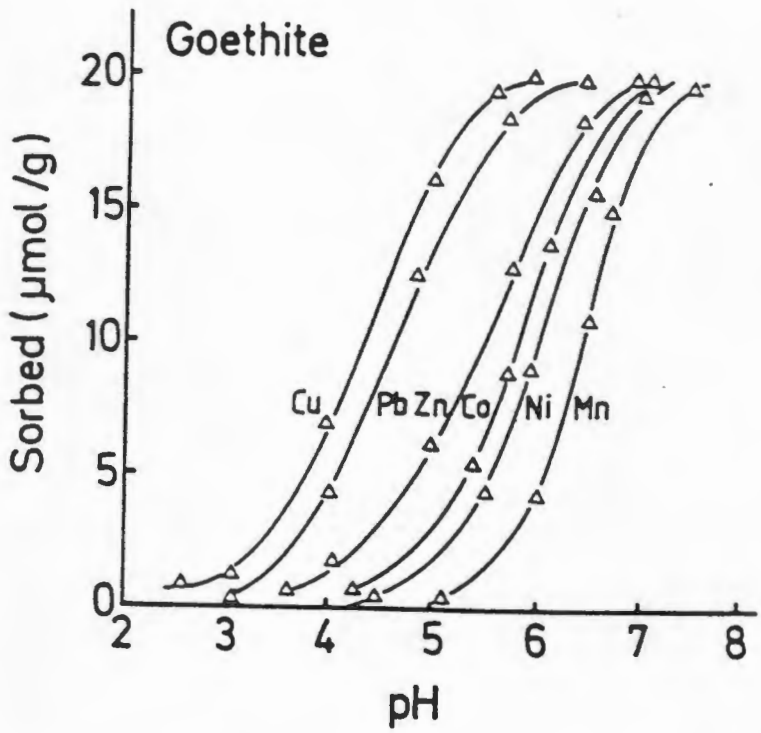

Figure 2.2 The pH dependent retention of some metals on synthetic goethite (Schwertmann and Taylor, 1989)

The distribution of acid mine drainage minerals was demonstrated as a function of pH (Figure 2.3) (Bigham *et al.*, 1992). The precipitation of ferric and aluminium hydroxides is also dependent on pH. At very low pH the metal ions are soluble but as the pH rises they precipitate out, iron(III) hydroxide at pH 2.3 and above, and aluminium hydroxides at about pH 4.5 to 4.7 and above. As the pH of AMD is often below these values the dissolved iron(III) salts will not precipitate out although previous precipitates might be visible (Kelly, 1989).

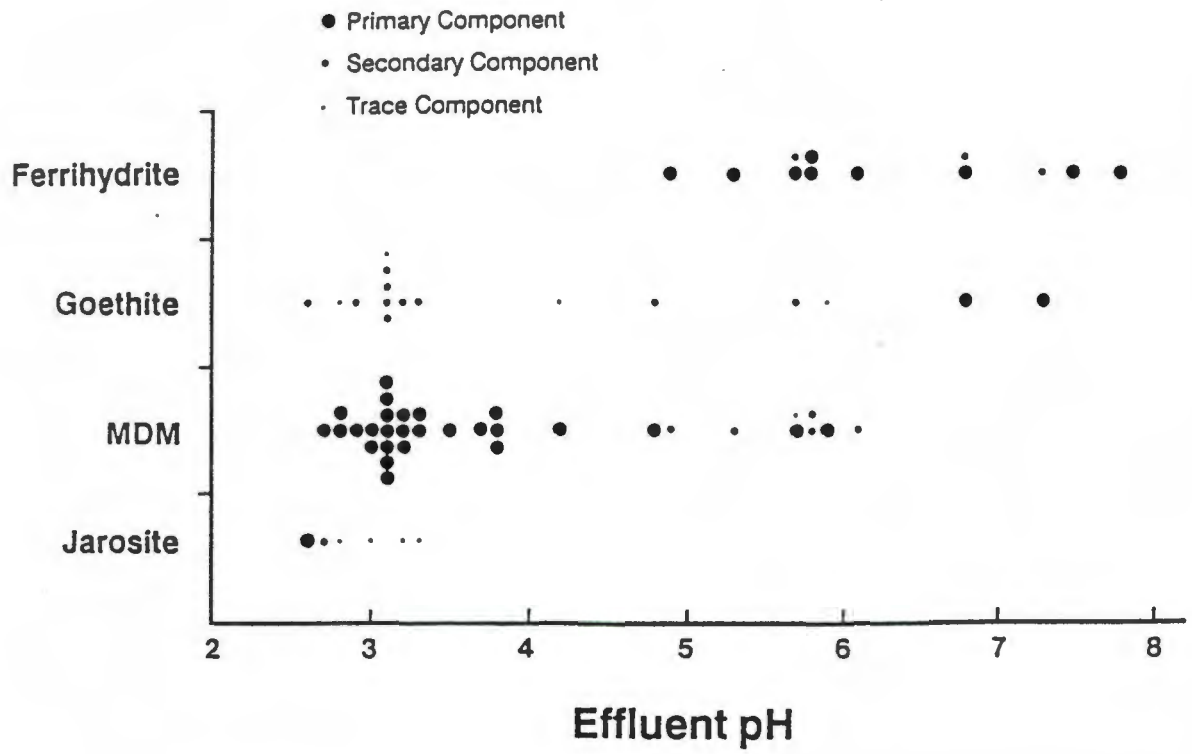

Figure 2.3 The distribution of mine drainage minerals as a function of effluent pH (Bigham *et al.*, 1992) MDM = Schwertmannite

Low pH values affect the adsorption of metals by various humic and fulvic acid fractions (Förstner and Wittmann, 1979). Crist *et al.* (1988) demonstrated that acidic waters also influence the interactions of metals with algae. Low pH generates high proton concentrations which in turn saturates anion sites on the cell surfaces. High metal concentrations were not able to displace these protons from their sites. The number of sites available for electrostatic bonding of metals to algae cell surfaces is determined only by the pH (Crist *et al.*, 1988).

2.3.2 Redox reactions and metal mobility

Oxidation reduction reactions can be described as reactions which involve the transfer of electrons or oxygen. They involve electron donors (reducing agents) and electron acceptors (oxidizing agents). The tendency of redox reactions to proceed is determined by the electromotive force (E) for the particular reaction. If a hydrogen electrode (platinum wire) and Zn electrode are immersed in an aqueous solution and electrically connected, the redox reaction (reaction 17) will proceed spontaneously when $E > 0$.

(17) $Zn + 2H^+ \rightarrow Zn^{2+} + H_2$

The E_h is the half-reaction potential of the hydrogen electrode, also described as a measure of the tendency of a substance to accept or donate electrons. The standard state potentials of all half-reactions can be symbolized as E_h^0 and are defined for standard state conditions of the reactants and products. Because in real reactions the reactants and products are rarely at unit activity, standard state potentials, E^0, must be corrected to the relevant conditions. This is done using the Nernst relationship which can be expressed as the redox reaction at 25°C between, a moles of reactant A and b moles of reactant B to produce c moles of C and d moles of D (Drever, 1988; McBride, 1994) by equation I:

(I)

$$E = E^0 - \frac{0.059}{n} \times \log \frac{[C][D]}{[A][B]}$$

As reduction potentials of half−reactions become more positive the tendency of oxidized species to be reduced increases. The redox intensity, pe, is defined in a manner analogous to pH (Drever, 1988; McBride, 1994) by equation II:

(II)

$$pe = -\log (e^-)$$

where pe expresses a hypothetical electron activity. It measures the relative tendency of a solution to accept electrons. Reducing solutions have low pe values and tend to donate electrons to species in the solution, oxidising solutions have high pe values and tend to accept electrons from species in the solution. pe-pH and Eh-pH diagrams can be used to display the stability relationship where redox reactions are involved (Figure 4). They show strictly equilibrium relationships, whereas natural waters do not necessarily comply with equilibrium conditions (Drever, 1988; McBride, 1994).

Oxidation reactions of reduced metal compounds (FeS_2, ZnS, Cu_2S) cause acidification and mobilisation of metals in solution. Bacteria are also capable of oxidising (*Thiobacillus* species) or reducing (*Desulfovibrio* species) sulphur compounds. These processes can result in either mobilizing or immobilizing metals in the respective environments (Pierzynski *et al.*, 1994). The oxidation of pyrite has been discussed in detail above as one of the principal components of AMD, affecting the mobility of metals in these solutions. Major components, Fe, Mn, organic matter of AMD are available for redox processes and will affect metal transport in AMD.

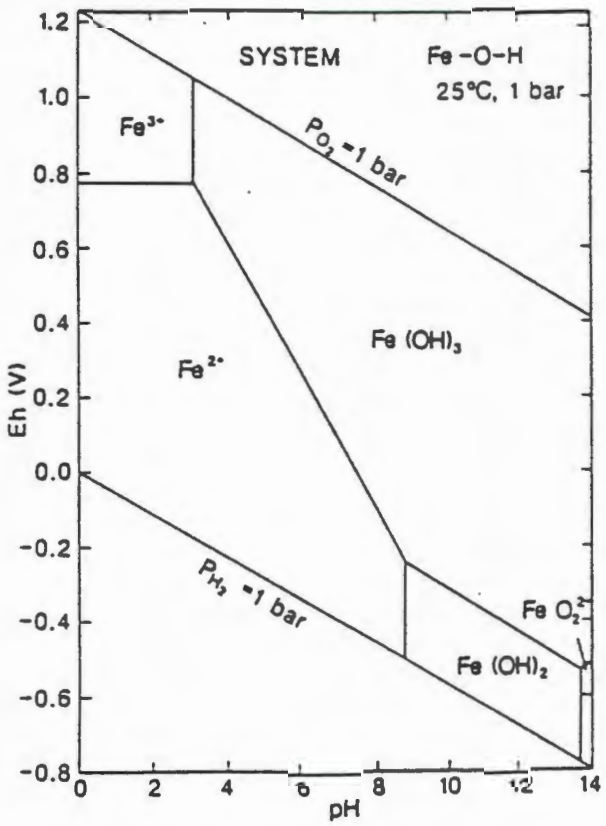

Figure 2.4 The Eh - pH diagram for Fe-O-H at 25°C and 1 atmosphere. The presentation assumes a total activity in solution of Fe = 10^{-6} M and that $Fe(OH)_3$ is the stable phase for the Fe(III) precipitate without considering magnetite (Schwertmann and Fitzpatrick,1992).

2.3.3 Precipitation and dissolution of minerals and metal mobility

The precipitation of metals as secondary minerals from AMD may occur with a change of pH or pe, mixing with natural waters, and contact with soils or sediments. Among the most important of these precipitates are the oxides, oxyhydroxides, hydroxides, sulphates, and carbonates, the phosphates and silicates are of lesser importance. In addition to these secondary precipitates, certain sulphide and sulphate minerals may form through the interaction of metals with hydrogen sulphide or sulphate (Evans, 1989; Karathanasis *et al.*, 1988). The extent of dissolution of a mineral in water, and conversely its precipitation, can be described by its solubility product (K_{SO}) and saturation index (SI) (Nordstrom and Munoz 1994; Drever, 1988).

Karathanasis *et al.* (1988) found that soil solutions contained high levels of dissolved Al, in areas of major coal mining activity and soils with low neutralizing capacity. They suggest that dissolved Al in these areas appeared to be controlled by the solubility of the basic aluminium sulphate minerals jurbanite and alunite, and not gibbsite and kaolinite. Soil solutions in contact with uncontaminated soil and geological strata supported soluble Al levels consistent with the solubility of kaolinite or gibbsite. In solutions with pH values < 4.5, pH and SO_4^{2-} activities can predict accurately enough the levels of soluble Al^{3+} in surface and ground waters.

The equilibrium of Fe is also significantly modified in an acid sulphate rich system. Although goethite and amorphous $Fe(OH)_3$ control Fe levels of most natural aquatic systems, dissolved Fe in acid sulphate rich solutions appears to be more consistent with the solubility of the basic iron sulphate mineral jarosite (Figure 2.3). Predictions similar to those for Al were made for soluble Fe^{3+} levels using amorphous $Fe(OH)_3$, goethite α-FeOOH, and jarosite $KFe_3(SO_4)_2(OH)_6$ as potential mineral phases controlling the activity of Fe^{3+} in solution. Karathanasis *et al.* (1988) suggested that most solutions (contaminated soil, uncontaminated soil, and contaminated surface water) were not in equilibrium with a single Fe-mineral.

2.4 Acid mine drainage mineralogy

2.4.1 Mineralization

The mineralogy of leachates from sulphide rich deposits and their oxidation products could help to predict effluent qualities and quantities. Minerals can be classified as primary minerals (FeS_2) which are those minerals that constituted the ore (coal) and surrounding material. Secondary minerals (goethite, jarosite) are those that form by precipitation of constituents derived from oxidation at the leachate emission point or in impoundments. Tertiary minerals originate in soil or tailings pores on drying and after removal from the contaminated site. Minerals that form during storage, after drying, are classified as quaternary minerals (Jambor, 1994).

Primary sulphide minerals present in South African coal and associated strata are summarized in Table 2.1. Oxide minerals such as quartz, magnetite and ilmenite in sulphide rich environments, have been observed to be resistant to alterations in comparison with associated sulphides. The formation of jarosite in oxidised environments is indicative of silicate-mineral dissolution as a source of K for jarosite. Sources for K release have been biotite, stilpnomelane, K-feldspar, and muscovite (Jambor, 1994). This would also result in the release of aluminium from these minerals. The oxidation of primary metal-sulphide (pyrite) minerals was discussed previously. The presence of primary carbonate minerals (Table 1) is geochemically important. Partial cation substitutions such as Fe and Mn for Mg in dolomite and Mg and Mn for Fe in siderite are the norm. These minerals are principal acid neutralizers and are the first to be attacked following acid generation. They are therefore the principal sources of Mn, Fe Ca, Mg, and other elements to the hyrogeochemical system. The reactivity of primary minerals will influence the availability of free metal ions in AMD (Jambor, 1994).

Some secondary minerals from the oxidation of coal and sulphide rich wastes are summarised in Table 2.2. The secondary iron containing minerals (goethite and jarosite) were found to be the most abundant minerals (Jambor, 1994). The yellow brown coloured goethite considered as the most stable form of the Fe(III) oxides is formed from the oxidation of pyrite, and typically occurs throughout the unsaturated zone (Figure 2.3). Goethite precipitates from solution via a nucleation-crystal growth process and tends to form granular or short rod like particles in AMD. Lower temperatures, higher activity of water and organic compounds capable of complexing Fe seem to favour goethite formation over other Fe oxides. Goethites formed in the presence of Al sources have Al incorporated into their structure in place of Fe.

Table 2.2 Secondary minerals identified in sulphide-rich tailings (Jambor, 1994 and Bigham, 1994)

Iron oxyhydroxides		Other minerals	
goethite	α-FeO(OH)	marcasite	FeS_2
lepidocrocite	γ-FeO(OH)	covellite	CuS
akaganeite	β-FeO(OH,Cl)	suphur	S
maghemite	γ-Fe_2O_3	cristobalite	SiO_2
ferrihydrite	$5Fe_2O_3.9H_2O$	vermiculite	$(Mg,Fe,Al)_3(Si,Al)_4(OH)_24H_2O$
		smectites	$M^+_{x+y}(Al_{2-x}Mg_x)(Si_{4-y}Al_y)O_{10}(OH)_2$
		kaolinite	$Al_2Si_2O_5(OH)_4$

Sulphates	
gypsum	$CaSO_4.2H_2O$
bassanite	$2CaSO_4.H_2O$
jarosite	$KFe_3(SO_4)_2(OH)_6$
schwertmanite	$Fe_8O_8(OH)_6SO_4$
melanterite	$FeSO_4.7H_2O$
goslarite	$ZnSO_4.7H_2O$
epsomite	$MgSO_4.7H_2O$
hexahydrite	$MgSO_4.6H_2O$
ferrohexahydrite	$FeSO_4.6H_2O$
siderotile	$FeSO_4.5H_2O$
rozenite	$FeSO_4.4H_2O$
anglesite	$PbSO_4$
alunogen	$Al_2(SO_4)_3.17H_2O$
copiapite	$Fe^{2+}Fe_4^{3+}(SO_4)_6(OH)_3.20H_2O$

Lepidocrocite (bright orange colour) is a polymorph of goethite, and found less frequently than goethite. The presence of high pH dependent carbonate ion concentrations suppresses the formation of lepidocrocite in favour of goethite. Ferrihydrite is most commonly precipitated from effluents having a pH > 5.0. The mineral displays poorly crystalline structure, but the small size and large surface area of the crystals makes this phase highly reactive. Many compounds of environmental importance such as arsenate, organics, and heavy metals are often adsorbed on the surface of these particles. Ferrihydrite is the least stable of the Fe(III) oxides (Figure 2.3). The remaining iron hydroxides are rare in comparison to the abundance of goethite, whereas the absence of haematite can be explained by unfavourable conditions for the formation of this mineral in AMD environments (Schwertmann and Fitzpatrick, 1992; Jambor, 1994; Bigham *et al.*, 1992).

The formation of minerals containing Fe(II) (siderite, vivianite, and magnetite) with the exception of rozenite,is limited to weak acidic to neutral environments. The various Fe-

sulphides occur where the *Eh* is low enough to reduce SO_4^{2-} to S^{2-} such as at the bottom of eutrophic dams and in anoxic sediments (Schwertmann and Fitzpatrick, 1992).

Iron sulphates are derived from the oxidation of iron sulphides, whereas the aluminium rich sulphates are derived from oxidised host shale rock. Jarosite is a common mineral in acid, high sulphate environments and frequently appears as straw coloured efflorescences. Jarosite was detected in samples formed under pH 3.5 and tends to form crystals of pseudocubic morphology. Schwertmannite (MDM) a poorly crystalline mineral species is a sulphate rich oxyhydroxide material with a tunnel structure. This yellow coloured mineral formed from effluents with pH value in the range of 3.0 to 4.0 and accounts for the lay term "yellow boy" given to AMD by US miners. The mineral has a characteristic pincushion morphology and can be readily identified and differentiated from other minerals common to AMD by its X-ray diffraction profile (Figure 2.5) (Bigham, 1994; Bigham *et al.* 1992).

Secondary gypsum is most abundant in the oxidized and saturated zones and has a relatively coarse grain size. In the oxidised zone the main source of Ca and SO_4^{2-} are carbonate mineral dissolutions and sulphide mineral oxidations respectively (Jambor, 1994). The reactivity of sulphides can differ immensely. These differences are the result of the different conditions (abiotic, biotic, etc.) under which oxidation occurs. The stability of sulphide minerals can be influenced by element substitutions which can either promote or detract from stabilization. Precipitation of secondary minerals can decrease metal ion concentrations in AMD if the chemical and physical conditions permit the formation of precipitates (Jambor, 1994).

Adsorption of trace elements to secondary minerals has been demonstrated for the elements Al, Cr, Mn, Ni, Co, Cu, Zn, Cd, As, and Pb (Evans, 1989). Goethite occurring in oxidizing environments has been shown to have spatial affinity rather than structural affinity for trace elements. Both arsenic and silicon also have affinity for goethite (Jambor, 1994). Metal ions can thus be scavenged and their mobility in AMD changed by precipitation or adsorption to iron(III) and aluminium precipitates (Karathanasis *et al.*, 1988). The absence of oxides and hydroxides other than Fe and Al in mine wastes, under conditions favourable for their formation, indicates other metal concentration limiting mechanisms. These mechanisms can be co-precipitation and adsorption. The difficulty of distinguishing between co-precipitation and adsorption, in areas where ferric oxyhydroxide phases are actively precipitating, should be kept in mind when suggesting metal removal mechanisms. Adsorption and co-precipitation is dependant on the mineralogical composition of ferric oxyhydroxide surface, solution

characteristics, and concentrations of competing cations and ligands (Alpers *et al.*, 1994).

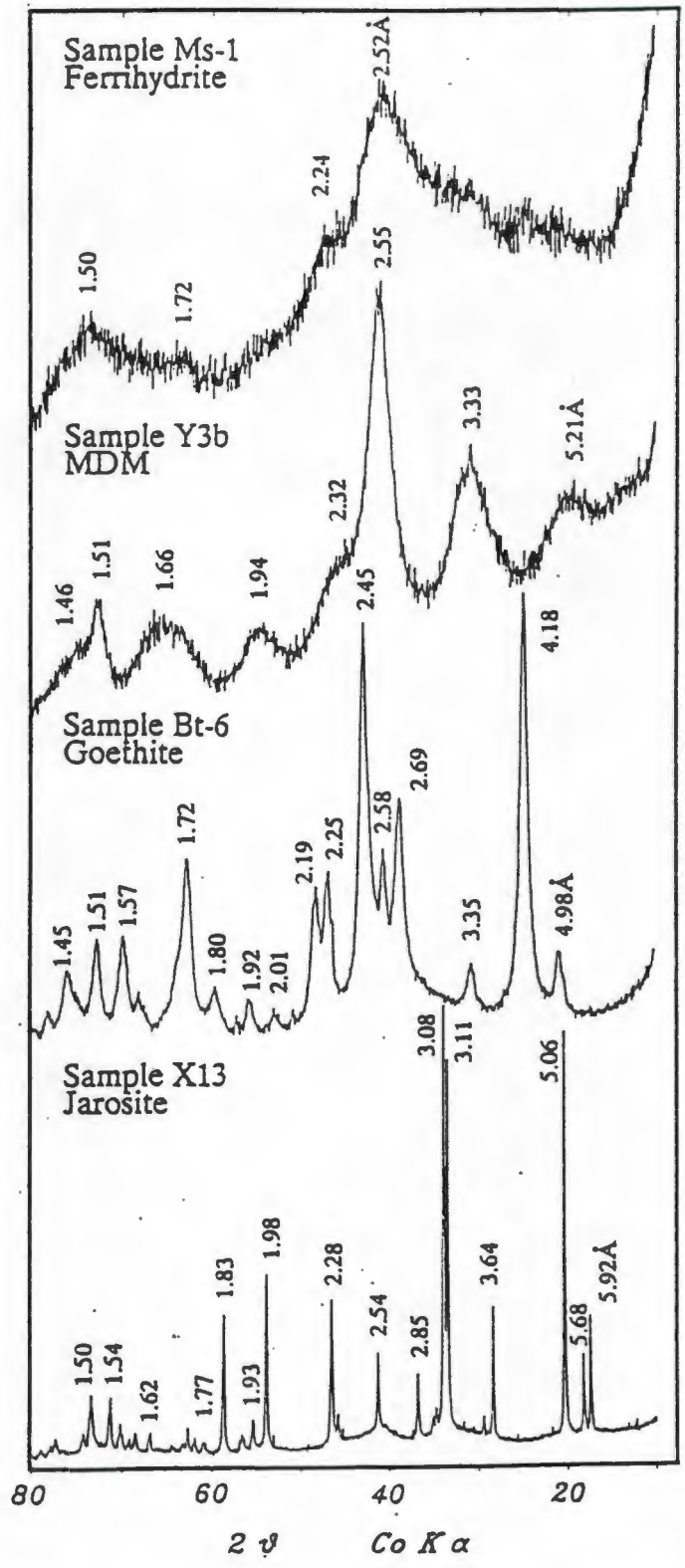

Figure 2.5 Representative X-ray diffraction traces from minerals common to mine drainage (Bigham *et al.*, 1992). MDM = Schwertmannite

2.4.2 Biomineralisation

Biologically induced mineral formation can be external to the organism and a result of metabolic activities and products changing the environment. Biologically controlled mineralisation is probably mediated by specific enzyme systems, organelles or matrices generating minerals within the cell or organelles. These minerals might be serving some essential biofunction (Schwertmann and Fitzpatrick, 1992). Microbiological activity is known to cause both the dissolution and the precipitation of Fe minerals. Organic compounds from the biomass complex the Fe brought into solution by microbial reduction of Fe(III) compounds and in this way mobilize the metal. The mobilized metal can then be transported to distant sites and reprecipitated by either biotic or abiotic oxidation. Ghiorse and Ehrlich (1992) give a summary of iron and manganese precipitating bacteria from natural environments, which includes species found in mine tailings drainage, acidic hot springs, and hydrothermal vent areas. Bacteria are thus directly associated with the precipitation/dissolution of iron and manganese and possibly other metals. Microorganisms, especially bacteria, alga, and fungi may also create environmental conditions (indirectly control the local environments through elevation of pH and Eh), which favour oxidation and precipitation of Fe and Mn. The role played by acidophilic bacteria in the aqueous oxidation of pyrite and related minerals is a good example of enzymatic catalysis of Fe and Mn oxidation (Bigham, 1994).

2.5 The prevention and remediation of acid mine drainage

Protection measures against the formation of AMD and resulting metal mobility begin with the choice of correct mining techniques, the shortest possible exposure of high sulphide bearing material, and the deposition site when mine tailings are involved. Of prime importance are the protection of air and water by preventing combustion of or leachate from abandoned coal mines or tailings. A few possible AMD prevention and remediation technologies and their effect on metal mobility are discussed below.

2.5.1 Inundation of pyritic material

Capping of mine spoils or sealing of coal mines by flooding and underwater disposal of pyritic tailings could prevent the formation of AMD. Water prevents the diffusion of O_2 from the atmosphere to the pyritic material. Thus the rate of oxygen consuming reactions is reduced, resulting in inhibition of bacterial pyrite oxidation. The continued availability

of Fe^{3+} as an alternative oxidant might prevent complete reduction of oxidation (Gould *et al.*, 1994; Evangelou and Zhang, 1995; Förstner and Wittmann, 1979). Singer and Stumm (1970) state that no complete and economically feasible method exists to totally exclude O_2 from abandoned mine workings.

2.5.2 Neutralization by alkaline materials

Alkaline chemicals, such as lime or sodium hydroxide, are usually applied or pumped into active mines where AMD is a problem. Alkalinity derived from limestone acts as pH buffer and AMD neutralizer, it also hydrolyses most heavy metals thus precipitating them as metal hydroxides. Metals such as Fe and Mn must be oxidized before being precipitated as stable compounds, which is why aeration and neutralization are combined in treating AMD. Other materials, such as alkaline fly ash and topsoil or their mixtures with lime have been found to significantly reduce drainage Fe, Mn, and SO_4^{2-} concentrations. Two or more stage treatments with combinations of limestone, lime slurry, or lime sludge and proper pH selection were found to be effective in the separation of heavy metals and subsequent recovery from AMD (Förstner and Wittmann, 1979; Evangelou and Zhang, 1995; Pulford, 1991).

2.5.3 Wetland treatment systems

The wetland processes identified as having the potential for removing metals from AMD include adsorption of metals by ferric oxyhydroxides, plant and algae uptake, complexation of metals to organic materials, precipitation of metals into oxides, oxyhydroxides, and sulphides. Only the precipitation as either oxides or sulphides has longterm potential. The low redox potential (Eh) of wetlands is not the ideal environment for the formation of metal oxides or oxyhydroxides. Therefore the optimisation of sulphate-reducing bacteria to consume acidity and produce hydrogen sulphide is the focus of recent studies. Hydrogen sulphide would in turn react with heavy metals to yield insoluble precipitates. However, for this process to significantly reduce SO_4^{2-} the sulphate rich AMD must flow through an anaerobic portion of the wetland (Department of Water Affairs and Forestry, 1995; Evangelou and Zhang, 1995). Bioaccumulation of metals by algae has been reported by Brady *et al.* (1994) and Crist *et al.* (1988). These authors found that algae cell surfaces containing anionic ligands were able to exchange protons for multivalent cations. This process was found to be pH dependant, and would be disadvantaged at low pH (Crist *et al.*, 1988)

2.5.4 Inhibition of metal-oxidizing bacteria

Anionic surfactants, organic acids and food preservatives can be used as pyrite oxidation inhibitors by controlling bacterial growth. In the presence of such compounds bacterial cell membranes become permeable and allow hydrogen ions in the acidic environment to enter the cell, causing cell deterioration. The presence of inhibitor degenerating acid resistant yeasts, high solubility and high adsorption capacity of most of these compounds to coal wastes would limit their widespread use (Bosch, 1990; Evangelou and Zhang, 1995).

2.5.5 Inhibition of pyrite oxidation by phosphate

Laboratory test have been described by Evangelou and Zhang (1995), in which the successful coating of pyrite particles by an iron oxide coating prevented further oxidation of pyrite. These experiments involved the leaching of pyrite waste with H_2O_2, KH_2PO_4 and a pH buffer. During the leaching process of this mixture through pyrite rich material, the H_2O_2 oxidizes pyrite and produces Fe^{3+} so that the iron phosphate precipitates as a coating on the pyrite surfaces. The possible use of these methodologies in abandoned coal mines is disputable since a well permeated waste body is needed for this process to succeed (Evangelou and Zhang, 1995).

2.6 Conclusion

The mobility of metals in aqueous systems is of importance to areas where potable water and its supply are crucial. Elevated metal concentrations in waters for domestic or agricultural use can result in toxicity to plants, animals and humans. Mining operations have been some of the major contributors to increases of metal concentrations in the environment. Abandoned coal mines are susceptible to the formation of AMD from the oxidation of metal sulphide rich minerals in the coal and associated geological strata. The mechanisms of metal disulphide oxidation rely on the availability of O_2 and water. The climate, groundwater table and hydrology of the mining area will affect the availability of these two components.

The presence of collapsed mine ceilings and seasonal rainfall would generate the necessary conditions for the generation of AMD from abandoned coal mines. Oxidation of pyrite (major metal sulphide) by O_2 and Fe^{3+}, accelerated by iron oxidising bacteria, generates waters with low pH values and high metal concentrations. Other primary minerals in the coal, surrounding strata, and contaminated soils will determine the metal elements involved in AMD. The

Chapter 3

DESCRIPTION OF THE STUDY AREA

3.1 Location

The study area is situated in Mpumalanga Province approximately 110 km north east of Johannesburg in close proximity to the town of Witbank. Witbank and its surrounding coal fields are located in the catchment of the Olifants River, upstream of the Loskop dam (Figure 3.1). The region has experienced rapid economic growth over the past two decades. Coal mining, power generation and industrial development were the dominant sectors contributing to this growth. Regional water quality is one element of the environment that has deteriorated as result of this development (DWAF, 1995).

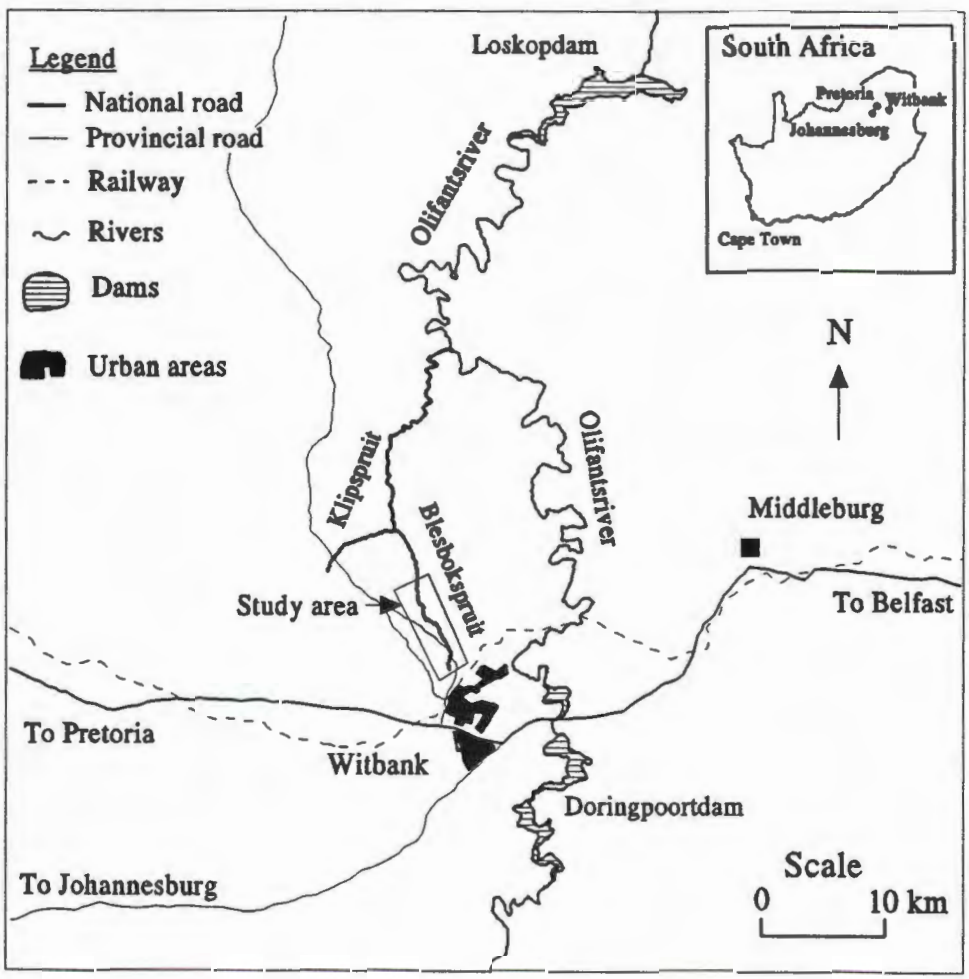

Figure 3.1 The position of the study area relative to Witbank and the Olifants River

Certain streams in the Witbank area have been of particular concern. These streams include the Klipspruit catchment (Figure 3.1). The headwaters of this catchment are dominated by old mining and active mining activities (Figure 3.2). Industrial operations and residential development are also present. The pollutant load exported by this catchment affects receiving water bodies of the Olifants River. These include the Loskop dam, situated downstream in the Olifants River. The dam supplies water for domestic, industrial and agricultural use. The Witbank area is situated on a watershed which drains in three directions. The north-western suburbs of Witbank and their environs drain to the Klipspruit via two smaller tributaries. One of these is the Blesbokspruit, which is the focus of this study.

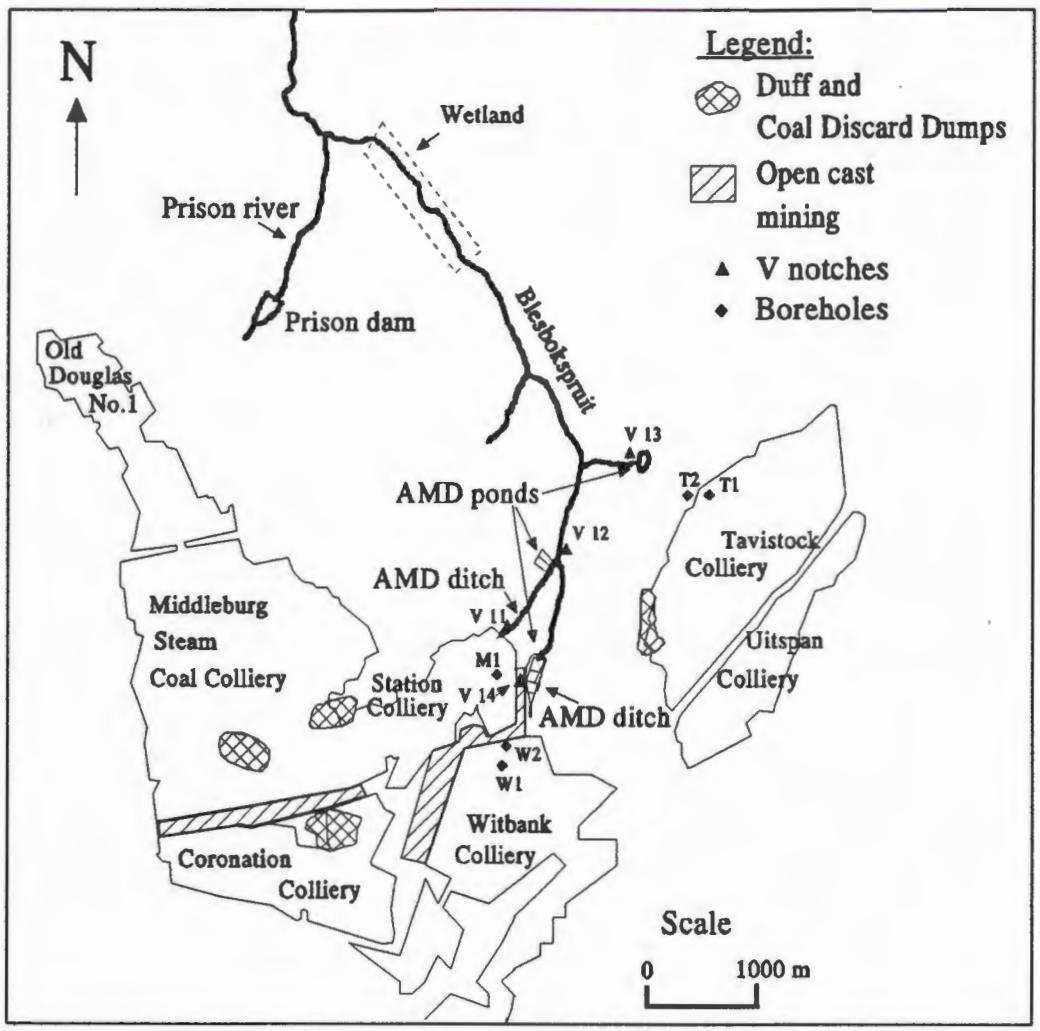

Figure 3.2 The Blesbokspruit catchment and the associated abandoned coal mines

3.2 Rainfall and surface hydrology

The Blesbokspruit and its catchment lie in the summer rainfall area of South Africa. The average summer rainfall for the period 1986 to 1993 is 93 mm, compared to an average winter rainfall during the same period of 14 mm (Appendix I, Table A I.1). However, 1996 was a particularly wet year, with summer and winter rainfall being, respectively, 227 mm and 23.7 mm (DWAF, 1995; Witbank Municipality, 1996).

The surface flow is increased by seepage/migration from old mine workings and attenuated by AMD collection dams. The monitoring points during the measuring period September 1986 - April 1994 were V-notches 11, 12, and 13 (Appendix I, Table A I.2). V-notch 12 was not found during the sampling trip in late July 1996 and had probably been washed away. The DWAF (1995) compared the annual rainfall for the period September 1986 to September 1994 to the recorded average flow rate of V-notches 11, 12, and 13 for the same period. A generally poor correlation of AMD flow and rainfall became evident from their comparison (DWAF, 1995). Acid mine drainage flows were generally higher during successive high rainfall years and generally lower during successive poor rainfall years (DWAF, 1995). The flow at all identifiable V notches during the sampling visit was noted as strong. The seepage from AMD outwelling points was considerable and the Blesbokspruit was flowing strongly. All AMD collection ponds were overflowing and rapid flow was observed in the AMD drainage ditches.

3.3 Geology and geohydrology

The geology of the area consists of alternating sequences of sandstones and shales of the Karoo Sequence, including structures such as minor slips, faults and some dolerite intrusives of varying thickness.

The Karoo sequence is comprised of Permian and Triassic age sediments of the Dwyka and Vryheid Formations of the Ecca group. The Dwyka Formation comprises products of Dwyka glaciation and are represented by diamictites, glacio-lacustrine siltstone, pebbly mudstones, fluvio-glacial gravels and conglomerates. The Ecca group consists of sediments deposited in shallow marine and fluvio-deltaic environments. Coal accumulated as peat in swamps and marshes associated with this environment. The coal seams of primary interest in the Blesbokspruit catchment are the No.2 Coal Seam and, to a lesser extent, the No.1 Coal Seam. The surface geology of the Blesbokspruit catchment consists of a silty sandy soil cover. This cover comprises hillwash, colluvium and residual soils to a depth of 5-10 m (DWAF, 1995).

Regionally the aquifer system in the Karoo Supergroup forms part of a non-continuous, multi-layered system. This system comprises the following aquifer types: 1) Shallow, perched aquifer; 2) Fractured Karoo rock aquifer; 3) Aquifers associated with dolerite intrusives; 4) Aquifers associated with coal seams. The depth of the permanent water table is generally in the order of 5-15 m below surface (DWAF, 1995).

Collapsed mines create local depressions in the geohyrological surface which accumulate excess water. Water from these old mine workings flows into the Blesbokspruit. Mine floor contour information indicates that mine water drains from the following mines towards the Blesbokspruit: 1) Middleburg Steam and Station Collieries; 2) Witbank Colliery; 3) Tavistock Colliery (Figure 3.2) (DWAF, 1995).

3.4 Mining

Mining of the Witbank coalfield started in 1889 near the present town of Witbank. The shallow coal seams were exploited by means of underground bord-and-pillar methods. These mining activities came to an end in the late 1940's and early 1950's. All underground mining has ceased in the Blesbokspruit catchment. Extensive collapse of the roof of the workings has occurred due to the shallow nature of the underground mining operations, extensive pillar robbing, and underground burning of support pillars. This has resulted in surface subsidence which seriously affects the groundwater quality and surface drainage patterns. Natural flooding of the old mine workings was thus facilitated resulting in the emergence of excess water into the Blesboksruit (DWAF, 1995; Bullock *et al.*, 1996).

3.5 Water quality

As a result of the mining methods used and the consequent surface subsidence,tension cracks, sometimes extending into the workings, developed. These allowed free passage of oxygen and water into mine workings which aided oxidation of pyrite in the coal and coal bearing strata. The kinetics of this reaction are slow but the oxygen encouraged and increased the rate of the exothermic oxidation reaction by offering an oxygen source for *Thiobacillus ferroxidans* bacteria which act as a catalyst. Increased heat associated with the oxidation reaction leads to the spontaneous combustion of the remaining underground coal. The increase in temperature due to the underground fires will accelerate the oxidation of pyrite (Bullock, 1996). The result is the acidification of the stagnant or flowing mine water. The mine water in the Blesbokspruit catchment is typified by low pH (2 - 4) and high TDS. Mine water quality from the different collieries which affect the Blesbokspruit catchment has been determined from recent exploration drilling (Table 3.1) (DWAF, 1995).

Tavistock Colliery has waters with low pH (<3) and high salinity (TDS ± 6000). The salinity is due to high concentrations of Ca, Mg, and SO_4^{2-}. The metal concentrations are also high. Mine water from the Witbank, Middleburg Steam, and Station Collieries have similar pH and metal concentrations as the Tavistock Colliery. The high salinity in these waters, however, is due to the dominance of the Na, Cl, Fe, and SO_4^{2-} ions (Table 3.1).

Table 3.1 The geochemistry of borehole waters associated with the Blesbokspruit catchment (DWAF, 1995).

Water Quality Variable	Boreholes related to the Blesbokspruit catchment (Fig. 3.2)					Water Quality Standards Target guideline range
	M1	W1	W2	T1	T2	
pH	2.8	2.7	2.7	2.8	2.9	6.0 - 9.0
Conductivity (mS/cm)	3.40	3.89	4.03	3.55	3.68	0 - 0.7
TDS (mg/ℓ)	3604	3048	3354	5778	7158	0 - 450
Total Alkalinity as $CaCO_3$	nil	nil	nil	nil	nil	
Na (mg/ℓ)	399	620	775	47	32	0 - 100
Ca "	84	42	40	509	462	0 - 32
Mg "	31	14	14	289	200	0 - 70
Cl "	611	951	989	18	4.8	0 - 250
SO_4 "	1440	910	1306	3233	3840	0 - 200
Nitrate " as N	5.3	2.3	2.9	6.4	15	0 - 6
Fe total "	193	99	122	198	726	0 - 0.1
Al total "	84	81	87	32	38	0 - 0.15
Mn total "	9.3	4.5	3.5	49	30	0 - 0.05

Note: All water quality variables are reported in mg/ℓ, except pH and conductivity (From DWAF, 1995 and DWAF, 1996).
M1 = Station colliery borehole; W1 and W2 = Witbank colliery boreholes; T1 and T2 = Tavistock colliery boreholes

Surface water quality was monitored over a period from February 1990 to November 1994 at V-notches 11, 12, and 13 (Table 3.2). It must be kept in mind that surface flow is also affected by seepage, surface run-off, and by the AMD collection dams. Mine water quality

data from Witbank Colliery and Middelburg Steam Colliery correlate with surface water quality data from V-notch 11 and 12. Water quality from V-notch 13 was found to be similar to water collected in Tavistock Colliery (Table 3.1 and 3.2) (DWAF,1995).

Table 3.2 The surface water geochemistry at V-notches associated with the Blesbokspruit catchment (DWAF, 1995).

Water Quality Variable	V-notch data related to the catchment (Fig. 3.2)			Water Quality Standards Target guideline range
	V 11	V 12	V 13	
pH	2.8	2.9	3.0	6.0 - 9.0
Conductivity (mS/cm)	4.30	4.81	3.91	0 - 0.7
TDS (mg/ℓ)	3330	3868	3335	0 - 450
Total Alkalinity as $CaCO_3$	nil	nil	nil	
Na (mg/ℓ)	193	211	29	0 - 100
Ca "	170	179	368	0 - 32
Mg "	86	94	173	0 - 70
Cl "	181	191	8	0 - 250
SO_4 "	2713	3172	2929	0 - 200
Nitrate " as N	0.09	0.04	0.15	0 - 6

Note: All water quality variables are reported in mg/ℓ except pH and conductivity
(From DWAF, 1995 and DWAF, 1996)
V11 = V-notch in AMD ditch from Station colliery; V12 = V-notch in Blesbokspruit; V13 = V-notch at Tavistock AMD pond.

3.6 Conclusion

Coal mining generates AMD when mine workings are brought into contact with oxygen and water. The collapsed and abandoned coal mines surrounding the Blesbokspruit catchment are no exception. The catchment collects and drains water from surface run-off, groundwater, and collapsed abandoned coal mines. The waters from abandoned coal mines have high TDS, low pH values and are metal rich. This AMD contaminates the Blesbokspruit resulting in a stream habitat devoid of fish, bird and in some instances plant life. The drainage of this water into the Klipspruit River could be detrimental to the downstream catchment and all users.

Chapter 4

AQUEOUS GEOCHEMISTRY OF THE BLESBOKSPRUIT WATERS

4.1 Introduction

The mechanisms controlling metal mobility in natural streams can differ from those in streams containing high metal concentrations (Chapman and Jones *et al.*, 1983; Bigham *et al.*, 1992). High metal concentrations typical of those found in AMD contaminated waters can rapidly saturate available surface sites in the stream-bed sediments and the natural organic and inorganic complexing agents in the water column.

The Klipspruit and tributaries (Blesbokspruit) are among the most heavily polluted streams in the upper Olifants River catchment. Acid mine waters have been seeping from the old mine workings along a weathered coal seam into the Blesbokspruit. This has a detrimental impact on the downstream environment. The waters generally have low pH and high salt concentrations. They are also capable of mobilizing toxic metal concentrations (Department of Water Affairs and Forestry, 1995).

The aqueous chemistry of the waters was thus determined. Acid mine drainage (AMD) from the Blesbokspruit catchment was characterized and analyzed for the presence of the major cations, anions and total element content.

The objectives of the analyses were the following:

1. To assess the quality of the Blesbokspruit water.

2. To determine either increases or decreases in metal concentrations in the waters.

3. To model the speciation of the ions in the catchment waters. This could give a theoretical indication of precipitate formation in the associated sediments.

4.2 Materials and Methods

4.2.1 Sampling

The study site is located to the north-west of Witbank in Mpumalanga Province, South Africa (Figure 2.1). The upper Blesbokspruit catchment was chosen to represent a specific area afflicted by AMD seepage from abandoned coal mines (Figures 2.1 and 2.2).

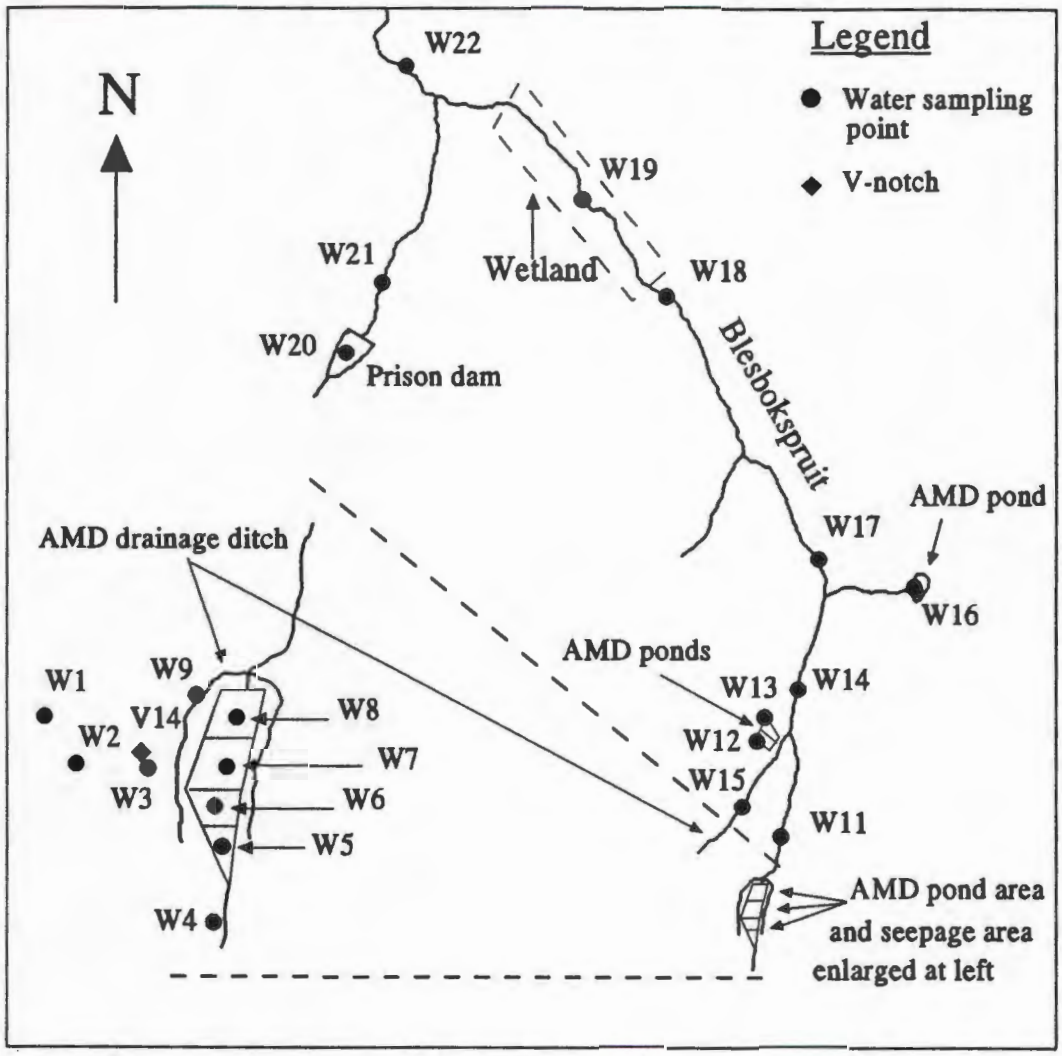

Figure 4.1 The water sampling points in the Blesbokspruit catchment

Site characteristics and descriptions of the collected samples are given in Tables 4.1 and 4.2. Twenty-two surface water samples from seeps, AMD ponds, streams, and reservoirs were collected. The positions of sampling points are indicated on the map of the Blesbokspruit catchment (Figure 4.1). Sampling positions were determined according to the presence of seepage, precipitation, tributaries, AMD ponds, and wetlands in the catchment (Figure 4.2).

Table 4.1 Catchment characteristics

Location	Prevalent rock types*	Prevalent soil types**	Area km²	Mining* dates
Tributary to Klipspruit and Olifantsriver	Shale, shaly sandstone, grit sandstone, conglomerate, coal in places near base and top; Tillite, shale; Sandstone, quartzitic in places, conglomerate; Ecca, Dwyka formations; Witbank coal field # 2 and # 1 coal seams.	Midslope - well drained reddish loam (Hutton form) and yellowish loam (Avalon form). Footslope - moderately drained, greyish, plinthic loam (Westleigh form) and poorly drained light greyish sand (Longlands & Kroonstad forms).	28	1889 - 1956 Small scale operations at present

* DWAF (1995)
** Verster *et al.* (1991)

Water samples were analyzed in the field for electrical conductivity, pH and temperature using a Corning field measurement kit. The equipment was calibrated on site using standard solutions. These were checked in the laboratory and were supplied with the laboratory equipment. Samples were collected in 250 ml polypropylene plastic bottles that were rinsed thrice with the water to be sampled. Four samples were collected for anion and elemental analyses. The low pH did not necessitate the acidification of the water samples destined for cation and element analyses. The bottles were filled to the top and capped carefully to minimise the presence of air and consequent oxidation of the samples. The sample bottles were stored at room temperature and transported via courier to Cape Town. On their arrival the samples were stored at 4°C. It was noted that a brown red precipitate was formed during transport and storage of most of the samples.

Table 4.2 Sample description (refer to Figure 4.1 for locations). Sediment (S), precipitate (P) and algae (A) numbers correspond to water sample (W) numbers.

Map No.	Sample type	Characteristics
W1	Water	Groundwater seeping from ridge, red, orange-yellow precipitates, bacteria
W2	Water	Upwelling point, red-brown crust, green dark purple algae, slow flow
W3	Water	V-notch, strong flow, orange yellow precipitate (crust)
W4	Water	Spruit origin above 4 AMD dams, clear water, organic matter, Eucalypts
W5	Water	Upper (1st) of 4 AMD collection dams in the main stream, full
W6	Water	2nd of 4 AMD collection dams in the main stream, full
W7	Water	3rd of 4 AMD collection dams in the main stream, full
W8	Water	Lower (4th) of 4 AMD collection dams in the main stream, full
W9	Water	AMD collection ditch west of AMD dams
W11	Water	300m downstream of AMD ponds in Blesbokspruit, strong flow, dark green algae
W12	Water	Upper (5th) AMD dam in AMD tributary, full
W13	Water	Lower (6th) AMD dam in AMD tributary, full
W14	Water	200m downstream of AMD dams 5 & 6, in main stream, strong flow, brown-purple algae
W15	Water	At V-notch in AMD collection ditch with strong flow; red-yellow precipitate
W16	Water	AMD dam (7th) on farm property, north east of bridge, full
W17	Water	300m downstream from bridge, in the stream, strong flow
W18	Water	At fence at upstream edge of the wetland, in small floodplain; strong flow
W19	Water	In wetland, below township
W20	Water	Dam on tributary on the west side of the stream, below prison, birds and fish noted
W21	Water	In tributary from prison dam upstream of the road
W22	Water	In the Blesbokspruit downstream of tributary inflow and wetland
S2	Sediment	Upwelling point (W2), stratified; top layer: rust dark-brown; bottom layer: grey dark-brown
S5	Sediment	1st AMD dam, stratified; Top: yellow brown; bottom: grey brown,
S6	Sediment	2nd AMD dam, top: grey red-brown, bottom: grey red brown, well mixed
S7	Sediment	3rd AMD dam, stratified; top: yellow brown; middle: grey yellow; bottom: dark grey + H_2S
S8	Sediment	4th AMD dam, stratified; top: red brown; middle: grey red-brown; bottom: dark grey
S11	Sediment	River sediment (W11), stratified; top: black dark-brown, sandy; bottom: black + H_2S smell
S12	Sediment	5th AMD dam, stratified; top: dark brown; middle: dark grey-brown; bottom: dark grey
S13	Sediment	6th AMD dam, stratified; top: grey; bottom: black + grey spots
S14	Sediment	River sediment (W14), stratified; top: dark brown; middle: grey; bottom: dark grey + H_2S smell
S19	Sediment	Wetland sediment (W19), not stratified; top: black + H_2S; bottom: black; peat-like + H_2S
S22	Sediment	River sediment (W22), stratified; top: dark brown; bottom: black + H_2S
A2	Algae	Green algae from seepage area downstream of upwelling point (W2)
A2	Algae	Black to brown-purple algae from seepage area downstream of upwelling point (W2)
P2	Precipitate	From upwelling point, rust coloured, spongy appearance
P2-3	Precipitate	From seepage area downstream of upwelling point, yellow appearance
P3	Precipitate	From V-notch, rust-red colour, precipitates on coal and rock pieces
P9	Precipitate	From AMD drainage ditch next to AMD dams 1-4, brown-yellow colour
P13	Precipitate	From AMD dam 6, yellow-grey colour
P15	Precipitate	From AMD drainage ditch towards AMD dams 5&6, red-orange colour

(A)

(B)

Figure 4.2 (A) The AMD outwelling point (W2), and (B) the seepage area on the west side of the Blesbokspruit. Algae growth and mineral precipitates are visible at both sites. Water seeps from the outwelling point and smaller seepage points along the ridgeline through the seepage area, collects and passes V-notch 14 before entering drainage ditch (W9).

(C)

(D)

Figure 4.2 (continued) (C) Acid mine drainage dams immediately east of the seepage area (W5, W6) collect AMD from the seepage area and were overflowing. Drainage ditch (W9) redirected excess flow from the seepage area directly into the Blesbokspruit. (D) Acid mine drainage ditch (W15) with red-brown precipitate clearly visible.

(E)

(F)

Figure 4.2 (continued) (E) A typical stream area upstream of the wetland and next to AMD dam W12 and W13 showing absence of surface vegetation. (F) The Blesbokspruit downstream of the wetland and prison river junction (W22).

4.2.2 Analytical Methods

4.2.2.1 pH and electrical conductivity

The pH and electrical conductivity (EC) of the samples were determined in the laboratory. pH was measured using a Crison micro 2001 pH meter and EC was measured using a Crison micro CM 2201 conductivity meter. The mean of three measurements for each sample was calculated and used as the representative value (Table 4.3). The pH meter was calibrated with Ciba-Corning pH 4 and pH 7 standard solutions. The electrical conductivity of supplied standard solutions (Corning conductivity standards: 12.88 mS/cm and 1413 μS/cm) was measured to determine instrument accuracy. Both instruments had temperature probes enabling temperature measurement and temperature compensation. Theoretical total dissolved salt was calculated from the EC values (Appendix II; subsection A II.2) (McBride, 1994).

Table 4.3 Laboratory pH and EC determination of the water samples. Three typical samples are shown. The results from the remaining 18 samples are summarized in Appendix II, Table A II.1.

Sample No.	Laboratory pH No.1	No.2	No.3	Mean pH	S.D.	RSD %	Laboratory EC in mS/cm No.1	No.2	No.3	Mean EC	S.D.	RSD %
W1	2.57	2.57	2.56	2.57	0.01	0.4	3.57	3.57	3.57	3.57	0	0
W11	2.71	2.71	2.71	0	0	0	3.09	3.08	3.08	3.08	0.01	0.32
W21	7.36	7.29	7.28	7.31	0.04	0.6	0.23	0.23	0.23	0.23	0	0

4.2.2.2 Eh determination

The Eh of the water samples was determined to give an indication of the ability of the samples to either donate or accept electrons. Sealed samples were opened and the Eh was immediately determined using a DTS 800 Multi titrator saturated calomel electrode and a platinum electrode (Appendix II, subsection A II.8) (Garrels and Christ, 1965). Eh measurement in complex solutions (such as AMD) via an electrode potential is subject to great uncertainty (Appendix II, subsection A II.8). Eh values can, therefore, give only a qualitative indication of the redox potential in complex solutions. They would be useful to broadly classify solutions as oxic, suboxic or anoxic (McBride, 1994).

4.2.2.3 Anion determination

The AMD samples were analyzed by ion chromatography (high performance ion chromatography - HPIC) using a Dionex 3000 ion chromatograph. Anions were separated on the Dionex HPIC-AS4A-SC anion exchange column with a carbonate/bicarbonate eluent. The run time was 8 minutes. Detection was by electrical conductivity.

Sample dilution was necessary to prevent exceeding the ion-exchange capacity of the separator column. Samples were diluted with deionized water (Milli-Q) to an EC < 50 μS/cm (Appendix II, Table A II.2). Deionized water was prepared by filtering tap water through 30 and 3 μm filters. This water was then passed through a reverse osmosis membrane and organic compound removal cartridge before being deionized (Milli-Q system, Millipore Corporation, Bedford U.S.A.). Before injection diluted samples were filtered through a 0.22 μm cellulose acetate filter membrane and a Dionex On Guard-P filter cartridge, containing polyvinylpyrrolidone polymers with high selectivity for organic compounds.

Five samples were run in duplicate, and 5 analyses were done for one sample to determine reproducibility of the results (Appendix II, Table A II.3). Accuracy of the instrument was determined by analysis of standard solutions with known concentrations (Appendix II, Table A II.4).

The run conditions were the following:

Sample loop volume:	50 $\mu\ell$
Guard column:	Dionex HPIC-IonPac AG4A
Separator column:	Dionex HPIC-IonPac AS4A-SC
Eluent:	1.80 mM Na_2CO_3
	1.70 mM $NaHCO_3$
Eluent flow rate:	2.0 ml/min.
Autosuppressor:	Anion MicroMembrane

4.2.2.4 Investigating the complexation of sulphate to iron or aluminium

Anion analyses on the Blesbokspruit AMD yielded high sulphate concentrations. Analysis of borehole and surface water from the catchment by the DWAF supports this finding (DWAF, 1995). The elevated sulphate and associated Fe and Al concentrations might affect the determination of the sulphate concentration by HPIC as a result of metal sulphate complex formation. Standard solutions (NaCl, Na_2SO_4, $Al_2(SO_4)_3.18H_2O$, $FeNH_4(SO_4)_2.12H_2O$) were prepared and diluted to an EC of a typical AMD sample. Sulphate and chloride concentrations in these samples were then determined by HPIC.

4.2.2.5 Acidity

Acids contribute to corrosiveness and influence chemical reaction rates, chemical speciation, and biological processes. Acidity can be defined as the amount of base required to raise the pH of the sample to the bicarbonate endpoint. Hydrolysable cations such as aluminium and iron contribute to the acidity. Oxidation of pyrite in coal generates strongly acidic waters. Very low pH and the presence of the sulphate anion in these waters also suggest a strong acid in these waters.

The acidity of the water samples from the Blesbokspruit was determined using an automated potentiometric titrator system (Radiometer DTS 800 Multi titrator) and 0.1 N NaOH as titrant. The following program was used for acidity determinations using the DTS 800 Multi titrator:

pH endpoint:	8.3
Delay time:	2 sec.
Sample volume:	8 ml
Titrant concentration:	0.1 M Titrasol NaOH

All samples were titrated in duplicate and the mean value was calculated. Repeat acidity determinations were made on 2 samples (Appendix A II, Table A II.5). The blank samples were 2 samples from a natural water source (W20, W21). They had no acidity. A control sample with 5ml 0.025 M Titrasol HCl was analyzed with the titrant to determine accuracy (Appendix A II, Table A II.5).

4.2.2.6 Monomeric silica determination

Degradation of silica containing rocks and minerals results in the presence of silica in natural waters as suspended particles. These particles might also be present in a colloidal or polymeric state, and can appear as silicic acid or silicate ions. The silica content of natural waters is in the 1-30 mg/ℓ range although somewhat higher Si values are expected for these acidic waters.

The heteropoly blue method was used to determine the concentration Si in the AMD samples (Standard Methods, 1985). In this determination ammonium molybdate reacts with Si and phosphate to produce heteropoly acids. Oxalic acid destroys any molybdophosphoric acid present. The remaining molybdosilicic acid was then reduced with 1-aminon-2-naphthol4sulphonic acid to heteropoly blue. The intensity of the blue colour was determined with a Turner Model 340 spectrophotometer. All samples were analyzed in duplicate and the mean value was used in the presented data. A calibration curve was prepared for the silica determination and used to determine the silica concentrations of the water samples (Appendix II, Figure A II.1).

The following calculations were used to determine silica concentration (Standard Methods, 1984):

A) From the standard curve: $Y = MX + C$

- Y: Absorbance of sample at 815 nm
- M: Slope of the standard calibration line
- C: Y intercept of the standard calibration line
- X: Sample value in $\mu g\ SiO_2$ / 55ml

B)

$$mgSiO_2/litre = 10^{-6} g\ SiO_2 \frac{55ml\ final\ volume}{ml\ sample}$$

4.2.2.7 Aluminium determination

Acidity from oxidising pyrite in abandoned coal mines, which is not neutralized by carbonate rock or in the soil zone, causes mobilization of aluminium into surface waters. This aluminium originates from aluminosilicate clays in the underground shale formations and surface soils. Aluminium will also contribute to the acidity of surface waters downstream of the AMD seepage. Aluminium was thus determined using Inductively Coupled Plasma-atomic emission spectrometry (ICP-AES) and the Chrome Azurol-S method (Appendix II, subsection A II.9).

In the latter method the metalochromic reagent chrome azurol-S (CAS) in hexamine buffer at pH 4.9 reacts rapidly with monomeric and polymeric forms of aluminium(III) (Kennedy and Powell, 1986). Aluminium concentrations determined by the CAS method were compared to those obtained by ICP-AES. The comparison showed good correlation between the CAS method and ICP-AES determinations and gives an indication of the accuracy of the ICP determination (Figure 4.3).

Aluminium in the water samples was determined using the extractable Al technique described by Kennedy and Powell (1985). To 10 ml hexamine buffer (0.8 M; pH adjusted to 4.9 with concentrated HCl), 10 ml ascorbic acid (0.5 g/ℓ) and 10 ml Chrome Azurol-S (1.64 M) was added 10 ml sample or standard. The mixture was allowed to stand at room temperature for 20 minutes and absorbance was measured at 567 nm using a Turner Model 340 spectrophotometer. The Al concentrations of the samples were determined against the calibration line (Appendix II, Figure A II.2). Aluminium was calculated as mg Al/ℓ. All samples and standards were analyzed in duplicate and the mean values were reported.

The following calculations were used to determine aluminium concentration:

From the standard curve: $Y = MX + C$

- Y: Absorbance of sample at 567 nm
- M: Slope of the calibration line
- C: Y intercept of the calibration line
- X: Sample value in mg Al/ℓ

4.2.2.8 ICP-AES determination of elemental concentrations

The total elemental concentration of the elements Na, K, Mg, Ca, Fe, Al, Mn, Si, Zn, Ni, Cu, Pb, Co, and Cr in nonacidified AMD samples was determined using ICP-AES. Water samples were diluted 10-fold and analyzed with a JOBIN YVON 70C ICP-AES. Instrument parameters, and plasma conditions are described in Appendix II subsection: A II.9. The results were compared with the results from the Al and Si chemical determination to give an indication of the accuracy (Figures 4.3 and 4.4).

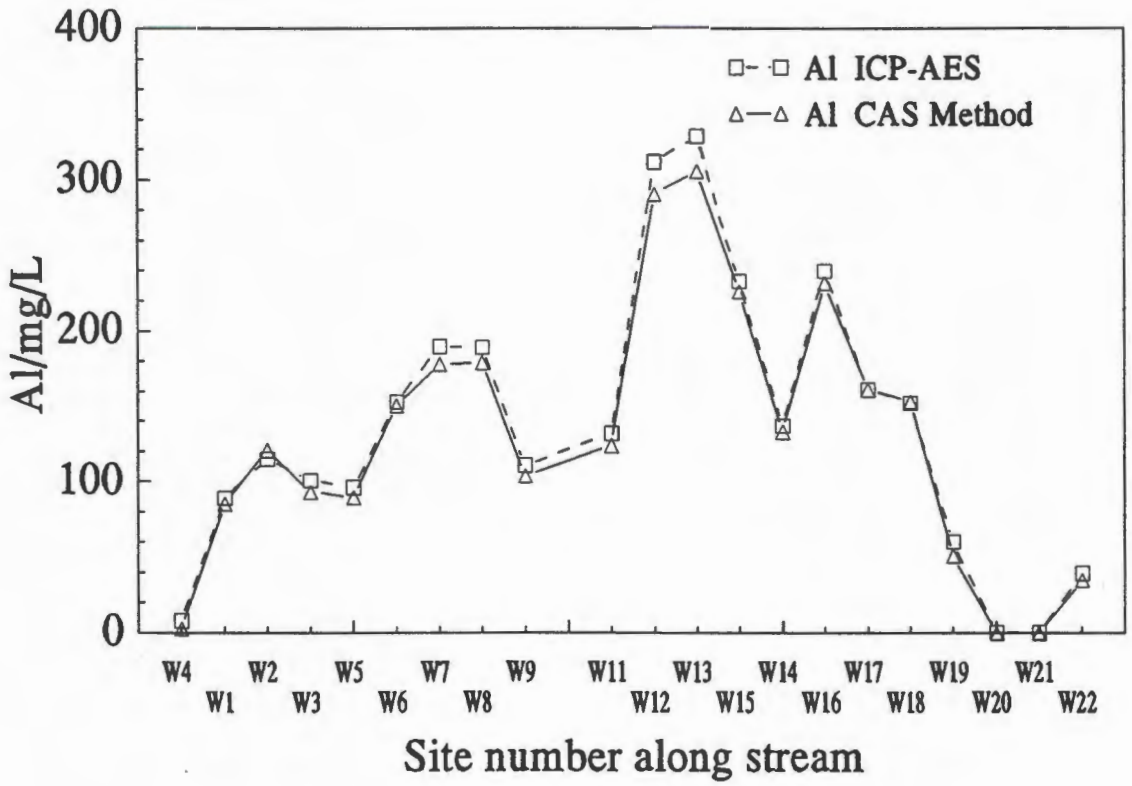

Figure 4.3 A comparison of Al concentration determinations by ICP-AES and the CAS method.

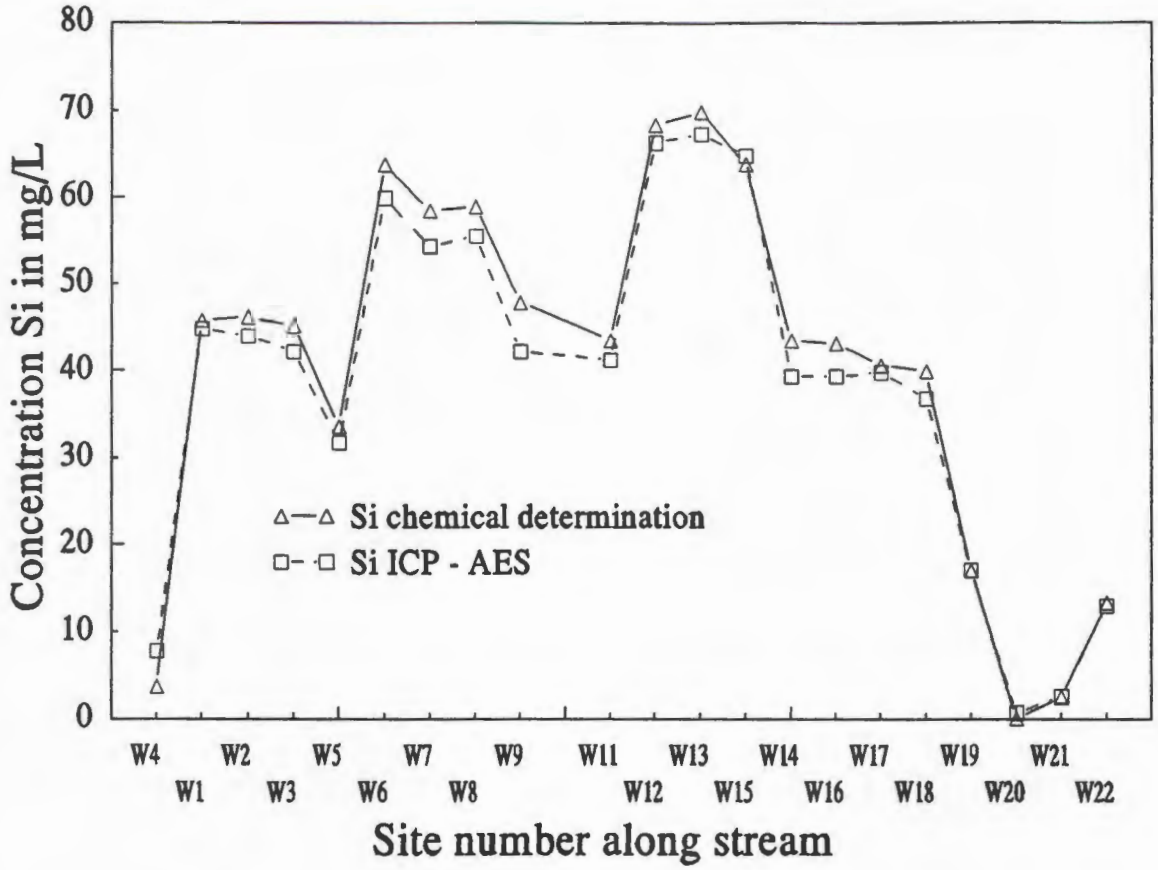

Figure 4.4 A comparison of Si concentration determinations by ICP-AES and the heteropoly blue method.

The results from both the chemical and ICP-AES analyses of the water samples for Si and Al content correlate very well with each other. This good correlation generated confidence in the remaining ICP-AES total element determinations.

4.2.2.9 Alkalinity (2 samples)

Alkalinity of water is its acid neutralizing ability. The alkalinity in most surface waters is primarily a function of carbonate, bicarbonate and hydroxide concentration in these waters (Murray and Wade, 1996). The alkalinity of the AMD is zero, and thus only samples W20 and W21 were analyzed for alkalinity. An automated potentiometric titrator system (DTS 800 Multi titrator) with 0.01 N HCl titrant was used for this determination.

Duplicate samples from a natural water source (W20, W21) were analyzed for their alkalinity using the DTS 800 Multi titrator.

The following program was used for alkalinity determinations:

pH endpoint:	4.5
Delay time:	10 sec.
Sample volume:	10 ml
Titrant concentration:	0.01 M Titrasol HCl

The alkalinity was calculated as follows (Standard Methods, 1985):

$$CaCO_3/litre = \frac{ml\ Titrant \times N\ Titrant \times 50000}{ml\ Sample}$$

where N = Normality of the titrant

4.2.2.10 Fluoride determination

The concentration of fluoride in the AMD samples was determined using a Corning ion analyzer 255 with a fluoride electrode as selective ion sensor. Fluoride ion activity depends on the solution's total ionic strength and pH. Fluoride complexing species (Al and Fe) and high acidity also affect fluoride ion activity. The addition of CDTA (cyclohexylenediaminetetraacetic acid), a chelator, to the fluoride buffer prevents these interferences.

The selective ion (F^-) electrode (Corning double junction 476067 reference electrode) of a Corning 225 ion analyzer was calibrated with three F^- solutions. The calibration slope is the difference in potential between the higher and lower standards when the standards differ by a factor of 10 in concentration. The three point calibration slope value obtained for the determination was -42.53 mV. Triplicate analyses of the three F^- standards were done during the sample analysis to check instrument accuracy and precision (Appendix II, Table A II.6). Fluoride was determined in ppm and reported in mg/ℓ. The electrode will respond to uncomplexed F^- activity over the range 0.1 -5 x 10^{-6}M (Standard Methods, 1985).

Standard and sample solutions were mixed 1:1 with fluoride buffer and allowed to equilibrate for 15 minutes. The instrument was calibrated using 0.1, 1.0 and 10.0 ppm F^- standards. A yellow-green colour was noticed on addition of the buffer to the AMD samples with elevated cation content. This colour developement can be due to Fe-CDTA complex formation. Each analysis was obtained in duplicate and the mean values were reported (Standard Methods, 1985).

4.2.2.11 Chemical speciation of Blesbokspruit waters

Ure and Davidson (1995) define speciation as either (a) process of identifying and quantifying the different, defined species, forms or phases present in a material; or (b) the description of the amounts and kinds of these species, forms or phases present. The unstable nature of the Blesbokspruit waters has to be taken into account when speciation of these waters is undertaken.

The MINTEQA2 speciation model was used for speciation modelling of the Blesbokspruit waters. MINTEQA2 (Allison *et al.*, 1991) is a geochemical speciation model based on equilibrium thermodynamics which can calculate the equilibrium composition of dilute aqueous systems among soluble, solid, adsorbed and gas phases. Calculations can be performed to take into account varied environmental conditions such as pH, ionic strength, temperature and redox conditions. The program also includes an extensive database which includes thermodynamic data for the soluble complexes, mineral solubilities, gas solubilities and redox couples (Lumsdon and Evans, 1995; Allison *et al.*, 1991).Input to the model required the total analytically measured concentrations of the compounds in the Blesbokspruit waters in mg/ℓ. The pH and temperature of the respective samples were also entered into the model. The Davies equation was defined to compute the activity coefficients. The equation is an extention of the Debye-Huckel equation and was preferred because only the ionic strength of the medium and the charge on the species were required to calculate the value of the activity coefficients (γ_i) (Lumsdon and Evans, 1995). Iron was assumed to be present as Fe^{3+} in all acidic samples and as Fe^{2+} in the freshwater samples (Drever, 1988; Yariv and Cross, 1979). Manganese was entered into the program as Mn^{2+} (Yariv and Cross, 1979).

4.3 Results and discussion of water analysis

The results of the Blesbokspruit water sample analyses are presented in Table 4.4.

Table 4.4 Laboratory analyses of Blesbokspruit waters

Variable	W4	W1	W2	W3	W5	W6	W7	W8	W9	W11	W12	M1**
pH[1]	3.5	2.6	2.7	2.6	2.8	2.7	2.7	2.7	2.6	2.7	2.9	2.8
EC[1] (mS/cm)	0.84	3.57	3.71	3.73	3.29	3.90	3.63	3.64	3.78	3.08	3.50	3.40
TDS (mg/ℓ)	578	2280	1748	2097	2356	2625	2295	2341	2504	2164	1758	3604
TDS* (mg/ℓ)	538	2285	2374	2387	2106	2496	2323	2330	2419	1971	2240	nd
Acidity[2] (mM)	2.2	19	26	21	18	28	32	31	24	22	45	nd
Alkalinity[2] in mg $CaCO_3$/ℓ	nil	nil	nil	nil	nil	nil	nil	nil	nil	nil	nil	nil
Eh (mV)	241	330	189	346	317	323	331	321	350	341	317	nd
Anions[3] (mg/ℓ)												
SO_4^{2-}	284	1345	987	1226	1416	1512	1509	1511	1470	1417	1077	1440
Cl^-	111	468	220	397	486	572	363	380	552	366	238	611
NO_3^-	BDL	BDL	BDL	BDL	BDL	BDL	BDL	BDL	BDL	BDL	BDL	5.3
F^-	1.1	1.2	1.2	1.3	2.0	1.3	1.3	1.2	1.3	1.3	0.04	nd
Total Elemental Concentrations (mg/ℓ) by ICP-AES:[4]												
Na	101	296	360	294	248	302	229	228	298	213	150	399
K	4.5	11.5	13.4	11.2	4.85	24.5	2.34	33.0	10.5	5.01	5.29	nd
Ca	49.2	110	116	117	139	145	136	134	122	111	205	84
Mg	24.7	43.1	47.1	45.4	56.7	56.9	51.9	51.3	47.0	44.6	72.9	31
Fe	1.3	31.6	25.5	46.2	29.6	38.6	34.6	74.4	36.1	27.2	20.4	193
Al	7.9	89.4	115	101	96.1	153	190	189	111	132	312	84
Al#	2.5	85.5	121	93	89.8	150	178	179	104	124	291	nd
Mn	2.9	10.6	11.5	13.4	12.4	13.8	12.8	12.7	13.4	12	24.1	9.3
Si	7.8	44.8	44	42.2	31.7	59.9	54.3	55.5	42.2	41.2	66.2	nd
Si##	3.8	45.8	46.2	45.2	33.6	63.7	58.4	59.9	47.8	43.3	68.3	nd
Zn	0.74	2.4	2.7	2.6	1.9	2.3	3.4	2.8	2.6	2.3	3.9	nd
Ni	0.87	1.9	1.8	1.9	1.71	2.2	2.1	2.2	1.9	1.9	2.7	nd
Cu	1.0	1.4	0.96	1.1	1.0	1.4	1.5	1.1	1.42	1.4	1.6	nd
Pb	1.2	1.6	1.5	1.4	1.4	1.6	1.4	1.4	1.4	1.6	1.7	nd

[1] Mean of triplicate analysis (Appendix II); [2] Mean of duplicate analysis (Appendix II); [3] Repeat analysis of random samples (Appendix II); [4] Multiple analysis; nd = not determined; BDL = below detection limit
* Theoretical TDS values; # Al concentration determined using the CAS method; ## Si determined using the heteropoly blue method; ** Data from borehole M1 and borehole T1 (From Table 2.1)

Table 4.4 (cont.) Laboratory analyses of Blesbokspruit waters

Variable	W13	W15	W14	W16	W17	W18	W19	W20	W21	W22	T1**
pH[1]	2.8	2.7	2.8	2.9	2.8	2.8	3.1	7.4	7.3	3.2	2.8
EC[1] (mS/cm)	3.73	4.38	3.16	4.75	3.30	3.30	1.66	0.33	0.23	1.26	3.55
TDS (mg/ℓ)	1580	2526	2215	3071	2225	2232	1070	230	180	360	5778
TDS* (mg/ℓ)	2387	2022	2803	3040	2112	2112	1062	211	147	806	nd
Acidity[2] (mM)	47	45	24	46	28	24	11	nd	nd	7.5	nd
Alkalinity[2] in mg $CaCO_3$/ℓ	nil	nil	nil	nil	nil	nil	nil	73.8	41.1	nil	nil
Eh (mV)	313	329	334	199	333	323	305	41	17	286	nd
Anions[3] (mg/ℓ)											
SO_4^{2-}	848	1587	1487	2242	1512	1510	716	45.8	22.9	128	3233
Cl^-	255	425	319	97.9	299	271	127	50.5	48.5	89.6	18.4
NO_3^-	17.4	BDL	BDL	BDL	BDL	BDL	BDL	10.5	1.9	1.8	6.4
F^-	0.08	0.04	1.4	0.06	1.5	2.1	1.7	0.1	0.08	1.2	nd
Total Elemental Concentrations (mg/ℓ) by ICP:[4]											
Na	153	266	228	73.4	188	199	111	23	18.2	56.4	47
K	4.4	8.9	6.7	10.8	5.9	7.4	4.3	3.3	1.9	4.5	nd
Ca	216	169	120	359	151	158	72.8	23.5	10.6	52.1	509
Mg	74.5	64.5	51	277	64.4	81.4	36.4	11.6	7.4	25.7	289
Fe	19.5	87.1	7.4	10.2	19.9	7.0	4.7	0.61	0.59	1.6	198
Al	329	233	137	240	161	152	60.3	0.33	0.27	39.6	32
Al#	306	226	133	232	161	153	51.3	BDL	BDL	34.9	nd
Mn	25	13.7	13.5	79.5	19.2	23.1	9.5	0.09	0.08	6.5	49
Si	67.2	64.8	39.4	39.4	39.8	36.8	17.1	0.75	2.67	13.0	nd
Si##	69.8	63.8	43.5	43.1	40.6	40.0	17.0	0.08	2.53	13.3	nd
Zn	4.0	4.3	2.2	10.4	2.7	2.8	1.4	0.4	0.4	1.1	nd
Ni	2.8	2.6	1.8	4.7	2.0	1.9	1.3	BDL	1.1	1.1	nd
Cu	1.4	1.5	1.0	1.1	1.1	1.0	1.0	0.94	0.95	0.97	nd
Pb	1.8	1.6	1.6	2.2	1.4	1.7	1.1	0.96	1.1	1.3	nd

4.3.1 pH

The pH values measured on site (Table 4.4; Appendix II, Table A II.1) compared well with the laboratory measurements. The pH of the catchment waters varies from pH 2.73 (sample W2) at the outwelling point to pH 3.17 (sample W22) downstream of the wetland (Figure 4.5). Most of the samples have a pH < 3.6 with the exception of the two natural water samples (W20 and W21). These two samples have pH values > 7 and reflect an AMD-free tributary of the Blesbokspruit. The very low pH values found throughout the rest of the catchment suggest a lack of neutralising capacity in the mine workings and the catchment. They also indicate the intensity of the acidic nature of the waters (Figure 4.5). Low pH results in the decomposition of silicate minerals and a subsequent increase in the concentration of metals (Al) associates with silicate minerals (Figure 4.6) (Karathanasis *et al.*, 1988).

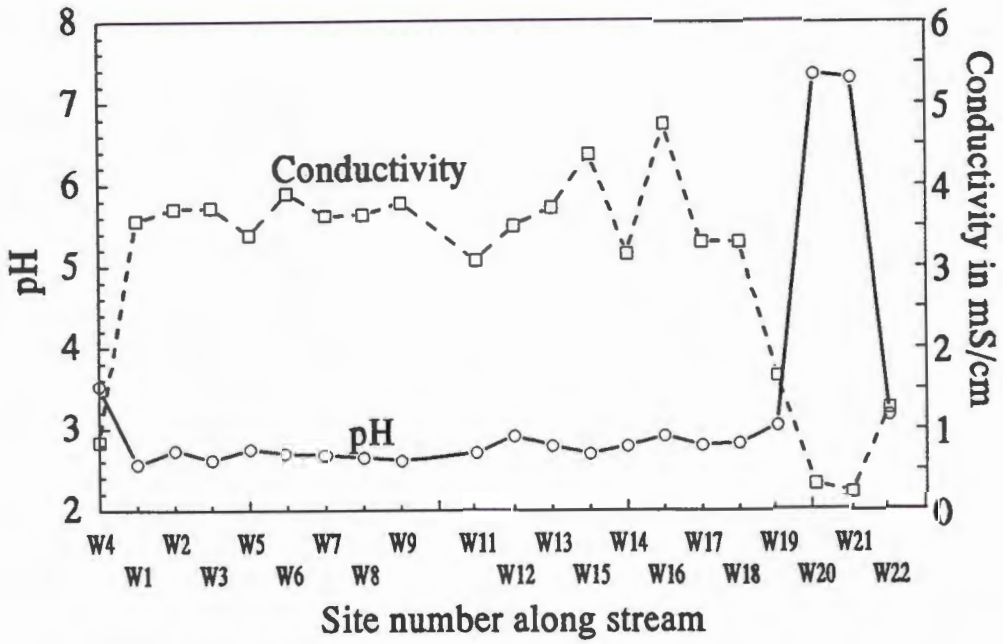

Figure 4.5 Conductivity and pH in the waters from the Blesbokspruit

4.3.2 Electrical conductivity (EC)

The field electrical conductivity of the water samples was similar to the values determined in the laboratory (Table A II.1 in Appendix I, Table 4.4). The EC values in the catchment vary from EC > 3 mS/cm, in all the samples with pH < 3, to EC < 1.5 mS/cm in samples with pH > 3 (Figure 4.5). Electrical conductivity of the

water provides an indication of dissolved salts and an approximate TDS can be calculated from the measured EC (McBride, 1994). Total dissolved salt values ranging from 1500 to 2500 mg/ℓ were calculated for the pH < 3 water samples and compared well with TDS values calculated by summing the dissolved constituents (Table 4.4). They indicate a slight brackish nature of these samples. Samples with pH > 3 had TDS values of 1000 mg/ℓ and less and could be defined as fresh waters (Drever, 1988).

4.3.3 Acidity

Pure water in equilibrium with atmospheric CO_2 has a pH of 5.66 at 25°C. Unpolluted rainwater has a pH of around 5.0 (Drever, 1988). The Blesbokspruit waters with pH < 4 can, therefore, be considered acidic (Table 4.4, Figure 4.6). The acidity of the Blesbokspruit water originates from the oxidation of pyrite with the release of acidity (H^+), dissolved ferrous iron and sulphate ions into the water (Table 4.4, Figure 4.7). The subsequent oxidation of the dissolved ferrous iron to ferric iron which then hydrolyses to form insoluble ferric hydroxide releases even more acidity to the catchment (Stumm and Morgan, 1970). The acidic waters enhance the dissolution of aluminosilicate minerals in the surrounding shale and soil (Karathanasis *et al.*, 1988; Drever, 1988; Nordstrom and Ball, 1986). High concentrations of aluminium correlate well with acidic waters (r^2 = 0.942) (Figure 4.6). The hydrolysis of Al(III) and Fe(III) in these waters contributes to the acidity (Drever, 1988; McBride, 1994).

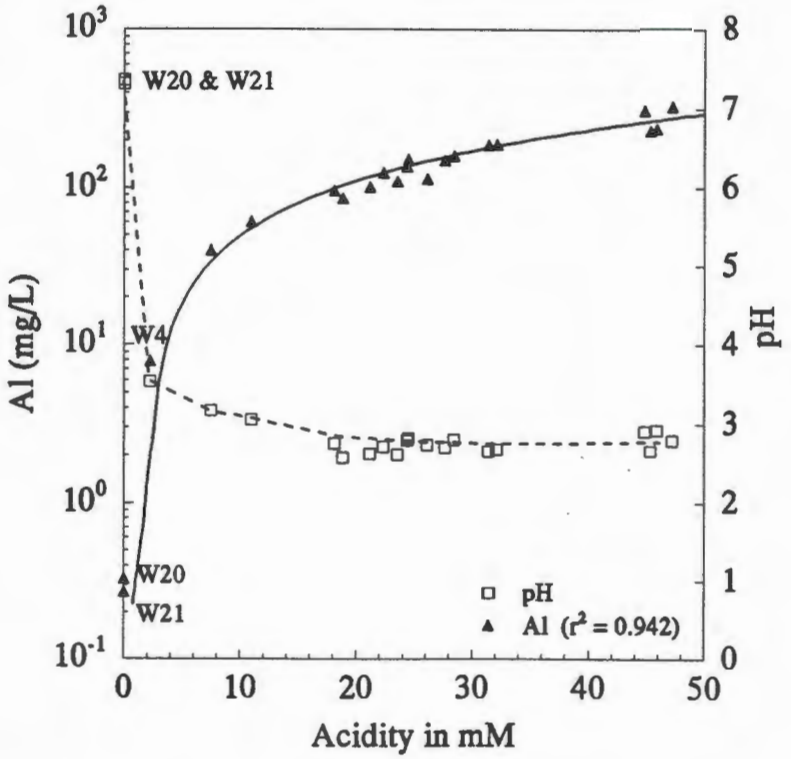

Figure 4.6 The relationship between acidity, dissolved Al and pH in the Blesbokspruit waters.

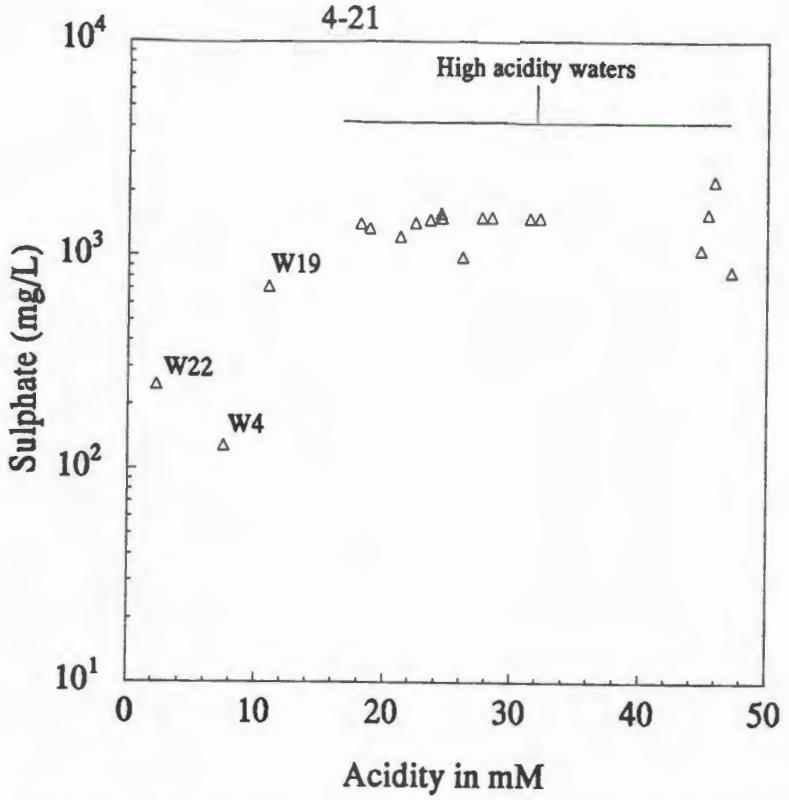

Figure 4.7 A plot of the relationship between acidity and sulphate in the Blesbokspruit waters.

4.3.4 Redox conditions in the Blesbokspruit

Water samples from the Blesbokspruit have Eh values > 100 mV with the exception of the two samples from the prison dam and prison stream and can therefore be classified as oxic (Table 4.4). The prison dam and prison stream samples can be described as suboxic (Table 4.4). Nordstrom and Munoz (1994), Garrels and Christ (1963), and Drever (1988) describe the Eh measurement in natural waters as a qualitative indication of the redox potential. The Eh measurements, therefore, indicate an oxidising environment in the analyzed waters.

4.3.5 Complexation of sulphate to iron or aluminium

Low pH waters with high sulphate content are known for their sulphate complex formation with aluminium (Yariv and Cross, 1979). Sulphate ion concentration in Al and Fe sulphate solutions was analyzed in an attempt to determine removal of sulphate ions due to complexation with Al and Fe. The concentration of SO_4^{2-} used in the preparation of the solutions was compared to the concentration of SO_4^{2-} determined by HPIC. The loss of SO_4^{2-} as the result of complexation to Al and Fe in samples with similar concentrations of SO_4^{2-} was found to be minimal (Figure 4.8). Sulphate and Cl^- concentrations determined by HPIC in the control solutions (Na_2SO_4 and NaCl) did not differ from the amount added (Figure 4.8). The removal of SO_4^{2-} in the AMD samples

due to complexation could be assumed to be minimal, and HPIC analysis of SO_4^{2-} was regarded as representative of the total concentration of SO_4^{2-} present in the Blesbokspruit waters.

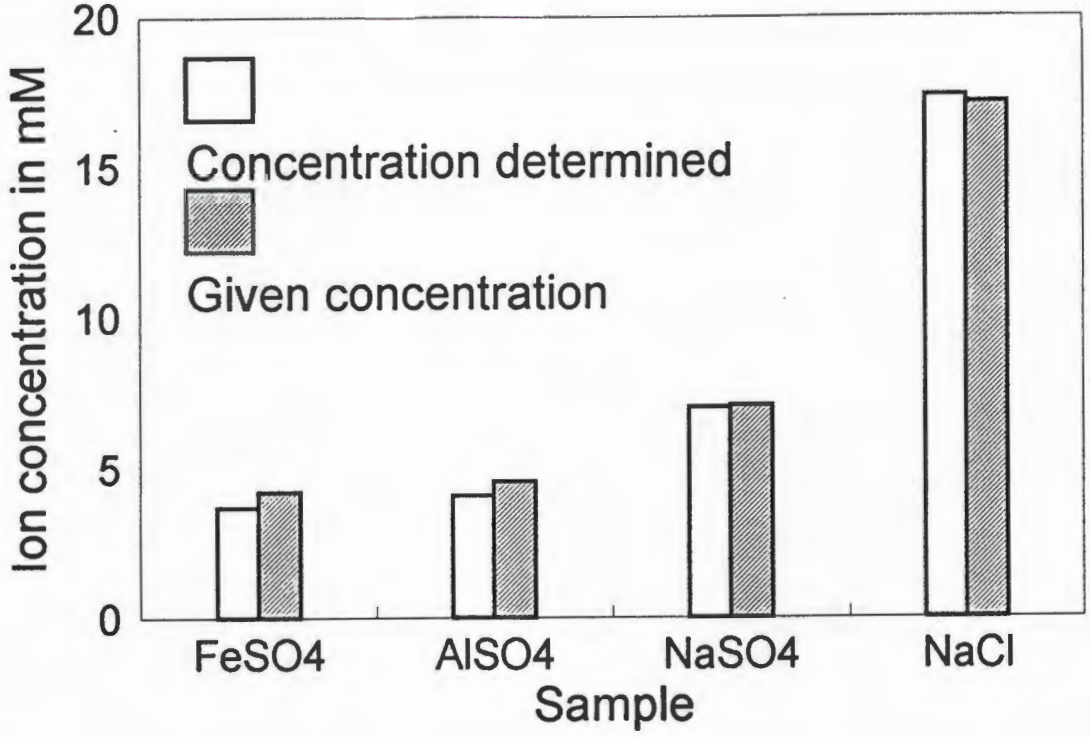

Figure 4.8 A comparison of added SO_4^{2-} and the SO_4^{2-} determined by HPIC. Control solutions (Na_2SO_4 and NaCl) were analyzed for their SO_4^{2-} and Cl^- concentrations.

4.3.6 Anion and elemental determination

The dominant anion present in the Blesbokspruit waters was SO_4^{2-} with concentrations between 128 - 2250 mg/ℓ while chloride ion concentrations were between 80- 580 mg/ℓ (Figure 4.9). Minor amounts of F^- (0.08 - 2.0 mg/ℓ) and NO_3^- (1.8 - 20 mg/ℓ) were detected (Table 4.4). Nitrate was found to be below the detection limit of the HPIC for most of the samples. Fluoride levels were determined with the fluoride electrode. The anion relationship of the AMD contaminated water in the Blesbokspruit catchment was $SO_4^{2-} > Cl^- > F^- > NO_3^-$. Anion concentrations in the waters from the prison dam and stream (W20, W21), with the exception of NO_3^- in the prison dam, are well within the target water quality range as proposed by the DWAF (Appendix VII, Table A VII.1). (DWAF, 1996).

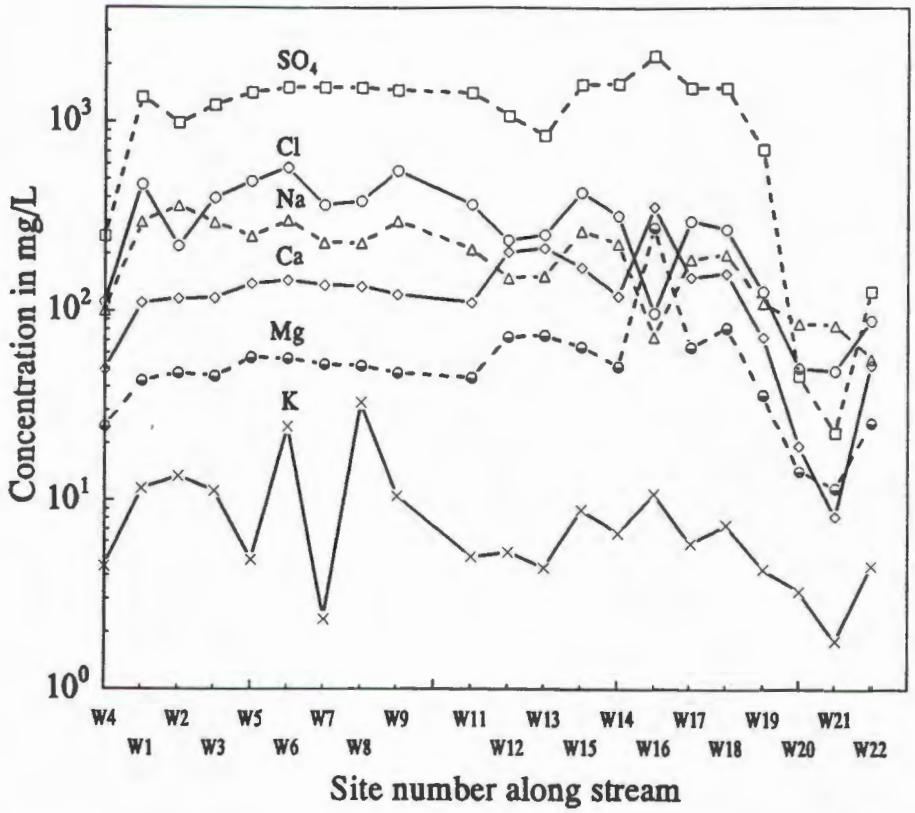

Figure 4.9 Concentrations of the dominant anions (SO_4^{2-} and Cl^-) and base metals in mg/ℓ in waters sampled along the Blesbokspruit.

The SO_4^{2-} and Cl^- values correspond well to the concentrations of these anions from the borehole and V-notch data (Tables 2.1 and 2.2). The high SO_4^{2-} (2242 mg/ℓ) and low Cl^- (98 mg/ℓ) concentrations from sample W16 are similar to the values found for these anions in the waters from V-notch 13 (2929 mg/ℓ SO_4^{2-} and 8 mg/ℓ Cl^-) and the boreholes T1 and T2 (T1: 3223 mg/ℓ; T2: 3840 mg/ℓ SO_4^{2-} and T1: 18.4 mg/ℓ; T2: 4.8 mg/ℓ Cl^-) from the Tavistock colliery. Water samples upstream of sampling point W16 compare well with water originating from the Middleburg Steam colliery, Station colliery and Witbank colliery (Table 2.1 and 2.2).

Sulphate is usually present at high concentrations in waters contaminated by AMD and low concentrations in normal stream waters (Nordstrom and Ball, 1986). Figure 4.7 demonstrates a rapid increase of SO_4^{2-} concentration from the "normal" stream waters (W4) to the waters in the seepage area. Once sulphate-rich AMD flows into the Blesbokspruit the concentration of sulphate in the stream stays either constant or is diluted by inflow from the prison stream (W22). Chemical processes that might remove SO_4^{2-} are negligible by comparison to dilution processes (Nordstrom and Ball, 1986).

The origin of Cl^- in these waters can be attributed to the leaching of Cl from the coal and to a lesser extent by Cl-rich groundwaters introduced during diagenesis (Bouska,

1981; Swaine, 1990).

Fluoride could originate from fluorapatite (Bouska, 1981) although phosphate concentrations in the Blesbokspruit waters were below detection limit. Alternatively F can leach from coal or associated clays (Swaine, 1990). The concentration F^- in the Blesbokspruit catchment fluctuates according to changes in the concentration Al in the waters (Figure 4.10). Low F^- concentrations appear at corresponding high concentrations of Al. The formation of AlF complexes would explain this variation in F^- concentration (Yariv and Cross, 1979). Fluoride concentrations in the waters from the study area, with the exception of water samples W12, W13, W16, W20 and W21, were exceeding the target water quality range proposed by the DWAF (DWAF, 1996) (Appendix VII). Water samples W12, W13 and W16 had the highest Al concentrations of the Blesbokspruit waters (Table 4.4) and the normal prison dam and stream water samples W20, W21 originated from surface runoff.

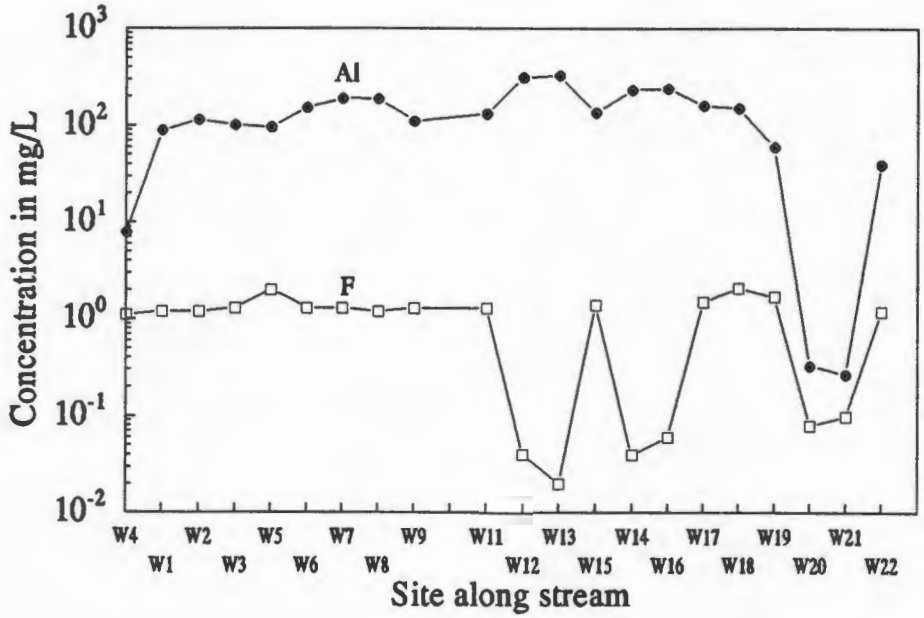

Figure 4.10 Changes in F^- concentration compared to changes in Al concentration in the Blesbokspruit catchment

Water samples were analyzed for total elemental content by ICP-AES. The results of the analysis are summarised in (Table 4.4). The dominant elements in the Blesbokspruit waters are (in descending order) Na, Ca, Al, Mg, Si, Fe, K, Mn, Zn, Ni, Pb, Cu. The concentrations of the base metals (Na, Ca, Mg, K) and major metals (Al, Fe, Mn, Zn) vary along the Blesbokspruit (Figure 4.9, Figure 4.11). The concentrations of the base metal and major metal elements correlate well with their associated borehole and V-notch concentrations (Table 2.1, Table 2.2). Iron is the only element which differs from this correlation.

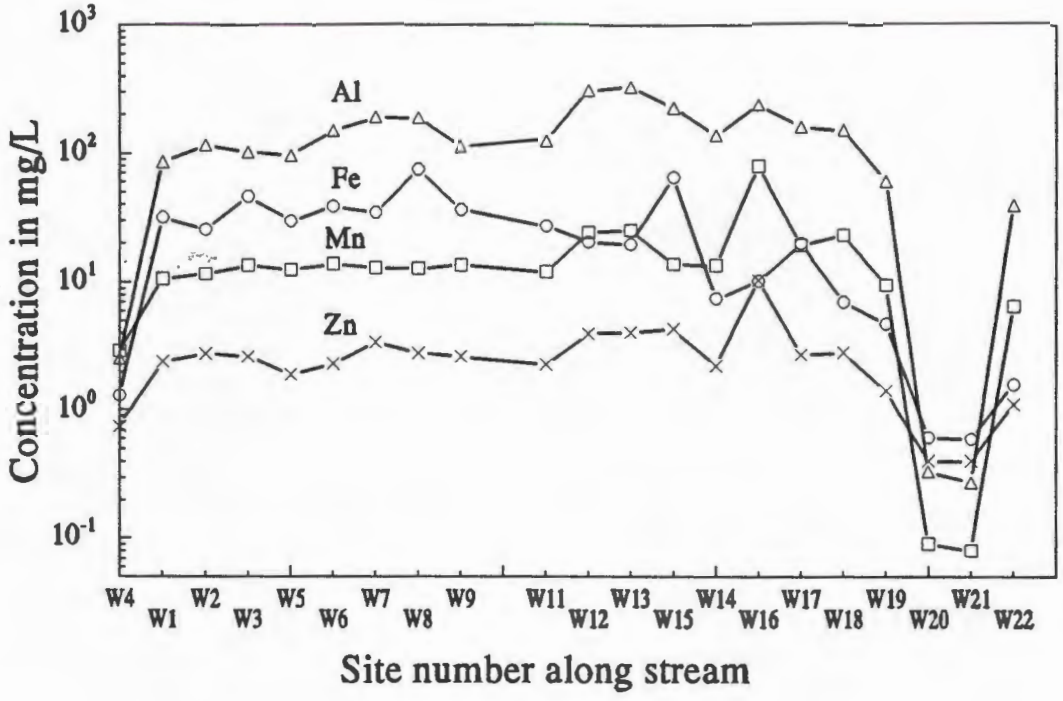

Figure 4.11 Changes in concentration of the major metal elements in the Blesbokspruit catchment

The base metal and major metal elemental concentrations in the prison dam and prison stream samples (W20, W21) are within the target water quality range proposed by the DWAF (DWAF, 1996) (Appendix VII). The low base metal and major metal elemental values for water sampled from the Blesbokspruit (W4) origin could be due to the lack of AMD inflow from the surrounding area. On contact with element-rich seepage from the outwelling point (W2) and numerous seepage (W1, W15) points along the stream the Blesbokspruit waters acquire high concentrations of elements typical of AMD (Figure 4.9 and Figure 4.11). A decrease in elemental concentration occurs as the Blesbokspruit flows through a small wetland (sample W19). Downstream of the wetland and the prison stream junction a further decrease in elemental concentrations occurs. The decrease can be attributed to precipitation, adsorption reactions in the wetland and dilution of waters leaving the wetland with waters from the prison stream.

Sodium and chloride concentrations with the exception of sample W2 (outwelling point), W20, W21 (prison dam and stream) correlate strongly (r^2 = 0.917), which suggest similar origins of these elements (Figure 4.12). Higher Cl^- values indicate the removal of dissolved Na from the waters by the precipitation of Na-jarosite. Both elements decrease in concentration in the AMD dam 7 (W16) on the east side of the stream, which indicates differences in Na and Cl concentrations in the different collieries. Calcium and Mg have similar concentration patterns in the Blesbokspruit waters. Their concentration,

however, increases in the farm dam sample supporting the suggestion of differences in geochemistry of the collieries located in and around the study area.

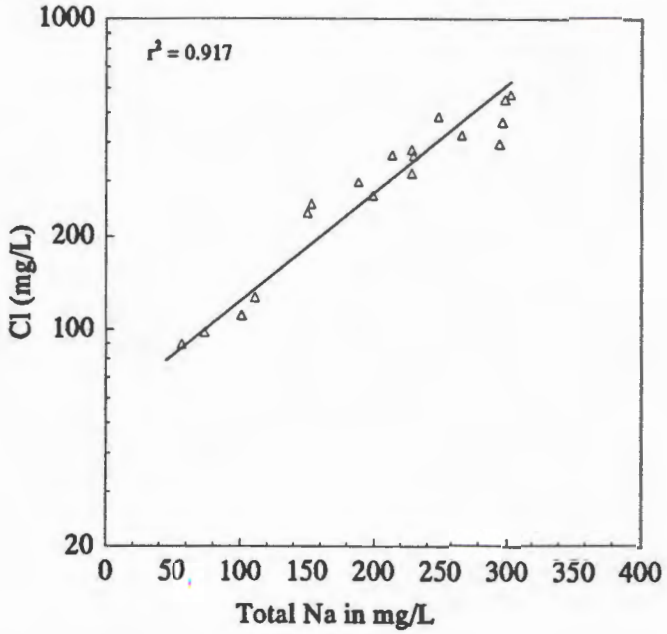

Figure 4.12 Comparison of total Na concentration with Cl^- concentration in the Blesbokspruit.

The oxidation of iron sulphide minerals leads to high concentrations of iron in the afflicted waters and to the subsequent formation of ochreous precipitates (Bigham, 1994; Bigham *et al.*, 1992; Winland *et al.*, 1991). Iron concentrations in the Blesbokspruit water were found to be much lower than the reported borehole iron concentrations (Table 4.4). The continuous precipitation of Fe in the sample bottles and during sample dilution and filtration could explain the low Fe concentrations in the samples.

The equilibrium of Fe is significantly modified in an acid sulphate system (Karathanasis *et al.*, 1988). Although goethite and amorphous $Fe(OH)_3$ control Fe levels in most natural aquatic systems (Stumm and Morgan, 1981) dissolved Fe in acid sulphate-rich solutions appears to be more consistent with the basic iron sulphate mineral jarosite (Karathanasis *et al.*, 1988). High Fe concentrations in samples W3 (V-notch 14), W8 (AMD dam) and W15 (AMD drainage ditch) are controlled by either dissolution of precipitates (W3, W8) or the inflow of fresh AMD from outwelling points (W15) (Figure 4.11). Precipitation, dilution and adsorption could result in the drop of Fe concentrations in sample W2 (outwelling point), W14 (stream), W19 (wetland), and W22 (downstream of wetland).

High concentrations of aluminium are typical in acid drainage seeping through soil and percolating through geological strata (Karathanasis *et al.*, 1988; Nordstrom and Ball, 1986; Nordstrom, 1982). The waters from the Blesbokspruit were found to have high

concentrations Al ranging from 80 - 240 mg/ℓ Al in the AMD afflicted parts of the catchment. The Al concentration range of the stream origin, and prison dam and stream varies from 0.59 - 8 mg/ℓ. Aluminium values in the water sampled downstream of the wetland had a concentration of 40 mg/ℓ (Table 4.4). All the water samples from the Blesbokspruit have Al concentrations above the target water quality range of 0 - 0.15 (DWAF, 1996) with the exception of the samples taken from the prison dam and stream. Although there is no evidence to show that dissolved Al is toxic to fauna or humans, it has a suffocating effect on fish and is toxic to roots and soil microbiota (Nordstrom, 1982; Drever, 1988). Consequently no fish were found in the AMD-contaminated Blesbokspruit waters and area between AMD dam 5 and 6 (W12 and W13) and the Blesbokspruit was devoid of plant growth with the exception of some eucalyptus trees.

Possible controls on Al chemistry of acid mine drainage are the leaching rate of Al from common aluminosilicate minerals in sulphuric acid solutions, and the solubility of basic Al-sulphate minerals known to exist under these conditions (Nordstrom and Ball, 1986). Kaolinite and gibbsite solubilities control the Al concentration in natural waters. However, the solubilities of gibbsite and kaolinite are dramatically altered under acidic conditions and in the presence of high concentrations of sulphate. Therefore, other less soluble minerals such as jurbanite, alunite and alunogen regulate the concentrations of Al in these acidic waters (Nordstrom, 1982; Karathanasis, 1988). The Si content of the Blesbokspruit waters correlates with the Al content of these waters (Figure 4.13), indicating a relationship between Si and Al which can originate from the presence of these elements in clay minerals. The increase in Al concentration from the Blesbokspruit origin (W4) to the AMD seepage area (W1, W2, W3) may be due to the dissolution of Al from aluminosilicate minerals (Figure 4.13) (Karathanasis *et al.*, 1988). Small decreases in Al concentration between the outwelling point and V-notch 14 are due to either precipitation reactions or adsorption on algae present in the seepage area (Figure 4.11). High aluminium concentrations were found in the stream and AMD dams with a two to four fold decrease in Al concentration in the wetland and after dilution with uncontaminated water from the prison stream (Figure 4.11).

High Mn concentrations were found in most of the water samples from the Blesbokspruit with exception of the prison dam and stream (Table 4.4, Figure 4.11). A maximum Mn concentration of 80 mg/ℓ was measured in AMD dam 7 (W16). All the water samples exceeded the target water quality range proposed for Mn (0 - 0.05 mg/ℓ) by the DWAF (Appendix VII) (DWAF, 1996). Zinc concentrations in the Blesbokspruit water samples W7, W12, W13, W15 and W16 were higher than the target water quality range for Zn (0 - 3 mg/ℓ) proposed by the DWAF (DWAF, 1996) (Appendix VII).(Table 4.4).

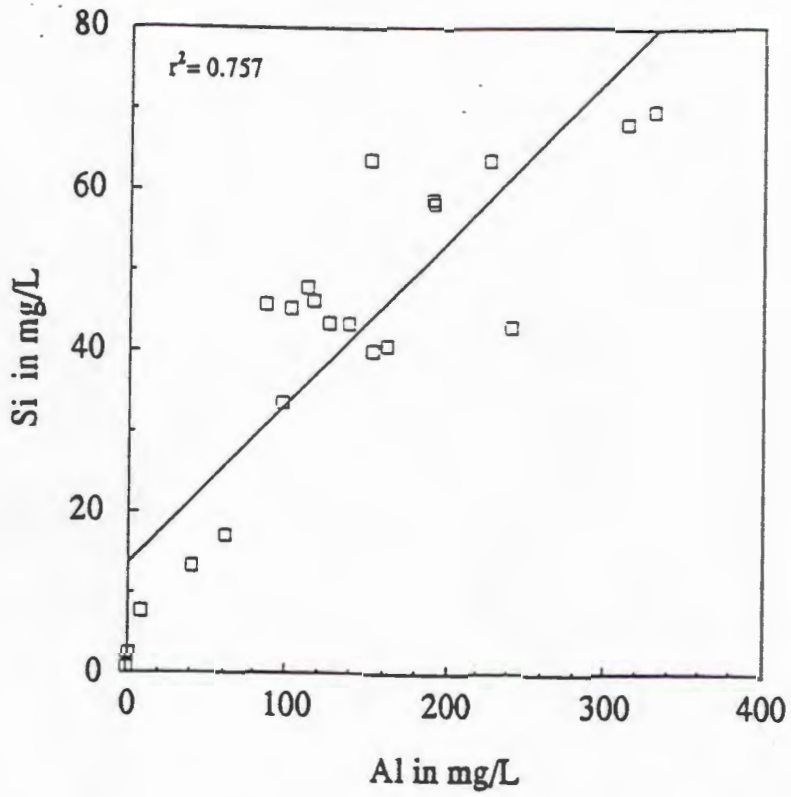

Figure 4.13 A plot of the Si concentrations in the Blesbokspruit waters as a function of the Al concentration of the waters.

Blesbokspruit waters contained toxic concentrations of Pb (0.9 – 2.2 mg/ℓ) which were much higher than the target water quality range concentrations of 0 - 10 µg Pb/ℓ proposed by the DWAF (Appendix VII) (DWAF, 1996). Krauskopf (1967) reported 20 ppm Pb in shales and Swaine (1990) reported a mean Pb value for South African, Australian and US coals of around 10 - 15 ppm. The dissolution of lead containing minerals such as galena (PbS) in the available oxidising environment suggests a possible origin for dissolved Pb in the Blesbokspruit catchment. Solubility diagrams of lead suggest that dissolved lead is present as Pb^{2+} in low pH (pH < 4) and positive Eh waters such as the Blesbokspruit catchment waters. The lower lead concentrations of the fresh waters (W20, W21) can be due to the higher pH of these waters and the presence of small concentrations of carbonate in the prison dam and stream (Stumm and Morgan, 1970). Lead concentrations remained high in water sampled downstream of the wetland (W22) (Appendix VIII). Förstner and Wittman (1979) reported toxicological tolerance levels of lead as 2g/kg for mammals and 0.33 - 200 mg/ℓ for fish. Liming or coagulation treatment processes can be used to remove lead from these waters (DWAF, 1996).

4.3.7 Charge balance

The anion-cation charge balance is a useful procedure for checking the quality of water sample analyses (Murray and Wade, 1996). Cation-anion charge balance results of the different Blesbokspruit water samples are presented in Table 4.4.

Table 4.5 Cation-anion charge balance results from the Blesbokspruit waters

Sample No.	Total anions meq/ℓ	Total cations meq/ℓ	Charge balance % difference
W4	9.10	10.2	5.50
W1	41.4	40.8	−0.70
W2	26.9	40.7	20.5
W3	36.9	37.1	0.30
W5	43.4	35.5	−10.0
W6	47.8	45.5	−2.40
W7	41.8	44.9	3.50
W8	42.4	47.5	5.70
W9	46.4	38.2	−9.60
W11	39.9	35.5	−6.00
W12	29.2	59.9	34.5
W13	25.2	62.0	42.1
W15	45.2	57.1	11.7
W14	40.1	36.7	−4.50
W16	49.6	75.1	20.4
W17	40.0	41.1	1.30
W18	39.3	41.9	3.20
W19	18.6	19.0	1.10
W20	2.50	3.20	12.3
W21	1.90	2.00	0.30
W22	5.30	12.2	39.8

Equation (A) and (B) were used to calculate the charge balance:

A

$$meq/L = \frac{mg/L\ cation}{molecular\ weight} \times ionic\ charge$$

B

$$\%\ difference = 100 \times \frac{\sum of\ cations - \sum of\ anions}{\sum of\ cations + \sum of\ anions}$$

Negative % difference values indicate an excess of anions in samples W1, W5, W6, W9, W11 and W14. According to Murray and Wade (1996) anion-cation differences of ±2 − 5% are considered acceptable for an anion range of 10 - 800 meq/ℓ. The data obtained for samples W4, W1, W3, W6, W7, W8, W14, W17, W18, W19 and W21 have an anion-cation charge difference of ≤ 5% and can, therefore, be considered to represent good quality data in terms of the charge balance criterion (Murray and Wade, 1996). Although the anion-cation charge balance of samples W2, W5, W9, W11, W12, W13, W15, W16, W20 and W21 is well outside the acceptable limits, the difference may be due to the fact that negatively-charged dissolved organic carbon was not measured in these waters. Another factor may be the hydrolysis of metal ions and the presence of high concentrations of sulphate that can affect the ionic strength of the solution and the species distribution (Murray and Wade, 1996).

4.3.8 Chemical speciation of the Blesbokspruit waters

Blesbokspruit waters were chemically speciated by dividing them into five subgroups: 1) Seepage area waters; 2) AMD dams W5, W6, W7, W8 and associated drainage ditch W9 waters; 3) AMD dams W12, W13, W16 and associated AMD ditch W15; 4) AMD contaminated stream waters; and 5) Fresh waters from the prison dam and stream. The reasons for separation were the different localities at which the water was sampled. The difference in the localities was determined by: 1) AMD seepage and origin (subgroup 1); 2) AMD retention and origin (subgroups 2 and 3); 3) AMD contaminated stream waters with multiple sources of contamination (subgroup 4); and 4) uncontaminated waters (subgroup 5).

If a natural water is at saturation equilibrium, then the ion activity product (IAP) calculated from the water sample should be the same as the solubility product constant (K_{sp}). The logarithm of this ratio is called the saturation index (SI) (Nordstrom and Munoz, 1994). A negative saturation index implies that the waters are undersaturated with respect to a mineral phase and the mineral should, therefore, be expected to remain in solution. Supersaturated samples have a positive saturation index where a mineral phase is expected to precipitate out of solutions. Saturation indices of approximately zero imply that the water is in equilibrium with a particular mineral phase which should, therefore, neither precipitate nor dissolve (Ure and Davidson, 1995; Nordstrom and Munoz, 1994).

The saturation indices calculated for seepage area samples (W1, W2, W3) are presented

in Table 4.6. The results of MINTEQA2 modelling indicate that the seepage area water samples are supersaturated with respect to nontronite, jarosite, goethite and quartz. The seepage area waters are undersaturated with respect to alunite, gypsum and ferrihydrite and in equilibrium with cupricferite. Sample W2 was supersaturated with respect to manganite.

Table 4.6 The saturation indices calculated for the seepage area samples using the MINTEQA2 modelling program.

Mineral name	Chemical formula	Saturation index		
		W1	W2	W3
GYPSUM	$CaSO_4.2H_2O$	-0.61	-0.62	-0.55
QUARTZ	SIO_2	1.1	1.0	1.2
JURBANITE	$AlOHSO_4$	-0.18	0.060	-0.036
ALUNITE	$(K,Na)Al_3(SO_4)_2(0H)_6$	-2.2	-0.89	-1.6
NA-NONTRONITE	$(Fe,Al)Si_2O_5(OH).nH_2O$	11	11	11
JAROSITE NA	$NaFe_3(SO_4)_2(OH)_6$	6.2	5.0	4.5
JAROSITE K	$KFe_3(SO_4)_2(OH)_6$	8.3	7.1	6.7
JAROSITE H	$HFe_3(SO_4)_2(OH)_6$	5.9	4.6	3.9
FERRIHYDRITE	$5Fe_2O_3.9H_2O$	-1.4	-1.6	-1.7
GOETHITE	α-FeO(OH)	2.6	2.4	2.1
MANGANITE	MnO(OH)	---*	4.0	---*
CUPRICFERITE		0.10	-0.074	-1.2

* The mineral manganite was not specified by MINTEQA2 in samples W1 and W3

MINTEQA2 saturation indices for the first 4 AMD dams and the associated AMD ditch are summarized in Table 4.7. The AMD dam waters are undersaturated with respect to anglesite, gypsum, alunite and cupricferite. Jarosite, quartz, goethite, nontronite are supersaturated in these solutions and the saturation index of jurbanite indicates waters in equilibrium with jurbanite. Saturation indices in the water samples from the remaining AMD dams and the Blesbokspruit stream show similar saturation indices as discussed for the other waters (Tables 4.8 and 4.9). Fresh water samples were undersaturated with respect to gypsum, quartz, jurbanite, jarosite H and anglesite and supersaturated or in equilibrium with respect to the remaining minerals (Table 4.9).

Table 4.7 Mineral saturation indices in water samples taken from AMD ponds (W5, W6, W7, W8) and the associated AMD drainage ditch (W9).

Mineral name	Saturation index				
	W5	W6	W7	W8	W9
GYPSUM	-0.44	-0.46	-0.49	-0.52	-0.52
QUARTZ	0.96	1.2	1.2	1.2	0.99
JURBANITE	0.075	0.19	0.27	0.22	-0.034
ALUNITE	-1.4	-0.45	-1.3	-0.35	-1.8
NA-NONTRONITE	10	11	11	12	10
JAROSITE NA	4.8	4.9	4.5	5.4	4.7
JAROSITE K	6.6	7.4	6.1	8.1	6.7
JAROSITE H	4.3	4.5	4.2	5.2	4.6
GOETHITE	2.3	2.3	2.2	2.5	2.1
CUPRICFERITE	-0.45	-0.38	-0.64	-0.23	-0.84
ANGLESITE	-0.38	-0.36	-0.38	-0.41	-0.43

Table 4.8 Mineral saturation indexes in water samples taken from the stream.

Mineral name	Chemical formula	Saturation index						
		W4	W11	W14	W17	W18	W19	W22
GYPSUM		-1.1	-0.56	-0.50	-0.40	-0.38	-0.80	-1.5
QUARTZ		0.41	0.97	1.0	1.1	1.1	0.72	0.61
JURBANITE		-0.33	0.15	0.27	0.36	O.36	0.19	-0.25
ALUNITE		0.25	-1.3	-0.55	-0.24	-0.078	0.060	-0.16
NA-NONTRONITE		11	10	10	11	10	10	10
JAROSITE NA		3.6	4.8	3.3	4.1	2.8	3.8	2.1
JAROSITE K		5.9	6.6	5.2	6.2	5.0	5.9	4.6
JAROSITE H		2.5	4.7	2.9	3.5	2.1	3.2	1.7
GOETHITE		3.1	2.3	1.8	2.1	1.7	2.5	2.6
CUPRICFERITE		2.8	-0.16	-1.2	-0.73	-1.6	0.57	1.1
ANGLESITE	$PbSO_4$	-0.56	-0.37	-0.32	-0.34	-0.24	-0.50	-0.87

Table 4.9 Mineral saturation indexes in water samples taken from AMD ponds (W12; W13; W16), the associated AMD drainage ditch (W15) and samples from the prison dam and river (W20; 21).

Mineral name	Chemical formula	Saturation index W12	W13	W15	W16	W20	W21
GYPSUM		-0.54	-0.62	-0.47	-0.034	-2.1	-2.7
QUARTZ		1.2	1.3	1.2	1.1	-0.69	-0.13
JURBANITE		0.53	0.35	0.28	0.59	-3.9	-4.2
ALUNITE		0.76	-0.096	-0.71	1.0	1.4	0.49
NA-NONTRONITE		13	12	12	11	17	19
PYROPHYLLITE	$Al_2Si_4O_{10}(OH)_2$	1.3	0.73	-0.59	-0.050	4.0	6.1
JAROSITE NA		5.1	4.2	5.9	3.4	2.1	1.6
JAROSITE K		7.1	6.2	7.9	6.2	4.3	3.4
JAROSITE H		4.8	3.9	5.6	3.1	-2.5	-3.0
GOETHITE		2.8	2.5	2.6	2.1	6.9	6.9
CUPRICFERITE		1.2	0.21	0.30	-0.52	17	17
ANGLESITE		-0.46	-0.52	-0.41	-0.14	-1.3	-1.5
		Saturated and supersaturated minerals in natural water samples W20 and W21					
DIASPORE	AlO(OH)					3.3	1.4
GIBBSITE (C)	$Al(OH)_3$					1.5	1.4
HALLOYSITE	$Al_2Si_2O_5(OH)_4.2H_2O$					1.9	2.8
KAOLINITE	$Al_2Si_2O_5(OH)_4$					5.3	6.2
LEONHARDITE	$CaAl_2Si_4O_{12}.4H_2O$					7.9	11
MUSCOVITE	$KAl_2Si_3AlO_{10}(OH)_2$					6.6	7.7
MONTMORILLONITE	$M^+_{x+y}(Al_{2-x}Mg_x)(Si_{4-y}Al_y)O_{10}(OH)_2$					4.7	6.6
FERRIHYDRITE	$5Fe_2O_3.9H_2O$					3.0	2.9
TENORITE	CuO					0.64	0.63
ZINK SILICATE	$ZnSiO_3$					0.84	1.3
LEAD HYDROXIDE	$Pb(OH)_2$ (C)					0.43	0.43
NICKEL HYDROXIDE	$Ni(OH)_2$					—*	0.037

* The mineral nickel hydroxide was not specified by MINTEQA2 in sample W20

Saturation indices of selected minerals were plotted as a function of pH to investigate the effects of dissolution or precipitation of minerals on the concentrations of metals in the Blesbokspruit waters (Figure 4.14).

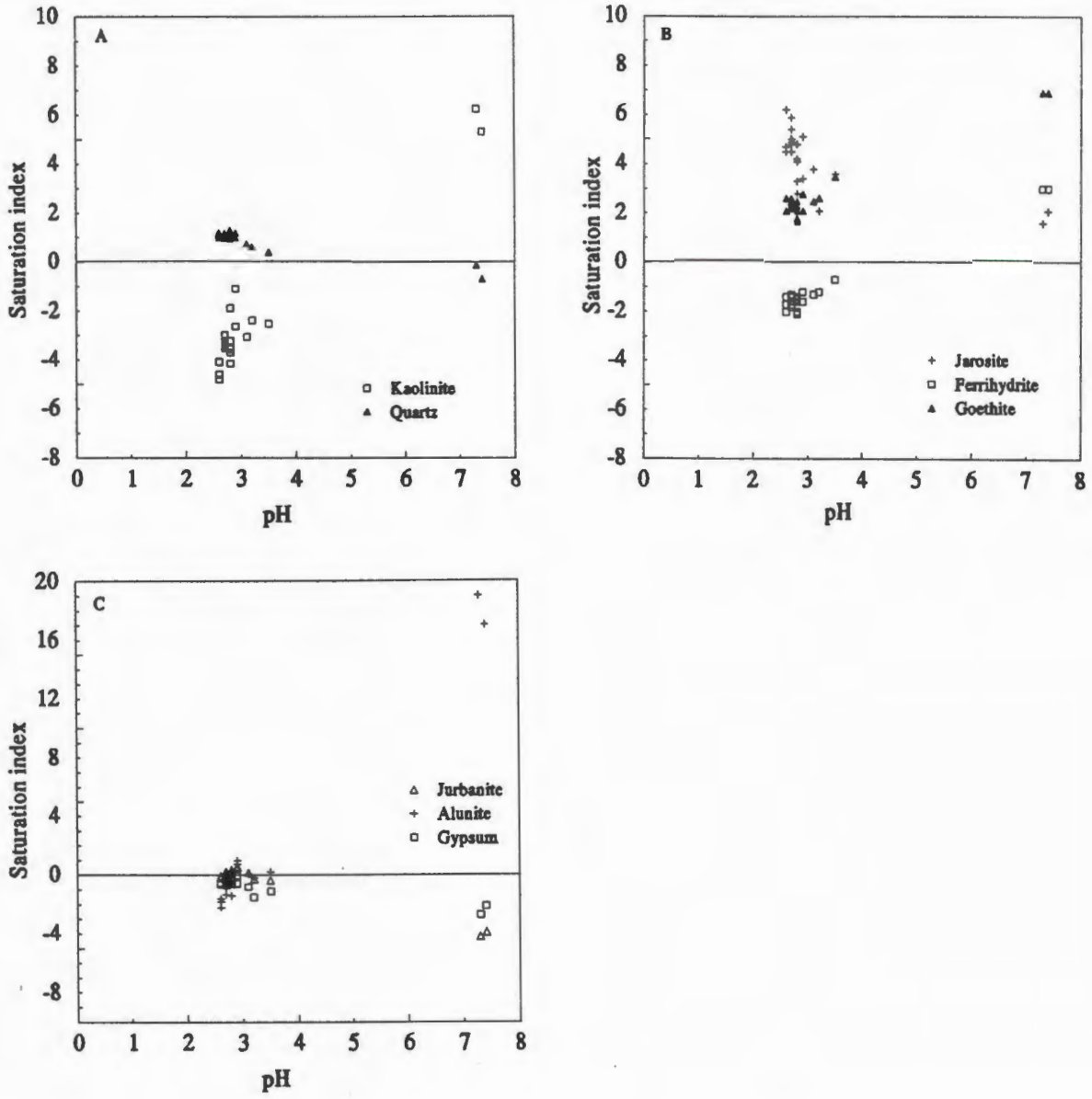

Figure 4.14 (A) The saturation index calculated for kaolinite and quartz in the Blesbokspruit waters; (B) The saturation index calculated for ferrihydrite, goethite and jarosite in the Blesbokspruit waters. (C) The saturation index calculated for gypsum, alunite and jurbanite in the Blesbokspruit waters. The saturation indices were plotted as a function of pH in all three plots.

Low pH waters are undersaturated with respect to kaolinite and saturated with respect to quartz (Figure 4.14 A). High concentrations of silica and aluminium correspond to low pH sites where kaolinite is undersaturated. Most samples at pH < 3 appear to be supersaturated with respect to jarosite and goethite and undersaturated with respect to ferrihydrite (Figure 4.14 B). Gypsum, alunite and jurbanite are at equilibrium or slightly undersaturated at low pH in most samples from the Blesbokspruit (Figure 4.14 C). Waters with pH > 7 (W20, W21) are undersaturated with respect to gypsum and jurbanite and supersaturated with respect to kaolinite, jarosite, ferrihydrite, goethite and alunite (Figure 4.14). The AMD retention dam, AMD drainage ditch and the Blesbokspruit stream water samples are slightly undersaturated with respect to anglesite ($PbSO_4$) indicating that lead remains in solution in these waters. The presence of hydrous ferric oxides (goethite) suggests that lead could be adsorbed by these minerals. The low pH of the Blesbokspruit waters would, however, counteract Pb adsorption to hydrous ferric oxides and result in high remaining Pb concentrations in these waters (Schwertmann and Taylor, 1989).

4.4 Conclusions

Sulphide ores exposed to the atmosphere and a fluctuating water table in abandoned coal mines release large quantities of sulphuric acid and elements such as Na, Ca, Mg, Al and Fe. An understanding of the distribution of these elements in the upper Blesbokspruit is essential to assess the potential impact of the contaminated waters on the Blesbokspruit and the rivers downstream of the study area.

The analysis of 21 water samples from the upper Blesbokspruit indicates a wide range in element composition and concentration. The waters are highly enriched with sulphate, chloride, aluminium, sodium, calcium, magnesium, iron, manganese and lead with the exception of waters sampled from a uncontaminated tributary. The water of the upper Blesbokspruit would be unsuitable for domestic, agricultural and recreational use. Changes in the concentration of the mentioned elements occur throughout the Blesbokspruit. The most significant of these changes appears in the waters associated with the small wetland through which the spruit flows. The general decrease in element concentrations in the wetland water can be attributed to element retention reactions involving adsorption, precipitation and coprecipitation. Dilution of the waters exiting the wetland by uncontaminated waters from a downstream tributary, further decreases the elemental concentrations of the Blesbokspruit.

All elements, with the exception of Al in the sample downstream of the wetland (W22), have similar concentrations to the waters sampled at the origin of the Blesbokspruit (W4). Lead

concentrations in the Blesbokspruit remained high and pose a possible health risk to users of this waters.

Speciation of the water from the Blesbokspruit indicates the precipitation of jarosite and goethite as possible removal mechanisms of iron from these waters. The solubility of basic aluminium sulphate minerals under acidic conditions explains the high aluminium concentrations in low pH water downstream of the wetland. Aluminium concentrations are sufficiently high to inhibit fish survival in the lower part of the Blesbokspruit and the downstream river environment.

The water analysis data from the Blesbokspruit suggests that metal mobility increases with an increase in acidity and is attenuated by precipitation and on contact with organic matter in the downstream wetland or as a result of dilution with uncontaminated water.

Chapter 5

CHEMICAL AND PHYSICAL ANALYSIS OF SEDIMENTS IN CONTACT WITH ACID MINE DRAINAGE

5.1 Introduction

High concentrations of metals (Al, Fe) are typical in acid drainage running off or percolating through soil or geological strata of collapsed subsurface coal mines (DWAF, 1995). It is also known that metal concentrations decrease downstream from the pollution source as is the case in the Blesbokspruit catchment (Chapter 3) (Förstner and Wittmann, 1979; Chapman *et al.*, 1983). Various physical and chemical processes may contribute to this attenuation. These include dilution, dispersion, precipitation-sedimentation-concretion, and adsorption-ion exchange on to stationary bed sediments and sedimenting suspended particulates (Förstner and Wittmann, 1979; Karlsson *et al.*, 1987; Chapman *et al.*, 1983). Under conditions where a constant release of effluent prevails a steady state will ultimately be reached. This, however, is not the case in most acidic waters including the Blesbokspruit catchment (Chapman *et al.*, 1983). Deviations from the idealized steady state in the Witbank area do occur due to fluctuations in climate and anthropological inputs (DWAF, 1995). These factors have to be kept in mind when analyzing sediment in contact with AMD. Other problems include the identification of all inputs of AMD and water into the Blesbokspruit. These problems are exacerbated in this highly disturbed area where numerous seepage sites exist (DWAF, 1995; Bullock *et al.*, 1996).

A large number of elemental and trace metal concentrations in solution are controlled by adsorption to solid phases in natural systems. Biogenic particles and Fe/Mn hydrous oxides play an important role in these processes (Johnson, 1986; Millward and Moore, 1982; Förstner and Wittmann, 1979). Data from numerous studies indicate the difficulty of assigning individual adsorption processes to particulate components in complex systems in which clays, hydrous oxides and organic material, either as particles or coatings may, compete as substrates for metal adsorption (Karlsson *et al.*, 1988; Johnson, 1986; Förstner and Wittmann, 1979).

In this chapter the sediments from the Blesbokspruit have been sampled and the results of the analyses were used to obtain an understanding of processes which are responsible

for metal ion attenuation in the stream.

The objectives of the sediment analyses were the following:

1) To determine the minerals and metals present in the sediments.

2) To compare sediment characteristics with metal concentrations in the sediment and overlaying AMD.

5.2 Materials and Methods

5.2.1 Sampling

Eleven sediment samples were collected from the Blesbokspruit catchment and associated AMD ponds. The localities of the samples are shown in Figure 5.1. Samples were taken using a hand held corer which consisted of a 400 mm long PVC pipe of 60 mm diameter. The core was pushed into the sediment by hand using a core handle. A slight rotational movement was then used to remove the core from the sediment, when it was immediately capped at both ends. The cores were maintained in an upright position where possible. They were then transported to Cape Town (two weeks) and frozen in a -20°C freezer. Frozen cores were later opened for analysis.

5.2.2 Sediment analysis

Sediment cores were inspected for the presence of stratification in the freshly opened specimens. Where possible, sediments were separated into their respective horizons and stored for further analysis in tightly capped plastic jars. Some sediments had no visible stratification, in which case the upper 5 cm were separated from the rest of the core and designated as the top horizon. Sediment sub-samples were air-dried, gently crushed to pass a 2 mm plastic sieve and stored in plastic bags. Material permitting, analysis of the sediments was done either on the top horizons, or on a 1:1 mixture of the top and middle horizons. Due to time constraints 5 of the 11 sediment samples (S2, S7, S14, S19, S22) were selected for detailed analysis.

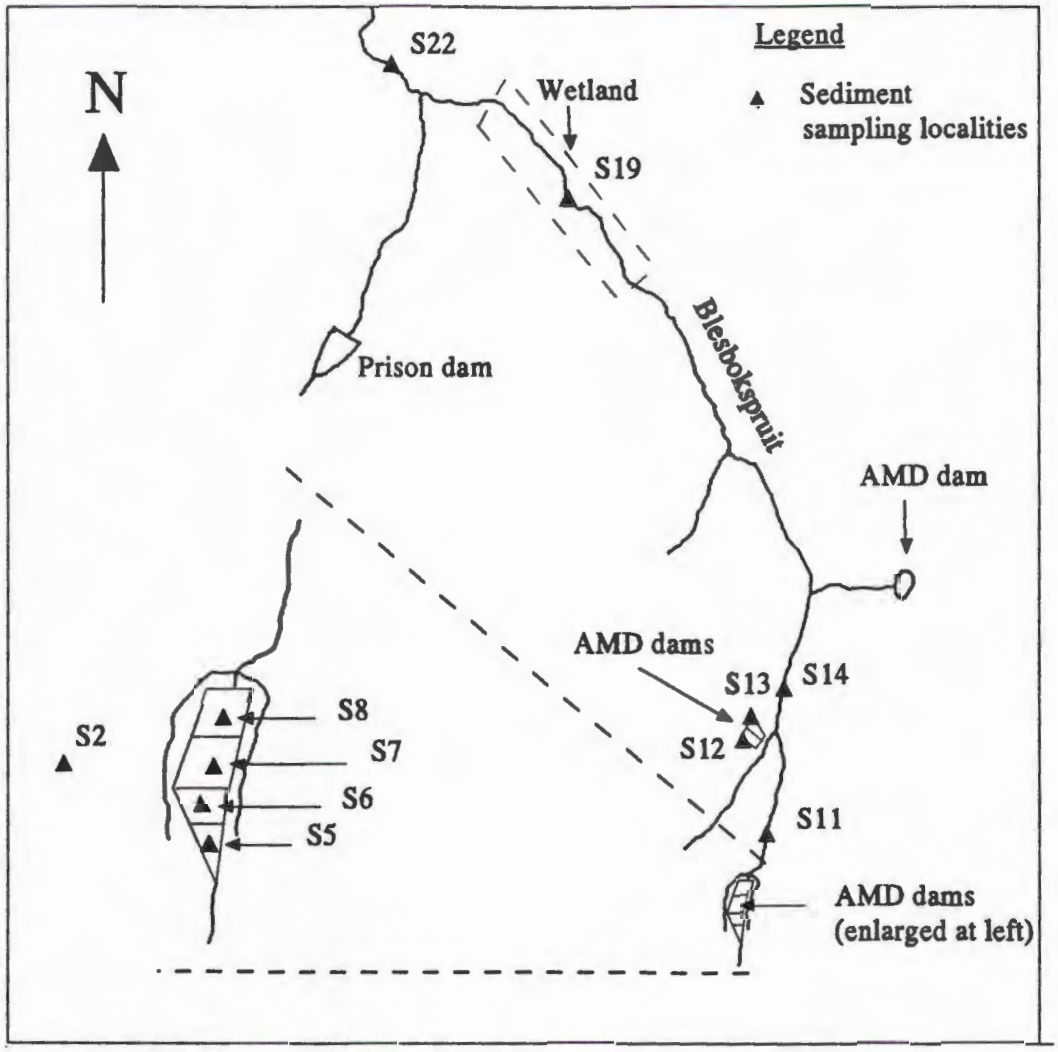

Figure 5.1 Sediment sampling locations in the Blesbokspruit catchment.

5.2.2.1 Sediment pH (H_2O and $CaCl_2$)

Sediment pH was determined in H_2O and $CaCl_2$. The different sediment fractions were mixed, in a 1:25 ratio, with either distilled water or (0.01 M) $CaCl_2$ solution. The pH of the settled solution was then measured using a Crison micro pH 2001 pH meter. The pH meter was calibrated against CIBA Corning standard solutions of pH 4 and pH 7 (Appendix III, Table A III.1).

5.2.2.2 Particle size distribution

Particle size analysis gives an indication of the surface area of sediments in contact with AMD. The percentage sand, silt and clay was thus determined for 5 sediment samples (top horizon only). The hydrometer method as described in Methods of Soil Analysis (1986) was used. This method allows for nondestructive sampling of suspensions undergoing settling. Multiple measurements on the same suspension can be performed to obtain detailed particle-size distributions. This analysis was performed by the South African Institute of Soil Science in Pretoria (RSA) (Gee and Bauder, 1986).

5.2.2.3 Organic carbon

Carbon is the major element in soil organic matter. Organic carbon determinations are therefore often used as the basis of organic matter estimates. The Walkley Black (dichromate oxidation) method was used to determine the organic carbon in the top horizons of all sediment samples. The method is simple and rapid, but the results are of a more semi quantitative nature because of possible interference by Fe(II) and Cl. Each sample as well as a blank were analyzed in duplicate (Appendix III, Table A III.2) (Nelson and Sommers, 1982).

5.2.2.4 Exchangeable acidity

Exchangeable acidity in 5 selected AMD sediments was determined using an automated potentiometric titration rather than the manual KCl method as described in Methods of Soil Analysis (Part 2). The automated method involved mixing the sediment fraction (2.5 g) in a 1:10 ratio with (1M) KCl. The solution was agitated for 30 minutes using an electric shaker and then filtered through Whatman (No.1) filter paper. The filtrate was titrated to an endpoint of pH 8.3 using (0.01 M) Titrasol NaOH and a Radiometer DTS multi-titrator system. Instrument calibration was ensured prior to measurements with a 0.005 M HCl (Titrasol) solution. Blank measurements (in mM) of the KCl solution were subtracted from the measured values (in mM). All determinations were done in duplicate and results were automatically obtained in mM and recalculated to mmol acidity/kg sediment quantities.

5.2.2.5 Exchangeable cation concentrations

The concentrations of exchangeable cations (Na^+, K^+, Ca^{2+}, Mg^{2+}, Fe^{3+}, Al^{3+}) were determined using 0.1 M $BaCl_2$ as a replacement ion for the native ions adsorbed to the sediment. In this method the sediments were saturated with 0.1M $BaCl_2$ and the supernatant collected and

analyzed for exchangeable cations. A Spectra Varian AA-30 flame atomic absorbtion spectrometer in the Department of Chemical Engineering at UCT was used for the analyses. Samples were diluted as deemed necessary by the spectroscopist. Hidden standards of 10, 50 and 100 ppm Fe^{3+} and Al^{3+} and 50, 10 and 2 ppm Ca^{2+} were incorporated into the analysis. Measured AAS cation values were recalculated from ppm to mmol$_c$/100 soil. The following equations was used (Thomas,1982):

$$meqM^{+} \; per \; 100g = \frac{100}{W} \times \frac{V}{1000} \times meqM^{+} \; per \; litre$$

W = soil weight
V = extract volume

5.2.2.6 Cation exchange capacity

Cation exchange capacity (CEC) is a measure of the quantity of readily exchangeable cations neutralizing negative charge in the sediments. The measurement of ion exchange capacity often involves the replacement of native, readily exchangeable ions by an "index" cation or anion whose surface excess is then determined (Sposito, 1989). For acid soils and soils bearing trivalent, readily exchangeable cations, Ba^{2+} is the index cation of choice (Sposito, 1989).The CEC of 5 selected sediments was determined using the CEC method of Gillman as described in Methods of Soil Analysis (Rhoades, 1982). Two grams of samples S19, S22, and S2 as well as 1:1 (top : middle horizons) mixtures of samples S14 and S7 were used in the experiment. The supernatant of the initial saturation solution step was retained for AAS analyses of the different displaced cationic species. The CEC of each sample was done in duplicate. The oven dry weight of each sample was determined by drying air dry samples for 72 h at 95°C. The final CEC calculation was done after AAS determination of the concentration of Mg^{2+} in the final supernatant (Rhoades, 1982):

$$CEC \; (meq/100g) = 100 \frac{(0.1 - C_1 V_3)}{W}$$

C_1 = concentration Mg in supernatant (meq/ml); V_3 = volume of added $MgSO_4$ (ml)
W = mass of oven dried sediment (g)

5.2.2.7. Clay mineralogy

The clay mineralogy of the sediment samples gives an indication of the clay types in contact with AMD. This could generate information on metal leaching from clay minerals and metal ion adsorption to clays.

The whole sample from 5 selected samples was pretreated with hydrogen peroxide to remove organic matter (Kunze and Dixon, 1986).

The clay fraction was isolated from the selected samples by dispersing the samples in a dilute (pH 10.00) Na_2CO_3 solution. The supernatant of this mixture was repeatedly collected after settling of the > 2 μm fraction. The clay collected in this way was then flocculated after adjustment of the supernatant to pH 7 and addition of NaCl. Flocculated clay was subsequently dialysed against distilled water for 48 hours to remove excess electrolyte. A 2 cm aliquot of the dialysed suspension was pipetted onto a glass slide to allow clay particles to settle out. This resulted in a preferred orientation of the clay particulates on the slide after drying at room temperature. The clay mineralogy of each sample was then determined by scanning the slides using a Philips PW 1390 X-ray diffractometer fitted with a LiF monochromator, scintillation detector and pulse height detector. A copper tube (CuKα = 1.542 Å) operating at 40 kV and 25 mA was used for the analysis. The samples were scanned through a range of 4 - 80^{0}2θ, with a step size of 0.1^{0}2θ and a counting time of 1 second / step.

5.2.2.8 XRD analysis of sediment

Dried sediments were crushed for 2 min in a carbon steel mill to - 300 mesh using a Siebtechnik swingmill. Sediment powder was then ground with an agate pestle and mortar to ensure uniform particle size. The powder was pressed into an XRD powder frame lying face down on a sheet of paper. This ensured a uniform orientation of the particles in the side of the frame presented to the X-rays. The mineralogy of each sample was determined by scanning the slides mounts a Philips PW 1390 X-ray diffractometer fitted with a graphite monochromator, scintillation detector and pulse hight detector. A cobalt tube (Co Kα = 1.790 Å) operating at 40 kV and 25 mA was used for the analysis. The samples were scanned through a range of 4 - 80^{0}2θ, with a step size of 0.1^{0}2θ and a counting time of 1 second / step.

5.2.2.9 XRFS elemental analysis

The 11 sampled sediments (top horizon) were analyzed for major and trace elements using a Philips X' Unique II (1480/00/10) X-ray spectrometer. Powder briquettes were prepared by taking 6 g oven dried sediment (- 300 mesh) and mixing with one drop Mowiol binding reagent (2% Hoechst Mowiol N 70 - 80 in distilled water) per 1 gram of powder. Boric acid was used as backing material and the powder was pressed at approximately 10 tons pressure into 30 mm diameter powder briquettes. Two grams of wax binder (Hoechst wax C) were used per 8 gram of powder in quartz-rich sediments where the Mowiol binding reagent was ineffective. The latter samples required a dilution correction factor of 1.25 in the determination of the analyzed element concentrations.

The trace elements determined were Zn, Cu, Ni, V, Mn, Co, Cr, Pb, Y, Sr, U, and Rb. Major element determination using powder briquettes was done to give a semi quantitative indication of high, medium, or low levels of the respective element in the sample. The major elements determined were: SiO_2, TiO_2, Al_2O_4, Fe_2O_3, MnO, MgO, CaO, BaO, K_2O, Na_2O, S, Cl and P_2O_5. Calibration of the XRF spectrometer was done with international standard rock reference materials. Instrumental parameters and data quality for routine trace element determinations were set up as described (Appendix VI) (Willis, 1996).

5.3 Results and discussion

5.3.1 Particle - size analysis

Four sediment samples from the Blesbokspruit catchment were analyzed for particle size to evaluate the sediment texture and reactivity (Table 5.1).

Table 5.1 Particle size distribution in 4 selected sediments.

Sample No.	Clay % < 2μm	Silt% < 50-2μm	Sand% < 2000-50 μm	Textural class
S2L	22.0	37.6	39.4	silty clay
S7T	21.0	21.2	57.8	clay sand
S14T	13.0	15.9	71.1	clay sand
S22T	9.0	22.4	68.6	clay sand

Note: Sediment texture classes were determined from the textural triangle for sediment textural analysis (Pettijohn, 1975).
S2L = outwelling point lower horizon fraction; S7T = AMD dam 4 top horizon fraction; S14T = stream bed top fraction, down stream of AMD dams 5 and 6; S22T = stream bed top fraction, downstream of wetland

The sediment samples analyzed covered a small textural range from loamy sediments to sandy clay loam sediments (Table 5.1) (Gee and Bauder, 1986). In general, chemical sorption of metals and other elements takes place on the fine grained particles with the < 2μm and the silt grain size fraction being the most reactive part of the sediment (Elsokkary, 1992). The major solids which have the capacity to sorb contaminants are: MnO_2, Fe hydroxides, clays and organic matter (Span *et al.*,1992). More than 20% of sediments S2L and S7 had a grain size fraction < 2μm (Table 5.1). Sediments S14 and S22 contained less clay and more sand suggesting that these sediments may be less adsorptive. The particle size of sediments suggests that sediment S2L is the most adsorptive of the sediments followed by sediment S7T; S14T and S22T (Table 5.1).

5.3.2 Physicochemical characteristics of the sediments

pH, exchangeable acidity, % organic carbon and cation exchange capacity of the sediment samples studied are reported in Table 5.2.

Table 5.2 Physicochemical properties of sediments sampled in the Blesbokspruit catchment.

Sample No.	pH H_2O	pH $CaCl_2$	Organic carbon %	Exchangeable acidity (mmol/kg)	CEC* (meq/100g)
S2L	3.5	3.4	2.6	51.9	1.76
S5T	3.0	3.1	0.3	nd	nd
S6T	3.0	2.8	0.5	nd	nd
S7T	2.9	2.7	0.5	23.7	3.56
S8T	2.6	2.5	0.6	nd	nd
S11T	3.4	3.4	1.8	nd	nd
S12T	3.1	3.0	0.5	nd	nd
S13T	3.7	3.6	0.9	nd	nd
S14T	3.2	3.1	0.7	32.1	4.05
S19T	3.0	2.9	9.5	114	4.13
S22T	3.8	3.7	3.9	44.9	4.12

* Gillman method - $BaCl_2/MgSO_4$ (Rhoades, 1982)
nd = not determined

5.3.2.1 Sediment pH

All the sampled sediments were in contact with AMD or the AMD contaminated waters of the Blesbokspruit over long periods of time. The pH (H_2O) of the sediment samples ranged from 2.6 to 3.8 with an average value of 3.2 (Table 5.2). The lowest pH value was measured in AMD dam 4 (S8T) and the highest pH value was measured in sediment sampled downstream of the wetland (S22T). Sposito (1989) states that a soil is acidic if the pH value of its aqueous-solution phase is < 7.0. These low pH values indicate the very acidic nature of the sediments and suggest the presence of dissolved Al^{3+} and Mn^{2+} (McBride, 1994) and Fe^{3+}. These ions consume base (hydroxyl) ions for neutralization

(McLean, 1982). The possibility of errors in the pH measurement as result of the suspension effect was investigated by measuring the pH in 0.01 M $CaCl_2$ (McBride, 1994). Minimal changes in pH were noted on comparison of the pH measured in H_2O and the pH measured in $CaCl_2$ (Table 5.2). The suspension effect on pH measurements in the sediment samples was, therefore, negligible.

5.3.2.2 Exchangeable acidity

The acidity measured as the moles titratable protons per unit mass displaced by an unbuffered KCl solution is termed the exchangeable acidity (Sposito, 1989). Exchangeable acidity is composed of four types of acidity. The first is the H ions obtained from the hydrolysis of exchangeable, trivalent Al. The second is from hydrolysis of partially hydrolysed and non exchangeable Al. The third type is from weakly acidic groups, mostly organic matter, and the fourth is exchangeable H (Thomas, 1982).

The exchangeable acidities of five representative sediment samples were determined and reported in Table 5.2 and Figure 5.2. The sediment sample from the wetland (S19) had by far the highest acidity. Sediment sample S2L sampled at the AMD outwelling point had approximately 45% of the acidity of the wetland sample with decreasing amounts of acidity in sediment samples S22T, S14T and S7T (Table 5.2). The exchangeable acidity data from the sampled sediments indicates that the wetland accumulates much more acidity from the surrounding acidic waters than the other sediments (Figure 5.2). The % organic carbon and exchangeable acidity correlate, indicating parallel trends for % organic C and exchangeable acidity (Figure 5.4).

This could be explained by metals, such as Al^{3+}, which are predisposed towards precipitation as well as complexation with organic compounds. The complexation of Al to anionic groups of organic matter is pH dependent, assuming that $Al(OH)_3$ precipitation-dilution controls Al^{3+} solubility (McBride, 1994). The relationship of exchangeable acidity and exchangeable Al (Table 5.4) is shown in Figure 5.3. The plot of these two variables shows a certain degree of correlation. This suggests a relationship between exchangeable acidity and exchangeable Al in the Blesbokspruit sediments (Thomas, 1982).

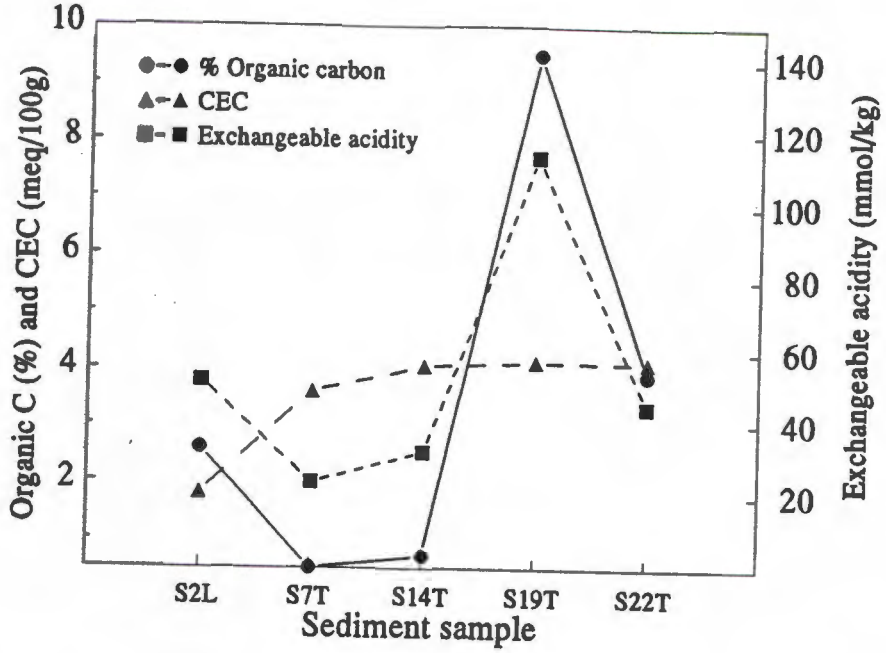

Figure 5.2 Exchangeable acidity, CEC values and % organic carbon in sediments sampled from different sites in the Blesbokspruit catchment

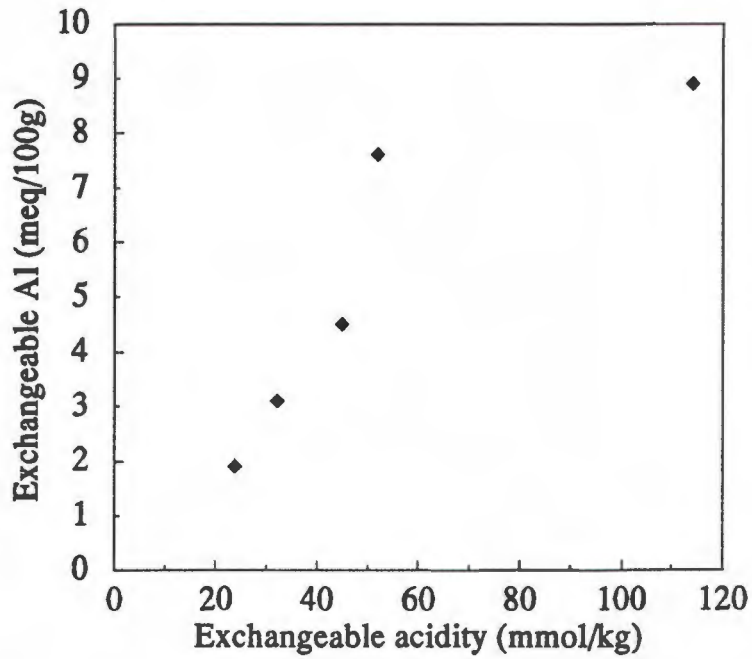

Figure 5.3 The relationship between exchangeable acidity and exchangeable aluminium

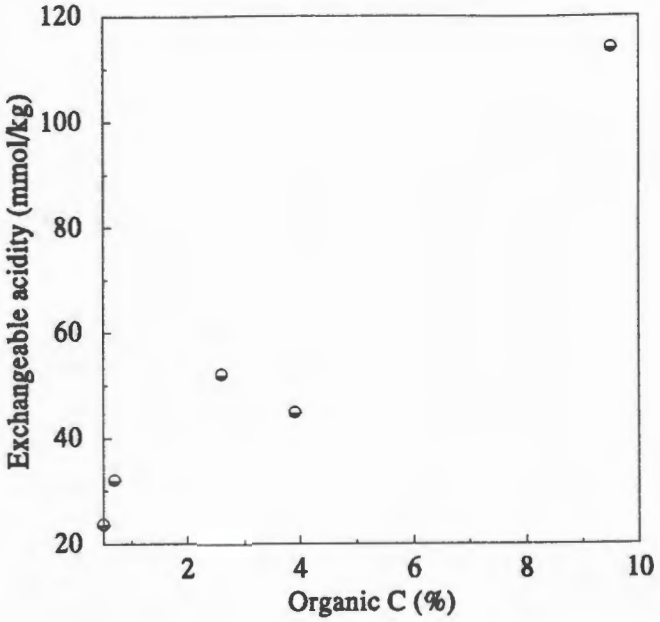

Figure 5.4 Plot of the relationship of % organic carbon with exchangeable acidity

The sorption of Al to organic compounds in the wetland is enhanced at pH 3 and 4 as dissolution of the mineral phase, $Al(OH)_3$ supplies Al^{3+} until complexation by organic matter is satisfied. Other metal ions for example, Fe^{3+}, have similar complexation and precipitation behaviour (McBride, 1994). The likely presence of increased amounts of organic acids in the wetland could also increase exchangeable acidity (Thomas, 1982).

5.3.2.3 % Organic carbon

Organic carbon is contained in the sediment organic matter fraction, which consists of the cells of microorganisms, plant and animal residues at various stages of decomposition and stable humus synthesized from residues. This complex material can be divided into a humic and non-humic fraction (Kabata-Pendias and Pendias, 1985). The humic substances are of a colloid polymer chain structure and contain large numbers of functional groups (CO_2, OH, C=C, COOH, SH, CO_2H) which have a great affinity for interacting with metal ions (McBride, 1994; Kabata-Pendias and Pendias, 1985; Jenkinson, 1988).

Jenkinson (1988) reported that arable topsoils commonly contain 1 to 3 % organic carbon, with grassland and forest soils somewhat more and Australian alpine humus soils 12 % organic carbon. The % organic carbon of selected sediments was determined and reported in Table 5.2. The wetland sediment sample (S19T) had the highest organic

carbon content (9.5%) similar to that of organic rich alpine humus soils. The sediment samples from the outwelling point (S2L) and the two stream samples (S11T downstream of AMD dam 4, S22T downstream of the wetland) had organic carbon <4% and >1.5%. The remaining sediment samples contained < 1% organic carbon (Table 5.2).

Metallic ions, particularly iron and aluminium, are tenaciously held by humic substances. The reaction with humic substances can lead to increased metal solubility. However, it is much more common for metals to form insoluble metal-organic complexes (Jenkinson, 1988). Strong ionic and covalent bonds are formed in these complexes. Metal adsorption on organic matter can, therefore, be viewed as a form of chemisorption (McBride, 1994). A typical affinity sequence of metals for soil organic matter as a function of electronegativity at pH 5 is given in Table 5.3 (McBride, 1994).

Table 5.3 Observed order of affinity of divalent metal ions for soil organic matter related to electronegativity (McBride, 1994).

Affinity sequence	Cu	>	Ni	>	Pb	>	Co	>	Ca	>	Zn	>	Mn	>	Mg
Electronegativity	2.0		1.91		1.87		1.88		1.0		1.65		1.55		1.31

Metal selectivity for organic matter depends on a number of factors beyond the properties of the metals themselves (McBride, 1994).

The factors are:

1. The chemical nature of the organic ligand.
2. The level of adsorption on the organic matter.
3. The pH at which adsorption is measured.
4. The ionic strength of the solution in which adsorption is measured.

Kabata-Pendias and Pendias (1985) report the order of affinity of metal ions to form water insoluble complexes with fulvic acid as:

$$Fe = Cr = Al > Pb = Cu > Hg > Zn = Ni = Co = Cd = Mn$$

The % organic carbon in the sediment samples can act as a measure of affinity of the

sediments for dissolved metals in the associated metal-rich waters. Therefore, it could be expected that the sediments with high organic carbon, content such as the wetland sediment, should show more affinity for metal ions.

5.3.2.4 Sediment cation exchange capacity

The cation exchange capacity (CEC) is the quantity of cations reversibly adsorbed per unit weight of sediment. CEC determination approximates the actual negative surface charge that can be balanced by acidifying cations (McBride, 1994).

The wetland sediment (S19T) contained the highest CEC (4.13 meq/100g) with CEC values < 4.13 meq/100g and > 3.5 meq/100g in sediments S22T, S14T, S7T and the lowest CEC value in S2L (1.76 meq/100g) (Table 5.2). Cation exchange capacity of the sediments increases from the sediment sampled at the outwelling point (S2L) to the sediment sampled in the stream bed (S14T) and then remains similar in the sediments sampled further downstream (Figure 5.2).

The appearance of similar CEC values in sediments sampled downstream of the AMD dams and containing different organic carbon concentrations can be due to the blocking of potential cation exchange sites in organic matter by Fe^{3+} and Al^{3+}. It is not uncommon for stable organic matter found in very acid soils or as in this case sediments, where Al^{3+} is soluble, to contribute little to the sediment CEC (McBride, 1994).

5.3.3 Exchangeable cations

The composition of readily exchangeable ions in the sediments can be determined by chemical analysis of the sediment solution after the reaction of the sediment with the "index" ion (Ba^{2+}). In acid soils the most important readily exchangeable metal cation is Al^{3+} followed by Ca^{2+} and Mg^{2+} (Sposito, 1989). The results of the exchangeable cation determination in selected sediments from Blesbokspruit are reported in Table 5.4.

Table 5.4 Exchangeable cations concentrations in meq/100g in selected Blesbokspruit sediments.

Sample No.	Exchangeable cations concentrations*(meq/100g) Na	K	Ca	Mg	Fe	Al
S2L	1.8	0.03	1.5	0.45	0.11	7.6
S7T	0.84	0.01	0.47	0.28	0.22	1.9
S14T	0.38	0.01	0.85	0.28	0.13	3.1
S19T	0.18	0.01	0.45	0.18	0.50	8.9
S22T	0.18	0.02	0.45	0.27	0.32	4.5

* in 0.1M $BaCl_2$ (Rhoades, 1982)

The data in Table 5.4 indicate that Al is the dominant exchangeable cation, followed by Na^+, Ca^{2+} and Mg^{2+}. The relatively high Al values in the outwelling point sediment (S2L) can be due to the large clay fraction of this sample, whereas the high exchangeable Al values for the wetland sediment (S19T) can be due to Al complexed to the organic matter in these sediments. Low exchangeable Al content in the AMD dam sediment (S7T) suggests the leaching of Al from the top layers of the sediment by the overlaying Al-rich acidic waters (Table 4.4 in Chapter 4)(Karathanasis *et al.*, 1988).

5.3.4 Sediment mineralogy

The mineralogical composition of whole sediment (< 2 mm) and clay (< 2 μm) fractions of selected sediment samples was determined by XRD.

5.3.4.1 Clay mineralogy of two sediment samples from the Blesbokspruit catchment

The clay mineralogies of sediments (S2L - outwelling point lower horizon) and S7T (AMD dam 3 - top horizon) were determined by XRD. X-ray diffractograms of the two clay fractions are shown in Figure 5.5.

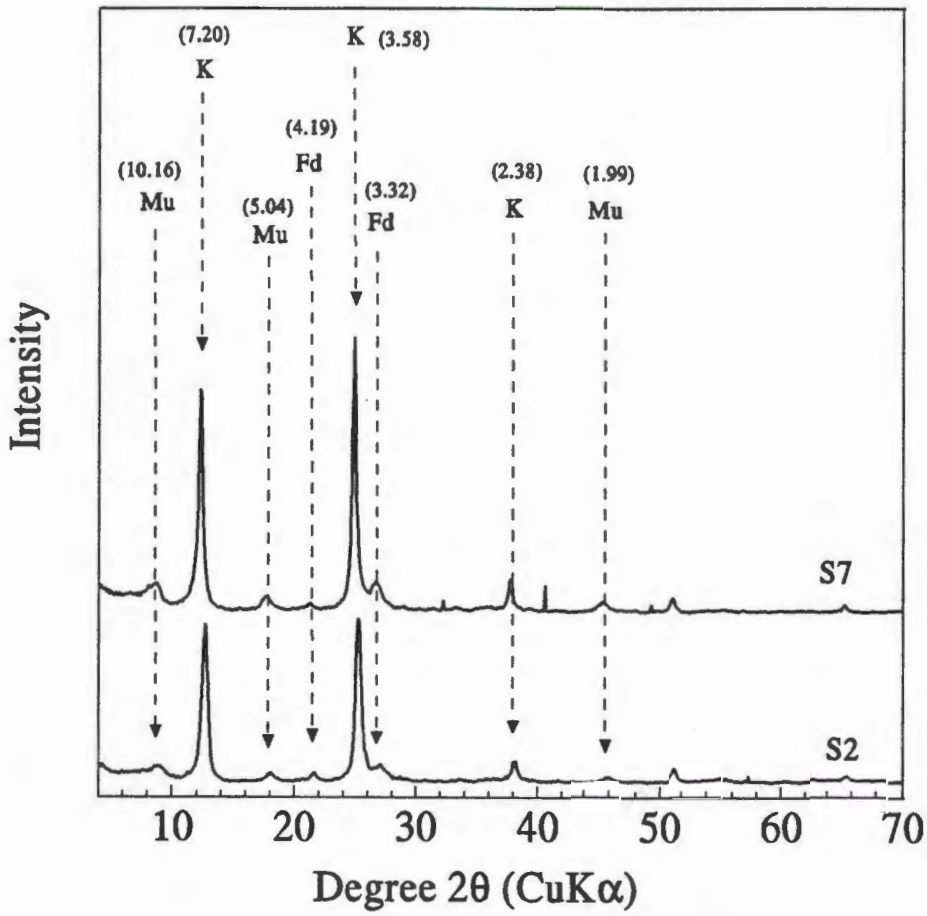

Figure 5.5 X-ray diffractograms of clay fractions extracted from Blesbokspruit sediment samples S2L and S7T. Peak locations are shown for kaolinite (K), muscovite (Mu) and feldspar (Fd). [*d* - spacings in Å are given in parenthesis.]

Muscovite [$KAl_2(Si_3Al)O_{10}(OH)_2$] representing the phylosilicates (micas) and feldspar [e.g. orthoclase $K(Si_3AlO_8)$] representing the tectosilicates were the principal primary minerals in both samples (Figure 5.5). Kaolinite [$Si_2Al_2O_5(OH)_4$] represented the secondary minerals in the clay fractions. Kaolinite dominated the aluminosilicate minerals in the clay fraction of both samples (Figure 5.5).

The low concentrations of Al in natural waters are assumed to be controlled by the insoluble nature of gibbsite and kaolinite in such waters (Chapter 3, Table 4.4, water samples W20 and W21) (Nordstrom, 1982). High concentrations of dissolved Al have been found in acid, sulphate rich mine waters including the AMD contaminated Blesbokspruit waters (Chapter 4, Table 4.4) (Nordstrom, 1982; Karathanasis *et al.*, 1988). At pH values < 4.5 kaolinite is more soluble than aluminium sulphate minerals found in sulphate rich waters (Nordstrom, 1982). Acid mine waters in contact with kaolinite in the Blesbokspruit sediments increases the solubility of this mineral, as predicted by MINTEQA2 modelling, resulting in the observed increase of dissolved Al in the associated waters (Figure 4.14 and Table 4.4 in Chapter 4). The calculated saturation indices of alunite and jurbanite show that these minerals are in equilibrium in the acidic waters (Figure 4.14 in Chapter 4). High dissolved Al concentrations in the Blesbokspruit may thus originate in the increased solubility of kaolinite and the equilibrium state of alunite and jurbanite in the Blesbokspruit catchment.

5.3.4.2 Mineralogy of whole sediment from selected Blesbokspruit sediments

X-ray powder diffractograms of sediments from the AMD dams are shown in Figures 5.6 and 5.7.

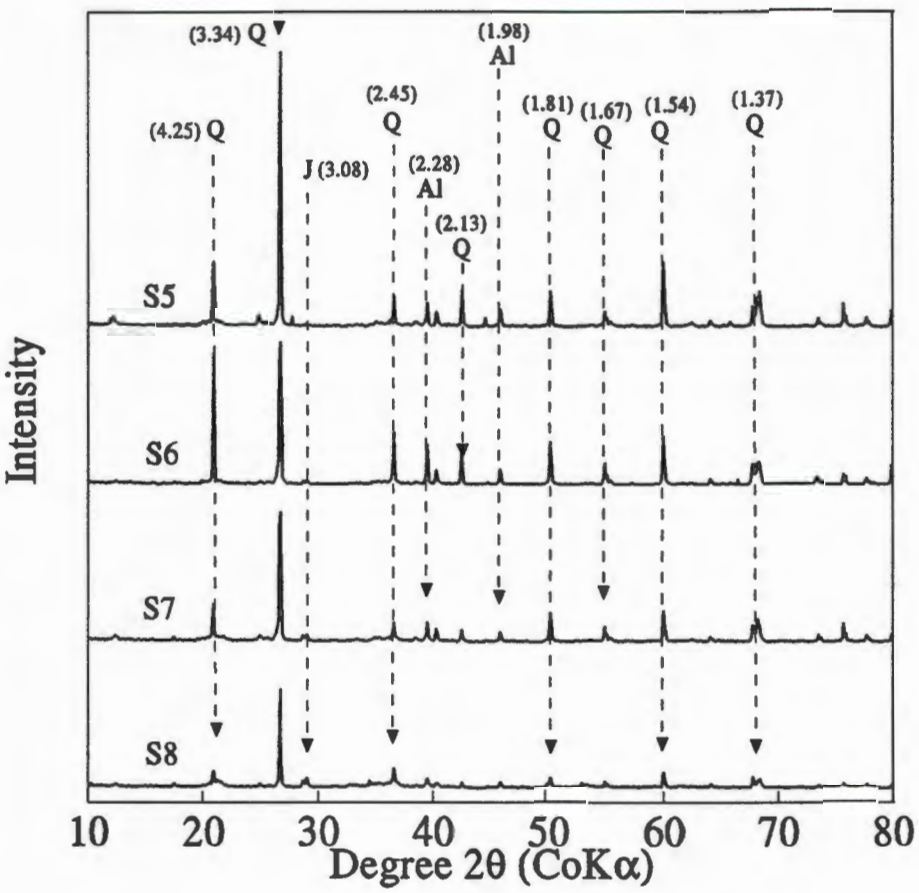

Figure 5.6 X-ray powder diffractograms of sediment samples from the AMD dams at the origin of the Blesbokspruit. S5 = top horizon of sediment from AMD dam 1; S6 = top horizon of sediment from AMD dam 2; S7 = top horizon of sediment from AMD dam 3; S8 = top horizon of sediment from AMD dam 3. Peak locations are shown for quartz (Q), jarosite (J), aluminium from Al XRD mount (Al). [*d*-spacings in Å are given in parentheses]

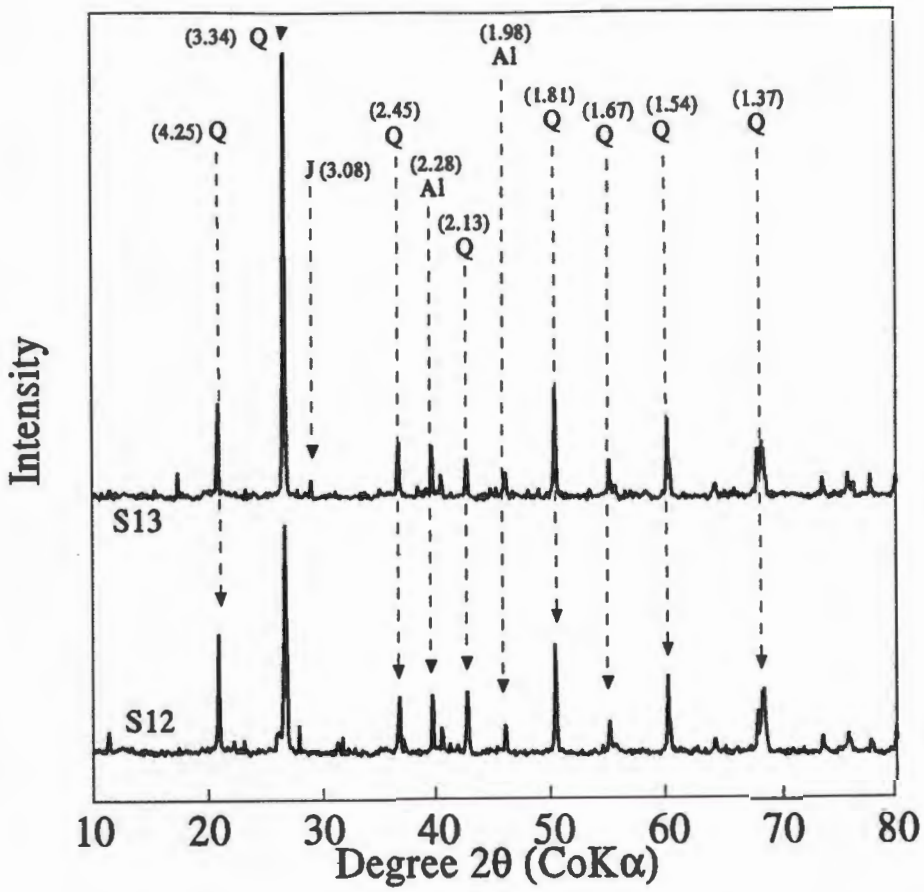

Figure 5.7 X-ray powder diffractograms of sediment samples from the two AMD dams downstream of AMD dam 4, receiving seepage from AMD ditch W15. S12 = top horizon of sediment from AMD dam 5; S13 = top horizon of sediment from AMD dam 6. Peak locations are shown for quartz (Q), jarosite (J), aluminium (Al) from Al XRD mount. [*d*-spacings in Å are given in parentheses]

The dominant mineral in the AMD dam sediments is quartz (SiO_2) (Figures 5.6 and 5.7). The mineral jarosite [$KFe_3(OH)_6(SO_4)_2$] was detected in sediments S13T, S6T, S7T and S8T (from AMD dam 2, 3 and 4) (Figures 5.6 and 5.7). The usefulness of X-ray powder diffraction data in identifying mineral phases is limited due to the dilution of precipitate peaks by large quantities of quartz. However, the diffractograms indicate the precipitation of jarosite from the sulphate rich waters retained in the AMD dams.

X-ray powder diffractograms of the sediments from the Blesbokspruit stream are shown in Figures 5.8.

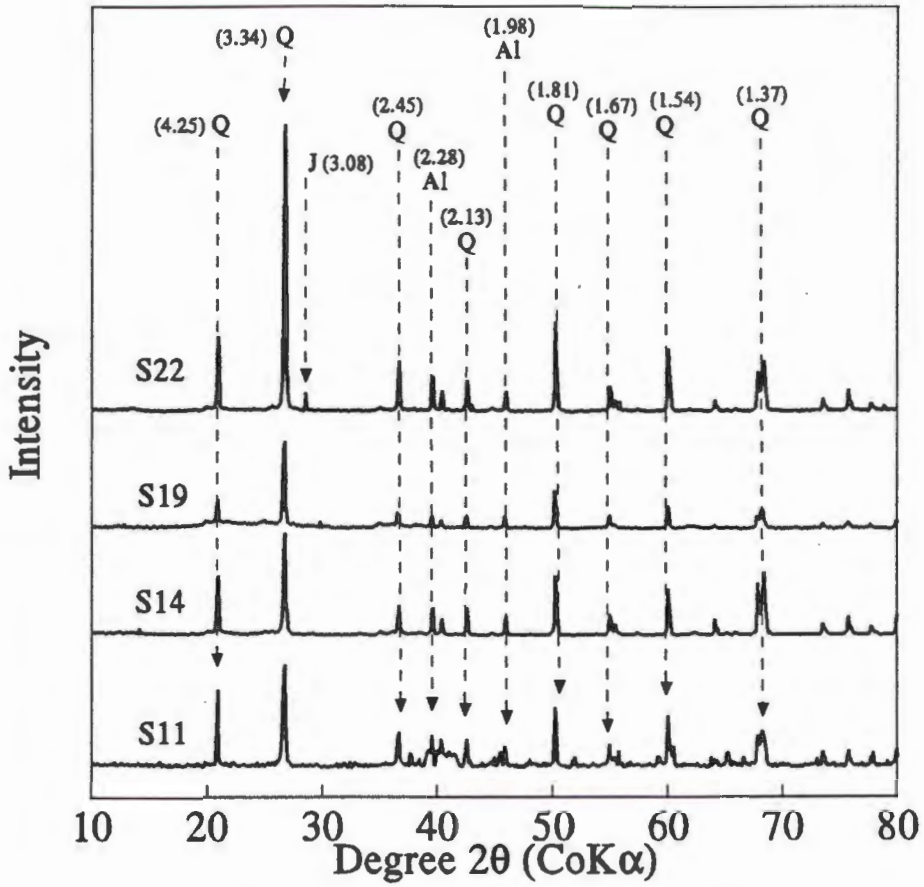

Figure 5.8 X-ray powder diffractograms of sediment samples from the Blesbokspruit stream. The top horizons of each sediment were analyzed. S11 = from streambed downstream of AMD dam 4; S14 = from the streambed downstream of AMD dams 5 and 6; S19 = in the wetland; S22 = in the streambed downstream of the wetland. Peak locations are shown for quartz (Q), jarosite (J), aluminium (Al) from Al XRD mount. [*d*-spacings in Å are given in parentheses]

The minerals in the Blesbokspruit streambed sediments are the same as those detected in the AMD dam sediments (Figures 5.6, 5.7, 5.8). The major peak in the streambed sediment diffractograms is the quartz peak (Figure 5.8). The mineral jarosite [$KFe_3(OH)_6(SO_4)_2$] was detected in sediment downstream of the wetland (S22) (Figure 5.8). The precipitation of secondary minerals such as jarosite from metal-rich solution

Table 5.5 Major elements in sediments from the Blesbokspruit catchment

Elements/oxides in weight %	Sediment sample S2L	S5T	S6T	S7T	S8T	S11T	S12T	S13T	S14T	S19T	S22T
SiO_2	52	80	83	67	46	84	87	76	87	64	102
TiO_2	0.91	0.53	0.42	0.56	0.49	0.27	0.51	0.59	0.43	0.83	0.59
Al_2O_3	22	7.7	3.8	8.4	7.9	3.9	4.6	8.1	2.0	8.4	7.4
Fe_2O_3	17	5.5	10	15	36	6.1	4.4	4.2	6.8	8.2	3.2
MgO	0.18	0.07	0.03	0.10	0.08	0.05	0.06	0.11	0.02	0.24	0.28
CaO	0.04	0.02	0.02	0.03	0.04	0.08	0.02	0.03	0.02	0.11	0.04
Na_2O	0.08	0.04	0.05	0.13	0.16	0.51	0.04	0.06	0.04	0.05	0.04
K_2O	0.93	0.34	0.26	0.78	0.97	0.16	0.18	0.35	0.12	0.68	0.73
P_2O_4	0.35	0.02	0.03	0.04	0.03	0.05	0.02	0.03	0.03	0.21	0.10
SO_3	1.6	0.4	0.85	1.9	4.0	0.85	0.35	0.83	0.48	1.0	0.83
Cl	0.04	0.01	0.02	0.02	0.03	0.02	0.04	0.01	0.01	0.05	0.02
BaO	0.05	0.01	0.01	0.01	0.02	0.01	0.01	0.01	0.01	0.04	0.03
H_2O	nd	nd	nd	nd	nd	nd	nd	nd	nd	nd	nd
% Organic carbon*	nd	0.33	0.48	0.47	0.61	1.76	0.48	0.94	0.68	9.5	3.9

* determined with the Walkley Black method; nd = not determined

Chemical sorption of metals and other elements takes place on the fine grained particles, and the major solids which have the capacity to sorb contaminants are MnO_2, Fe hydroxides, clays and organic matter (Span *et al.*,1992). The grain size of these sediments, therefore, can have a major effect on the elemental concentrations in sediments (Förstner and Wittmann, 1979). Iron oxide content in the top horizons of the sediments sampled in the Blesbokspruit catchment is generally higher than the values reported for iron in the top horizons of sediments impacted by gold-mining operations (Horowitz *et al.*, 1988). The values correspond well to those found in intermediate and mafic rocks with the exception of sample S2L, S6T, S7T and S8T. Sample S2L is the lower horizon to the ferrihydrite rich crust covering the outwelling point. Ferrihydrite contamination from the overlying horizon can result in the high Fe_2O_3 values in this sample. The sediment diffractograms of samples S6T, S7T and S8T (Figure 5.6) indicates the presence of increasing amounts of jarosite in these sediments which can explain the elevated sediment Fe content. The relationship of Fe_2O_3 with SO_3 showed a strong degree of correlation (Figure 5.9), suggesting that iron sulphate minerals control the iron content in sediment samples S6T, S7T and S8T (Karathanasis *et al.*, 1988).

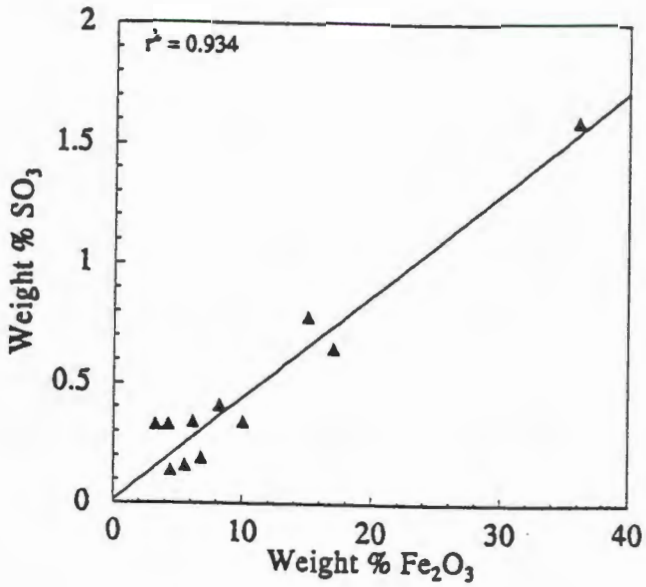

Figure 5.9 A plot of the relationship of Fe_2O_3 and SO_3 in the Blesbokspruit sediments

The silica content of the sediments reflects the sand (quartz) fraction of the sediments and Al_2O_3 the silt-clay fraction of the sediments, explaining the high SiO_2 content in the sand-rich samples (Table 5.1) (Kabata-Pendias and Pendias, 1985). The clay rich sample S2L (22% clay) has the highest Al_2O_3 content of the sediments.

Table 5.6 Trace elements in sediments from the Blesbokspruit catchment

Elements	Sediment sample										
in mg/kg	S2L	S5T	S6T	S7T	S8T	S11T	S12T	S13T	S14T	S19T	S22T
Zn	67	13	12	25	38	140	13	16	14	73	43
Cu	39	13	16	21	30	24	26	26	27	56	21
Ni	29	14	20	16	11	41	26	28	35	63	40
V	181	49	47	92	109	56	71	148	68	107	47
Cr	157	118	165	305	225	169	179	186	204	244	138
Mn	141	82	112	108	108	181	147	106	209	243	158
Co	9.7	3.9	4.1	3.8	5.0	14	3.9	5.7	3.9	25	19
Zr	271	617	624	514	383	294	655	442	920	240	345
Y	42	19	15	25	23	14	17	24	13	77	45
Sr	152	14	11	29	30	17	8.5	14	9.4	14	8.0
Rb	26	19	16	38	44	10	15	25	7.2	36	36
Pb	34	7.8	10	23	36	21	21	64	21	26	10
U	6.0	2.6	1.9	4.1	5.3	3.2	1.8	3.9	2.9	11	3.3

Numerous authors have found high trace element contents in sediments affected by mining activities (Johnson and Thornton, 1987; Karlsson *et al.*, 1988; Horowitz *et al.*, 1988; Förstner and Wittmann, 1979). Trace element analysis of whole sediment samples gave an indication of the amount of trace elements present in the top horizon of the Blesbokspruit sediments. In the Blesbokspruit sediments there is a certain degree of correlation between Cu, Ni, Mn and % organic carbon (Appendix III, Table A III.3). Cobalt shows strong association (r^2 = 0.858) with % organic carbon (Figure 5.10) and is accumulated in the organic carbon rich sediments (S19T – wetland sediment, S22T – sediment downstream of the wetland).

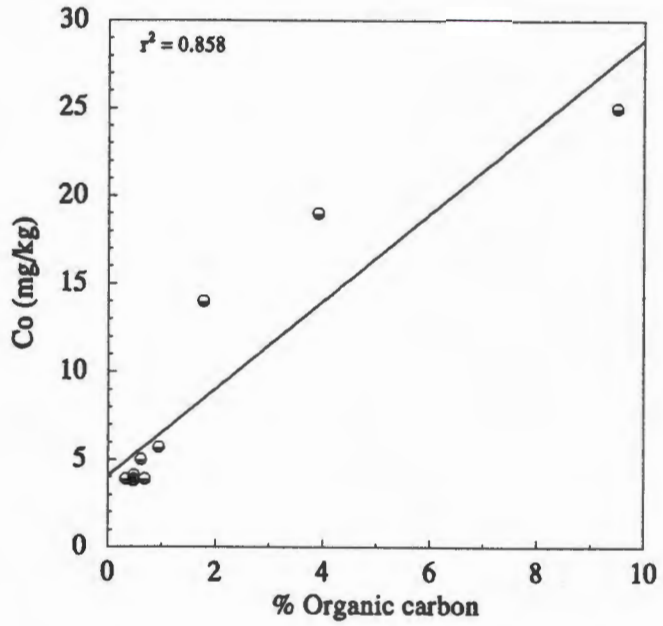

Figure 5.10 Plot of the relationship of Co and % organic carbon in the Blesbokspruit sediments

The average Co content (8.9 mg/kg) is , however, below that reported for the average Co content found shales (19 mg/kg) (Krauskopf, 1967). Comparison of Co values with those in sediments affected by gold mining operations (Horowitz *et al.*, 1988) shows lower Co content in the Blesbokspruit sediments. The sorption of Co to Mn minerals is pH dependant, resulting in less Co sorption of Co on Mn minerals at the low pH values of the studied sediments (Smith and Patterson, 1995).

Numerous authors have found high trace element contents in sediments affected by mining activities (Johnson and Thornton, 1987; Karlsson *et al.*, 1988; Horowitz *et al.*, 1988; Förstner and Wittmann, 1979). Trace element analysis of whole sediment samples gave an indication of the amount of trace elements present in the top horizon of the Blesbokspruit sediments. In the Blesbokspruit sediments there is a certain degree of correlation between Cu, Ni, Mn and % organic carbon (Appendix III, Table A III.3). Cobalt shows strong association ($r^2 = 0.858$) with % organic carbon (Figure 5.10) and is accumulated in the organic carbon rich sediments (S19T – wetland sediment, S22T – sediment downstream of the wetland).

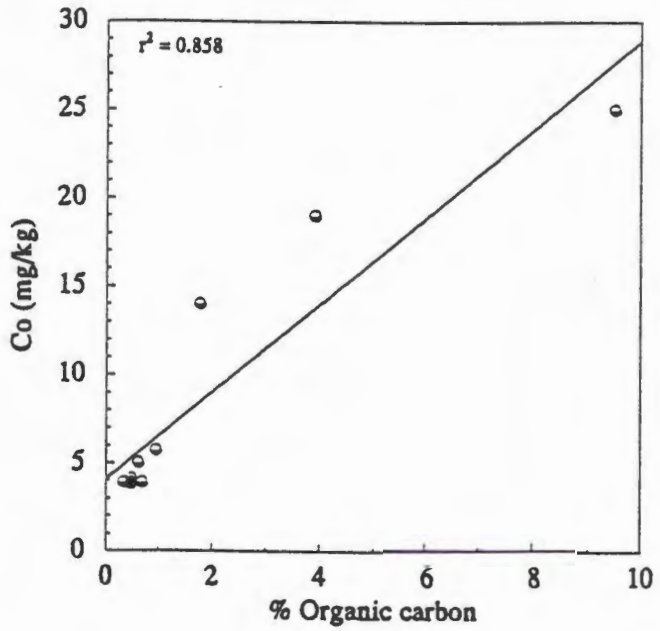

Figure 5.10 Plot of the relationship of Co and % organic carbon in the Blesbokspruit sediments

The average Co content (8.9 mg/kg) is , however, below that reported for the average Co content found shales (19 mg/kg) (Krauskopf, 1970). Comparison of Co values with those in sediments affected by gold mining operations (Horowitz *et al.*, 1988) shows lower Co content in the Blesbokspruit sediments. The sorption of Co to Mn minerals is pH dependant, resulting in less Co sorption of Co on Mn minerals at the low pH values of the studied sediments (Smith and Patterson, 1995).

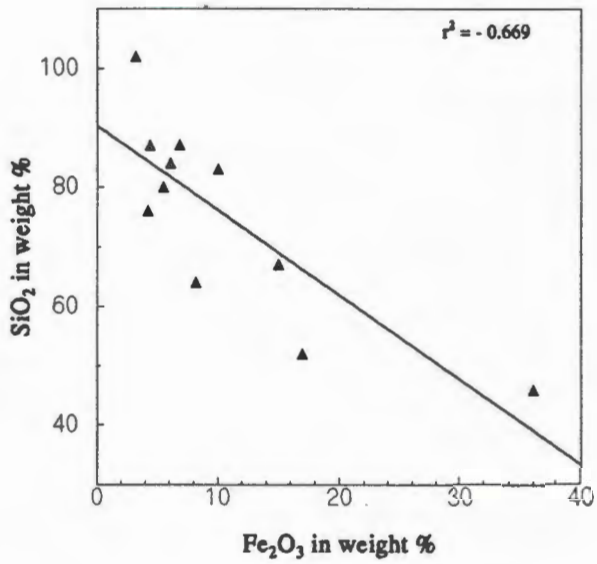

Figure 5.11 Plot of the relationship of Fe_2O_3 and SiO_2 in the Blesbokspruit sediments

A negative correlation (r^2 = -0.669) exists between Fe_2O_3 and SiO_2 indicating an increase of Fe_2O_3 in the sediment with a subsequent decrease of SiO_2 (Figure 5.11). The dissolution of aluminosilicate clay material in the sediments and the precipitation of iron sulphate minerals (jarosite) explains this correlation (Karathanasis *et al.*, 1988). MINTEQA2 modelling of the acidic waters from the Blesbokspruit (Figure 4.14 in Chapter 4) shows undersaturation for kaolinite and supersaturation for jarosite supporting the Fe_2O_3 and SiO_2 relationship seen in Figure 5.11. Coprecipitation or adsorption of trace metals to solid phases, including iron oxide or iron sulphate minerals, appears to control the trace element concentrations in these acidic waters (Johnson, 1986).

Strong correlation (r^2 = 0.976) between Rb and K_2O was observed in the sampled sediments (Figure 5.12). The Rb/K_2O correlation has been reported by Kabata-Pendias and Pendias (1985). The good correlation between Rb and K_2O is expected because Rb has atomic properties similar to K and can, therefore, interchange with K in K-minerals. The average K/Rb ratio for the Blesbokspruit sediments is 145 and compares well with the average K/Rb ratio of 150 reported for shales (Heier and Billings, 1970).

No significant correlations were found between Pb and the other elements in the sediments. However, the average Pb content (25 mg/kg) of the sediments was somewhat higher than the average Pb content (20 mg/kg) reported in shales (Krauskopf, 1970) and in sediments from the AMD contaminated Cheyenne river arm (18 mg/kg) (Horowitz

et al., 1988). The sediment from AMD dam 6 (S13T) had the highest Pb content and no Pb accumulation was detected in the wetland sediments.

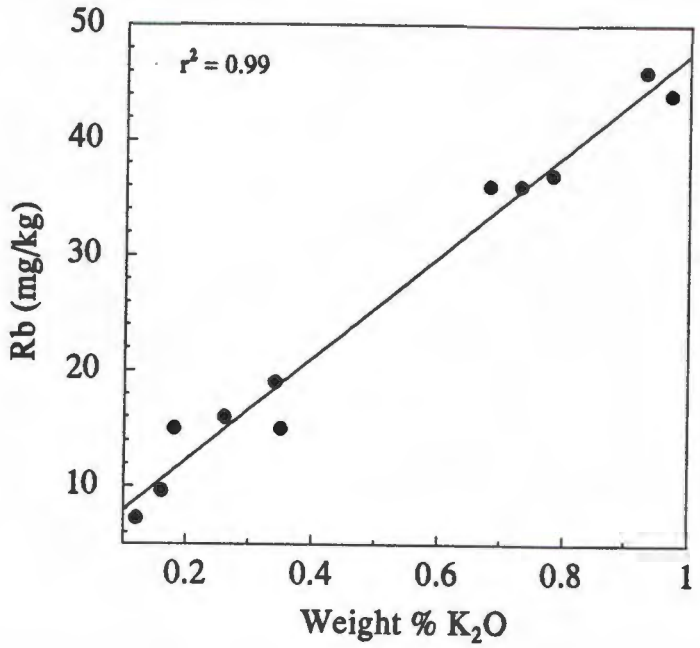

Figure 5.12 The correlation plot of Rb and K_2O in the Blesbokspruit sediments

Average zinc (41 mg/kg), Ni (27 mg/kg), and Cu (29 mg/kg) content of the Blesbokspruit sediments is similar to, or lower than the reported average values of these elements in sediments affected by gold mining operations (Horowitz *et al.*, 1988). No significant correlations with organic carbon were found for these elements. The presence of iron oxyhydroxides, clay and organic matter in the sediments affects adsorption of Cu, Zn and Ni (Millward and Moore, 1982; Kabata-Pendias and Pendias, 1985). However, the low pH of the Blesbokspruit waters counteracts adsorption of metals to organic matter and precipitating minerals, although at the higher pH values in the wetland and downstream of the wetland (Table 4.4 in Chapter 4) an increase in metal sorption to these sediments was observed (Evans, 1989).

Average U (4.3 mg/kg) sediment content is somewhat higher than the average U content (3.7 mg/kg) reported for shales (Krauskopf, 1970) indicating U accumulation in the sampled sediments.

The manganese content in the Blesbokspruit sediments is below the range of Mn values reported for U.S. surface soils. Manganese is accumulated in soils rich in Fe oxyhydroxides and or organic matter (Kabata-Pendias and Pendias, 1985). The highest concentration of Mn in the Blesbokspruit catchment is detected in the organic carbon rich wetland sediment (S19T) (Table 5.5). All the Blesbokspruit sediments contain > 100 mg/kg Cr which is above the reported average Cr value of 76 mg/kg in AMD contaminated sediments (Table 5.5) (Horowitz *et al.*, 1988). Reduction of Cr(VI) to Cr(III) is more rapid in acid, organic rich sediments. In such environments the relatively insoluble and less mobile Cr(III) form predominates and generally occurs as insoluble hydroxides and oxides (McGrath, 1995).

5.4 Conclusions

The sediment characteristics such as the particle size, organic carbon, CEC and mineral content affect the metal attenuation capacity of the Blesbokspruit sediments.
The high exchangeable acidity found in the organic and clay rich sediments indicates the presence of adsorbed Al to these phases. In the organic carbon rich sediments this adsorbed Al saturates part of the CEC. The high exchangeable Al values in the wetland sample indicate that Al is indeed accumulated in this sediment. The Al originates in the mica, feldspar and kaolinitic clay minerals present at the AMD outwelling area and in the AMD dams. No precipitation of Al minerals was detected as predicted by MINTEQA2 modelling (Figure 4.14 in Chapter 4) suggesting attenuation of dissolved Al in the Blesbokspruit waters by sorption to organic matter in the sediments. However not all Al is removed from the Blesbokspruit by the wetland and toxic concentrations of 40 mg/ℓ Al (DWAF,1996) remain in the waters downstream of the wetland. The presence of the iron sulphate mineral (jarosite) in some sediments suggest that this mineral controls the iron content of the Blesbokspruit waters at certain sites in the catchment.

According to the South African water quality guidelines Fe, Mn and Pb values downstream of the wetland are still above the target water quality range (DWAF, 1996). The low pH and the saturation with Al of the wetland sediment CEC, counteract adsorption of these metals. The available data however, suggests that the wetland sediment accumulates some metals more efficiently than the remaining sediments and acts as a sink to metals such as Zn, Ni and Cu. The construction of small artificial wetlands in the Blesbokspruit downstream of the existing wetland can, therefore be recommended. This may further attenuate the metal concentrations in the Blesbokspruit waters.

Chapter 6

CHEMICAL AND PHYSICAL ANALYSIS OF PRECIPITATES ASSOCIATED WITH ACID MINE DRAINAGE IN THE BLESBOKSPRUIT CATCHMENT

6.1 Introduction

Oxidative weathering of iron sulphide minerals leads to the formation of a variety of precipitates (Bigham, 1994; Karathanasis *et al.*, 1988; Nordstrom and Ball, 1986 and Chapman *et al.*, 1983). The formation of secondary minerals depends on the availability of oxygen, changes in pH and Eh, mixing with natural waters and contact with soils, organic matter or sediments. The degradation of water quality in the Blesbokspruit due to contamination with AMD results in the precipitation of secondary minerals in the affected catchment. Chapman *et al.* (1983) and Filipek *et al.* (1987) implicated the formation of secondary minerals in regulating toxic trace element concentrations through adsorption and coprecipitation reactions.

The most common minerals associated with AMD are poorly crystalline oxyhydroxides and sulphates of Fe, jarosite, and ferrihydrite. The latter is the dominant phase at pH > 5 and in organic rich environments. Goethite occurs as a secondary component in AMD affected areas (Bigham *et al.*, 1992). Karathanasis *et al.* (1988) reported that Al concentrations in AMD contaminated waters at pH < 4.5 were primarily controlled by the solubilities of poorly crystalline jurbanite and alunite. In this chapter mineral, major and trace element content of the precipitates collected in the Blesbokspruit catchment are reported and discussed.

The objectives of the analyses were the following:

1) To determine the microscopic structure of the precipitates.

2) To determine the minerals present in the precipitates.

3) To characterize the major and trace element composition of the precipitates.

6.2 Materials and Methods

6.2.1 Sampling

Precipitates were obtained from the Blesbokspruit catchment (Figure 6.1). The sample area was wet after uncharacteristic rain and snow falls a few days prior to sampling. Six grab samples were collected using a small shovel and stored in sealed plastic bags and capped plastic jars. Samples were in close proximity to or in contact with sampled AMD.

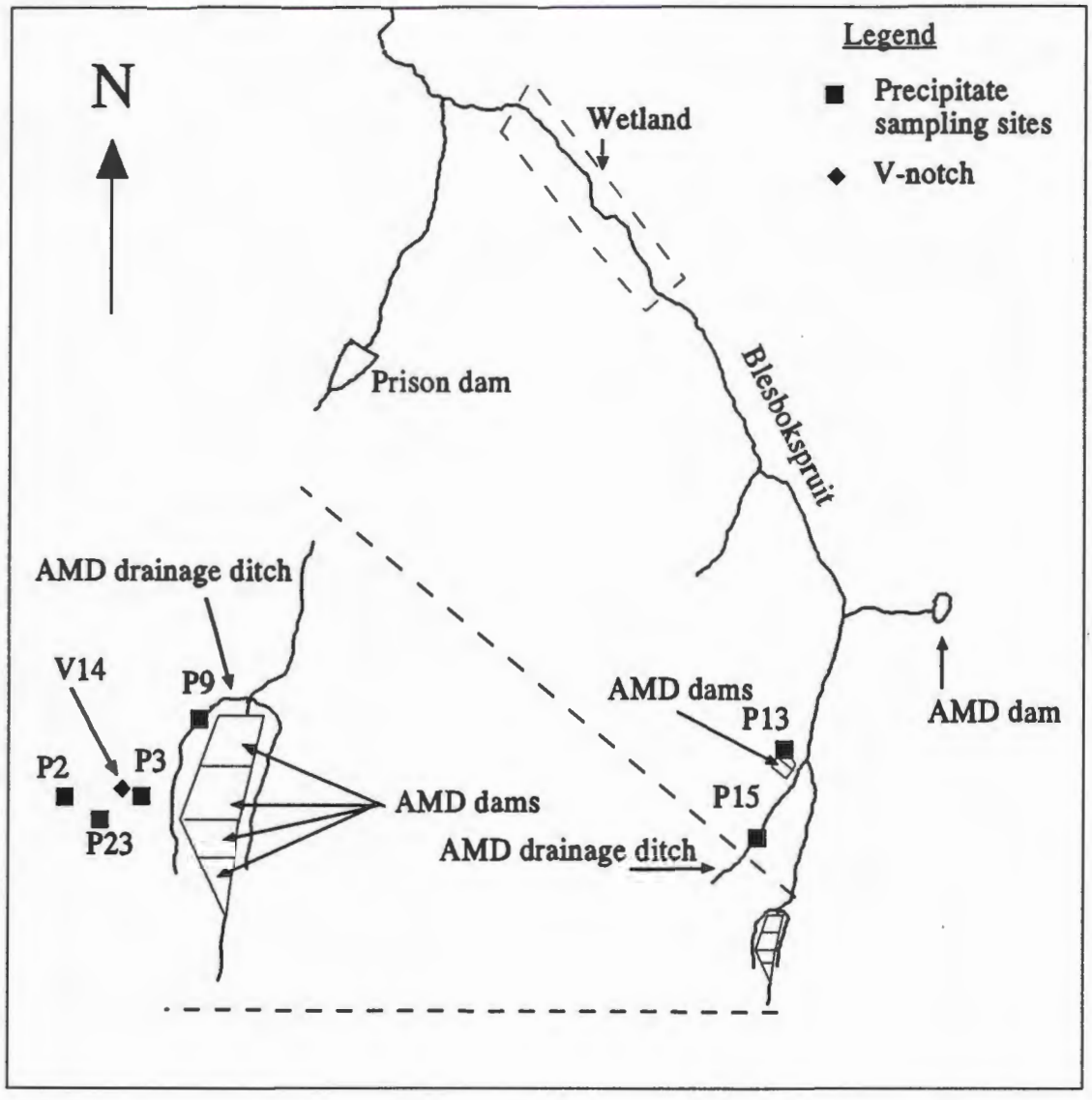

Figure 6.1 The precipitate sampling sites in the Blesbokspruit catchment.

6.2.2 Analysis

6.2.2.1 Precipitate colour

The colour of precipitates was determined and described using the Munsell colour chart (Table 6.1).

Table 6.1 Precipitate colour description of dry samples (Munsell, 1992)

Precipitate	Verbal description	Munsell notation
P2	Dark red	2.5YR 4/6
P2-3	Pale yellow	2.5YR 7/4
P3	Red	2.5YR 5/6
P9	Light reddish brown	5YR 5/6
P13	Light yellowish brown	10YR 6/4
P15	Red	2.5YR 5/8

6.2.2.2 XRD mineral analysis

Precipitates associated with AMD contaminated areas were analyzed with XRD to determine their mineralogy.

Dried precipitates were crushed to −300 mesh using an agate pestle and mortar to ensure uniform particle size. The powder was pressed into an aluminium XRD powder frame lying face down on a sheet of paper. This ensured a preferred orientation of the particles in the analytical surface presented to the X-rays. The mineralogy of each sample was determined by scanning the mounts using a Philips PW 1390 X-ray diffractometer fitted with a graphite monochromator, scintillation detector and pulse height selector. A cobalt tube (Co $K\alpha$ = 1.790 Å) operating at 40 kV and 25 mA was used for the analysis. The samples were scanned through a range of 4 - 80°2θ, with a step size of 0.1°2θ and a counting time of 1 second / step.

6.2.2.3 Elemental analysis with XRFS

X-ray fluorescence spectrometry was used to determine major and trace elements in the precipitate samples. The results of the analysis would give an indication of adsorption and coprecipitation of metal ions in the precipitates.

Six precipitate samples were analyzed for major and trace elements using a Philips X' Unique II (1480/00/10) X-ray spectrometer. Powder briquettes were prepared by taking 6 g oven dried sediment (- 300 mesh) and mixing with one drop Mowiol binding agent (2% Hoechst Mowiol N 70 - 80 in distilled water) per 1 gram of powder. Boric acid was used as backing material and the powder was pressed at approximately 10 tons pressure into 30 mm diameter powder briquettes. In quartz-rich sediments where the Mowiol binding reagent was ineffective, 2 grams of wax binder (Hoechst wax C) were used with 8 gram of powder. The latter samples required a dilution correction factor of 1.25 in the reporting of the analyzed element concentrations.

The trace elements Zn, Cu, Ni, V, Mn, Co, Cr, Pb, Y, Sr, U and Rb were determined quantitatively (Appendix VI). Semi quantitative major element determination using powder briquettes was done to give an indication of high, medium, or low levels of the respective elements in the sample. The major elements determined were: SiO_2, TiO_2, Al_2O_4, Fe_2O_3, MnO, Na_2O, MgO, CaO, S, Cl, BaO, K_2O and P_2O_5.

6.2.2.4 SEM analysis

Qualitative elemental analysis of the precipitates was carried out using scanning electron microscopy (SEM). This analysis generated qualitative element areal and point distributions from the precipitates.

In SEM an electron beam is focused to a nanometre sized probe and used to excite various signals. Secondary electrons are electrons mostly used for imaging and electron micrographs. Backscatter electrons give rise to two types of images: a topographical image, and a compositional image. These two electron signals can be used to study the morphology of the sample. The X-ray photons emitted as a result of the interaction of the electron beam with the specimen atoms can be detected by wavelength- or energy – dispersive spectrometers. These two techniques can be used for chemical and elemental analyses of the sample (Van Grieken and Xhoffer, 1992).

Scanning electron microscopy analysis was done on selected samples (P2, P3, P13 and

P15). Samples were studied and photographed using light microscopy. This was done to help with orientation during SEM analysis. Samples were mounted on an SEM stub and carbon coated prior to SEM microscopy.

To examine the samples the Leica Stereoscan 440 SEM with a 3 lens system was used at a vacuum of 10^{-4} - 10^{-6} torr. A lanthanum hexaboride (LaB_6) crystal was used with a 15kV source giving 6-10 times more brightness than tungsten and better resolution. The maximum resolution with this instrument was 3nm. The instrument used secondary electrons for imaging, backscattered electrons for atomic number determination, and X-rays for elemental analyses. Three types of analyses were done: 1) Image analyses; 2) point elemental analyses; 3) elemental scan analyses of a selected area.

6.3 Results and discussion

6.3.1 SEM analysis of the precipitates

An optical microscopy image of precipitate P2 is shown in Figure 6.2.

Figure 6.2 Optical microscopy image (20x magnification) of precipitate P2 sampled from the deposit on top of the outwelling point. The sponge like appearance of the precipitate probably originates from the encrustation of algae covering the outwelling point.

Scanning electron microscopy was used to identify crystal morphologies in the different precipitates (Figure 6.3, Figure 6.4, Figure 6.5 and Figure 6.6).

(A)

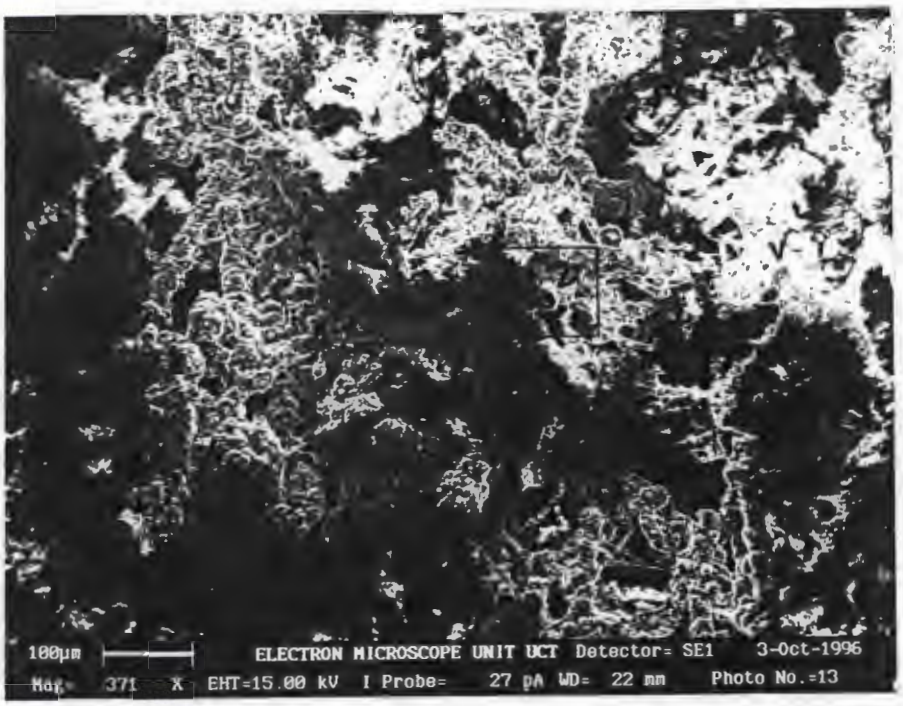

(B)

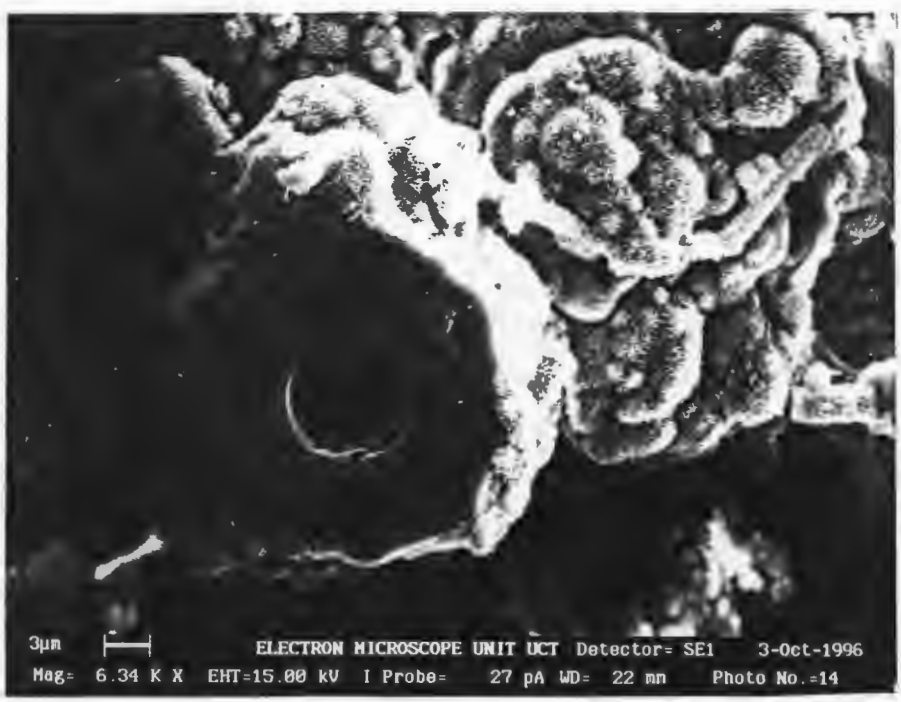

Figure 6.3 (A) Scanning electron micrograph of precipitate P2 sampled from the outwelling point depicting encrustation of dead algae filaments (arrows). Bar = 100 μm. (B) Enlargement of an encrusted algae tube. Bar = 1μm.

(A)

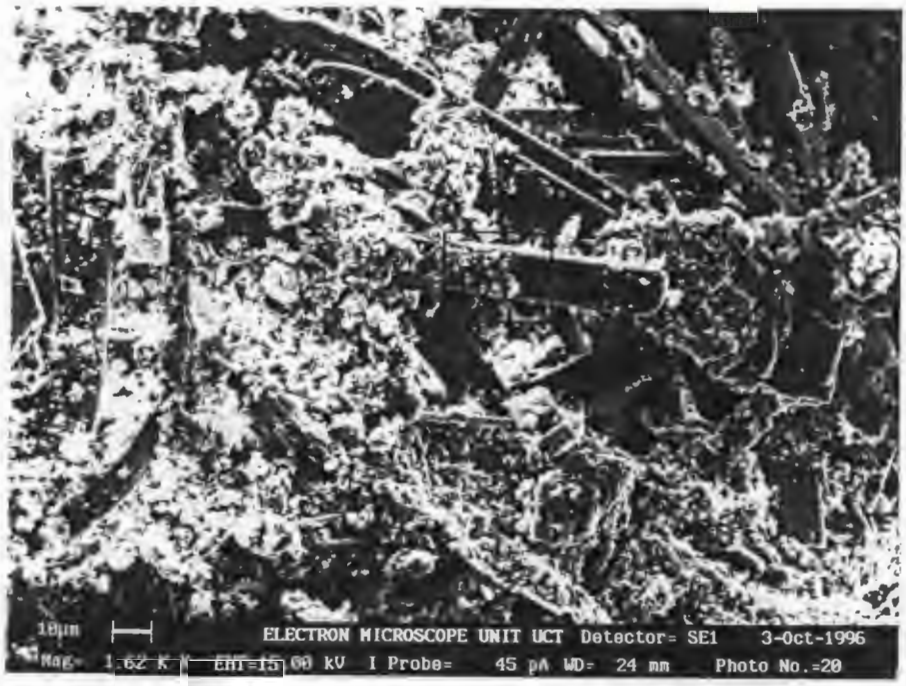

(B)

Figure 6.4 Scanning electron micrograph of precipitate P13 depicting two different crystal morphologies. (A) The large crystals have needle type crystal morphology and are covered by smaller crystals. Bar = 10 μm. (B) An enlargement of Figure 6.5 (A). The small crystals overlaying the needles have hexagonal morphology. Bar = 1μm

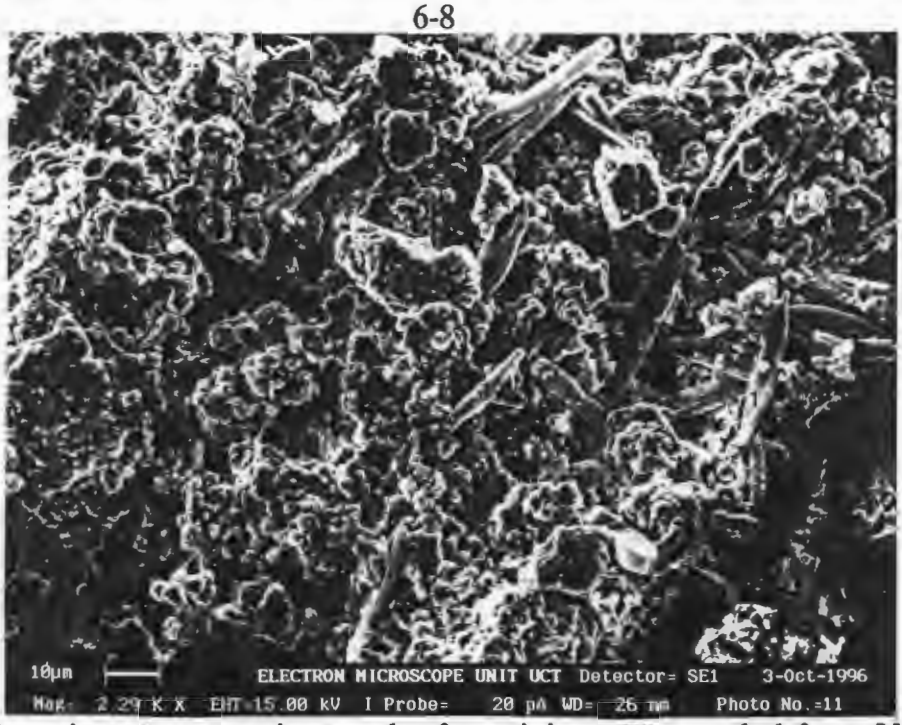

Figure 6.5 Scanning electron micrograph of precipitate P3 sampled from V-notch 14. Spindle shaped crystals (1) and conglomerate crystals (2) are depicted in this image. Bar = 10 μm

Figure 6.6 Scanning electron micrograph of precipitate P15 depicting spherical pincushion type crystal morphology. Bar = 1μm

The spherical, needle-covered crystal morphology of precipitate P2 (Figure 6.3 B) suggests the presence of ferrihydrite as the dominant mineral in the algae encrustations (Schwertmann and Taylor, 1989). The electron micrograph of precipitate P3 (Figure 6.4)

depicts two distinct crystal features: a spindle shaped crystal morphology (1), similar to the shape of some diatom species, is embedded in an unidentifiable conglomerate. Large needle shaped crystals covered with fine hexagonal crystals were depicted in the precipitate P13 micrograph (Figure 6.5 (A)). Doner and Lynn (1989) described needle shaped gypsum crystals. The fine hexagonal crystals covering the needle shaped crystals suggest the presence of jarosite in precipitate P13 (Figure 6.5 (B)) (Schwertmann and Taylor, 1989). The spherical crystal morphology of crystals in precipitate P15 (Figure 6.6) is similar to the spherical crystal morphology of ferrihydrite (Schwertmann and Taylor, 1989). The crystals are, however, 200-500 times larger than the reported size of ferrihydrite crystals (Schwertmann and Taylor, 1989). The pincushion type crystal morphology suggests the presence of schwertmannite (Bigham, 1992) although no further evidence of this mineral was detected in the precipitates.

The precipitates were analyzed using EDS to determine the elemental composition of the identified crystals and conglomerates. The ratios of the Kα peak intensities were used as a relative measure of the concentrations of the elements present in the precipitate. Results of the EDS analysis of the different crystal structures in the precipitates are summarized in Table 6.2 (Appendix IV).

Table 6.2 A qualitative appraisal of the elements present in crystal structures identified by SEM using EDS. The ratios of the Kα peak intensities were used to indicate elemental concentration.

Sample description	A comparison of element Kα peak ratios in descending order of peak intensities*
Precipitate P2: Total area	O, Fe, S, Al, Si, P, Cl (100 : 84 : 65 : 12 : 9 : 9 : 9)
Precipitate P2: Encrustation	O, Fe, S, Al, Si (100 : 66 : 44 : 9 : 8)
Precipitate P3: Total conglomerate	O, Fe, S, Si, Al (100 : 70 : 54 : 16 : 11)
Precipitate P3: Spindle shaped structure	Si, O, Al, S, Fe, K (100 : 58 : 21 : 15 : 15 : 3)
Precipitate P13: Needle structure	S, Ca, O (100 : 74 : 17)
Precipitate P13: Hexagonal structure	S, O, Fe, Si, Al, K (100 : 91 : 47 : 18 : 12 : 10)
Precipitate P13: Rounded features	Si, O, Al, Fe, S (100 : 100 : 92 : 31 : 17)
Precipitate P15: Pin cushion structure	O, Fe, S, Si, Al (100 : 81 : 63 : 11 : 9)

* > 50 = Major element (M); 50 − 10 = minor element (m); < 10 = trace element (t)

The major elements detected in precipitate P2 were O, Fe and S, with minor amounts of Al and trace amounts of Si, P and Cl (Table 6.2). High peak intensities for O, Fe and S suggest iron oxyhydroxide and oxide or iron sulphate minerals present in the surrounding solution (Persson and Lövgren, 1996; Karathanasis *et al.*, 1988). Minor and trace element peak intensities for Al, Si, P and Cl suggest adsorption or complexation of these elements to the mineral surface or adhesion of silicate particles to the precipitate (Table 6.2) (Winland *et al.*, 1991; Chapman *et al.*, 1983).

The major elements (O, Fe, Si) detected in the conglomerate material from precipitate P3 suggests the presence of iron oxyhyroxide and oxide or iron sulphate minerals with Si and Al adsorbed to the surface of the mineral (Table 6.2) (Chapman *et al.*, 1983). Peak intensities of the spindle shaped structures indicate high Si and O concentrations and suggest the presence of silica as biogenic opal in diatoms (Table 6.2) (Drees *et al.*, 1989).

The needle structures in precipitate P13 display major peak intensities for S and Ca and minor O concentrations suggesting gypsum as the mineral phase of the needle structures (Table 6.2) (Doner and Lynn, 1989). High S, O, Fe EDS peak intensities for the hexagonal structures covering the gypsum crystals indicate the deposition of an iron sulphate mineral similar to jarosite (Schwertmann and Taylor, 1989). The rounded feature in precipitate P13 had major Si, O and Al peak intensities indicating the presence of quartz or clay particles adhering to the sampled precipitate (Table 6.2).

EDS analysis of precipitate P15 indicates high peak intensities for the elements O, Fe and S suggesting the presence of iron oxyhydroxide and oxide or iron sulphate minerals in the precipitate. These minerals can act as sorbents for inorganic anions (Si), organic anions and cations such as Al (Table 6.2) (Persson and Lövgren, 1996; Karathanasis *et al.*, 1988; Schwertmann and Taylor, 1989).

6.3.2 Precipitate mineralogy

Precipitate powders were analyzed with XRD and the resulting diffractograms were presented in Figure 6.7. The precipitates were divided into two groups: 1) precipitates from the seepage area (P2, P2-3, P3); and 2) precipitates from AMD dam 7 and the two AMD drainage ditches (P9, P13, P15). Precipitate P2-3 and P3 from the seepage area displayed 4.26 Å and 3.34 Å quartz peaks and 3.06 Å and 5.06 Å jarosite peaks. No quartz or jarosite was present in precipitate P2 and the only mineral detected by XRD was ferrihydrite as two broad peaks at 2.54 Å and 1.51 Å (Figure 6.7).

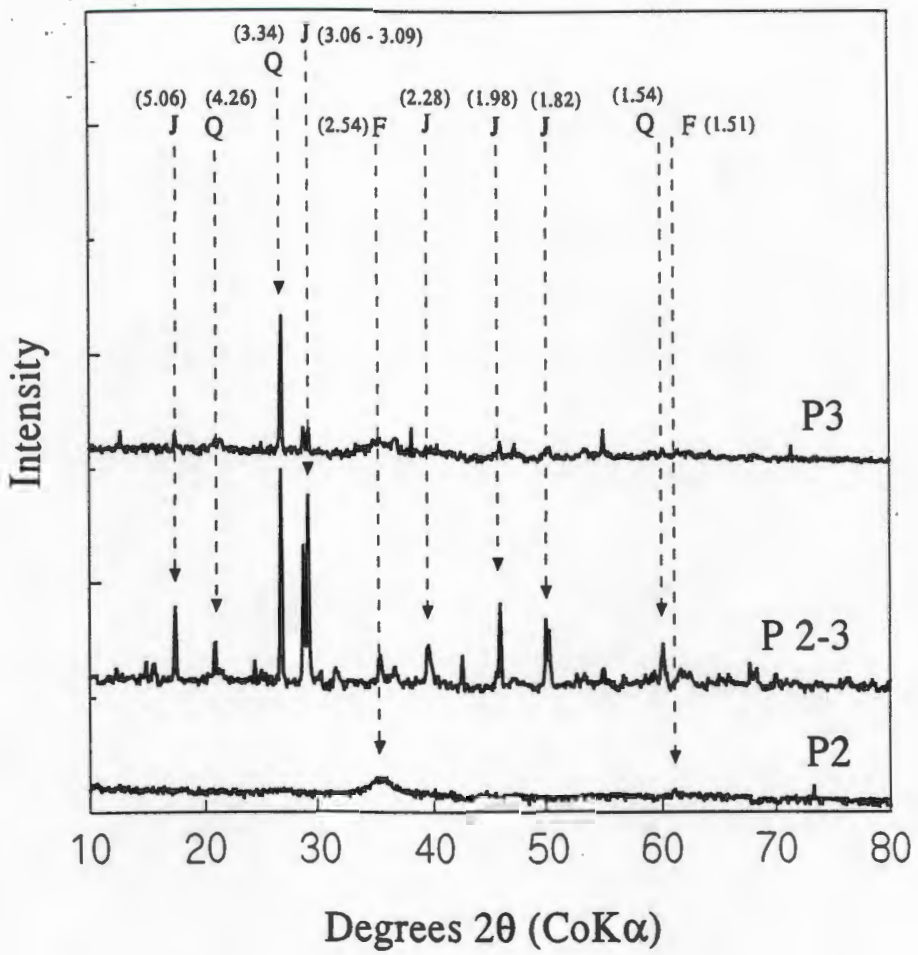

Figure 6.7 X-ray diffractograms of precipitates from the seepage area: P2 - precipitate from the outwelling point; P2-3 - precipitate from seepage area between outwelling point and V−notch 14; P3 - precipitate from V-notch 14. Peak locations are shown for: J = jarosite, Q = quartz, F = ferrihydrite. [*d* - spacings in Å are given in parentheses]

The X-ray diffractogram of the precipitate from the outwelling point (P2) suggests that ferrihydrite is the dominant mineral precipitating from upwelling iron-rich acidic waters at the outwelling point (Figure 6.7). Ferrihydrite is a wide spread and characteristic component of young Fe-oxide accumulations such as ochreous precipitates from ferriferous waters (Schwertmann and Taylor, 1989). Dried samples of ferrihydrite have Munsell hues ranging from 7.5YR to 2.5YR (Bigham *et al.* 1992) which compare well with the Munsell hues reported for the precipitate in Table 6.1. The sudden appearance of Fe^{2+}-bearing waters at the surface followed by rapid oxidation and hydrolysis of Fe^{2+} results in the deposition of ferrihydrite. The presence of an algae mat overlaying the outwelling point will assist this

oxidation process (Schwertmann and Fitzpatrick, 1992; Bigham *et al.*, 1992). Most of the mine drainage ferrihydrites examined to date have given very broad 2 to 4 peak XRD patterns similar to the XRD pattern for ferrihydrite in precipitate P2 (Figure 6.7 A) (Bigham *et al.*, 1992). Milnes *et al.* (1992) described the presence of minor goethite and poorly crystalline lepidocrocite peaks in AMD precipitates. Minor peaks of goethite and lepidocrocite may be present in the outwelling point sample P2, although ferrihydrite would dominates these peaks if present.

The diffractogram of precipitate P2-3 suggests that jarosite is the dominant mineral in seepage area (Figure 6.7). This area is characterized by AMD seepage from the upslope outwelling point through the surface material towards V-notch 14, eventually entering drainage ditch W9 and the Blesbokspruit. Jarosite was also detected in precipitate coatings (P3) from rocks at V-notch 14 (Figure 6.7). Bigham *et al.* (1992) describe jarosite as a common, straw coloured (Munsell hue of 2.5y) mineral in acid, high sulphate environments. Jarosite is typically a well crystalline material with narrow peak widths in its XRD pattern (Bigham *et al.*, 1992). This corresponds well with the XRD pattern of jarosite in precipitates P2-3 and P3. The presence of quartz peaks in the XRD pattern of precipitate P2-3 and P3 can be due to the entrapment of sand particles by the precipitate, amorphous silica and the presence of diatoms (Figures 6.5 and 6.7).

Precipitate from the AMD dam (P13) and the drainage ditch (P15) displayed strong quartz peaks at 4.26 Å and 3.34 Å (Figure 6.8). No quartz was detected in precipitate P9 (Figure 6.8). Jarosite peaks were detected in precipitate P9, P13 and P15 at 3.07 Å, 5.07 Å, 1.97Å and 2.27Å (Figure 6.8). Diffractograms from precipitate P9 and P13 indicated the presence of goethite at 4.19 Å and a possible ferrihydrite-goethite peak at 2.56-2.45 Å (Figure 6.8). Milnes *et al.* (1992) detected a similar mixture of poorly crystalline lepidocrocite, minor goethite and ferrihydrite in iron precipitates from waters contaminated by effluent from uranium mine spoils.

Goethite is considered a minor constituent of mine drainage precipitates with a typical yellowish brown colour (Munsell hue 7.5YR-10YR) and is associated with the minerals lepidocrocite and ferrihydrite (Schwertmann and Fitzpatrick, 1992; Bigham *et al.*, 1992).

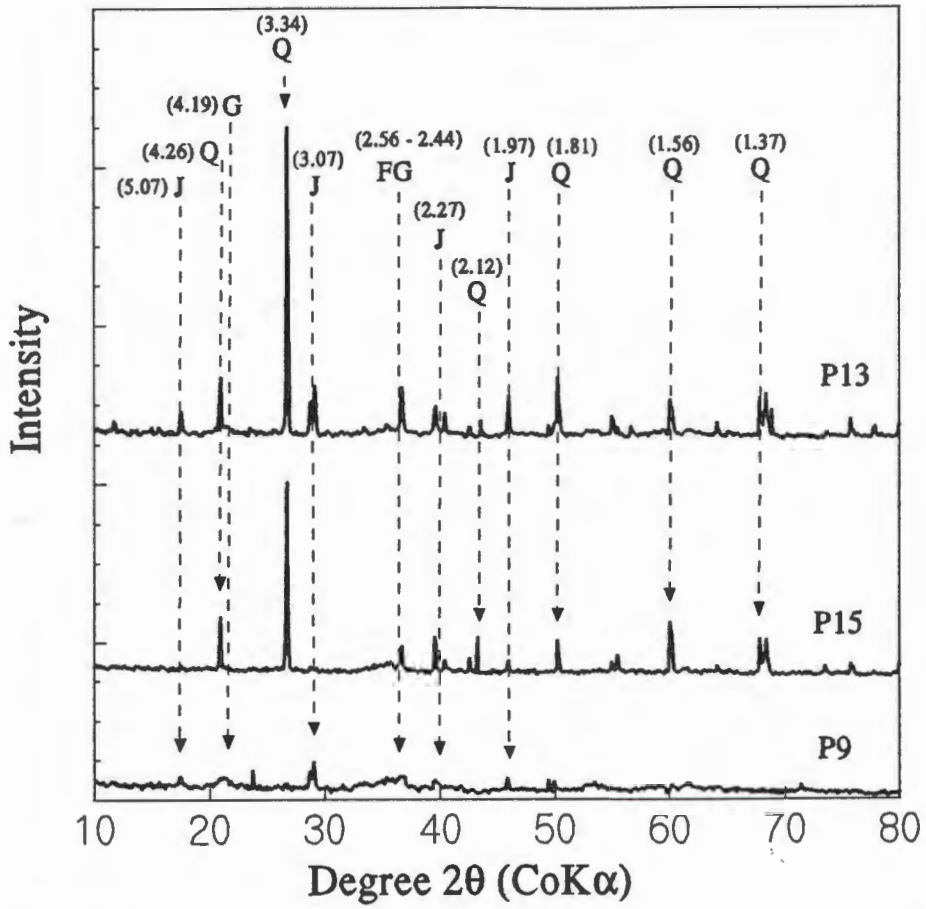

Figure 6.8 X-ray diffractograms of precipitate from an AMD dam and the two drainage ditches: P9 - precipitate from AMD drainage ditch draining AMD from the seepage area; P15 -precipitate from AMD drainage ditch draining AMD towards AMD dam 5 and 6; P13 - precipitate from AMD dam 6. Peak locations are shown for: J = jarosite, Q = quartz, F = ferrihydrite, G = goethite. [*d* - spacings in Å are given in parentheses]

The particular mineral species of iron oxyhydroxide, oxide and sulphate formed depends on environmental factors such as pH, Eh, temperature, water activity and solution composition. These factors may in turn influence the level of supersaturation, oxidation state of the Fe and the rate of Fe supply and crystal growth, which will determine the species of mineral formed (Schwertmann and Fitzpatrick, 1992). Therefore, Fe(III) oxide and sulphate minerals may serve as indicators to the type of environment in which they are formed. The presence of iron sulphate minerals such as jarosite is indicative of the oxidation of iron sulphide minerals (pyrite) and high sulphate concentration (Figure 6.9) (Doner and Lynn, 1989) in waters from the Blesbokspruit catchment.

Sulphate is the primary dissolved anionic species in all the acidic waters from the Blesbokspruit (Table 4.4), whereas total Fe concentrations are relatively low indicating that most of the dissolved Fe has precipitated through oxidation/hydrolysis reactions. Goethite has been implicated in the formation of outer sphere surface complexes with SO_4^{2-} which can influence the adsorption of trace elements (Persson and Lövgren, 1996; Winland *et al.*, 1991). Although goethite or amorphous $Fe(OH)_3$ control Fe levels in most natural waters (Stumm and Morgan, 1981), the control of dissolved Fe in acid sulphate-rich solutions appears to be more consistent with the solubility of the basic iron sulphate mineral jarosite (Karathanasis *et al.*, 1988). The strong supersaturation of the acidic waters with respect to jarosite (Figure 4.14 B in Chapter 4) supports the precipitation of jarosite from these waters. However, Bigham *et al.* (1992) and Karathanasis *et al.* (1988) noted that a poorly crystallized oxyhydroxysulphate Fe mineral with similar stoichiometry and greater solubility might control Fe^{3+} in solutions. This mineral was identified and characterized by Bigham (1992) and named schwertmannite. Schwertmannite was not detected by XRD analysis of precipitates from the Blesbokspruit. The pincushion crystal morphology of precipitate P15 and P2 (Figures 6.3B and 6.6), however, indicates the presence of this mineral. The strongest schwertmannite peak coincides with the strongest ferrihydrite line, making distinction difficult in poorly ordered materials (such as P2 and P15) with weak XRD patterns. There is enough sulphate present (Table 6.3) relative to the Fe to suggest that at least some of the material in precipitate P15 may consist of schwertmannite given the particle morphology (Figure 6.6). Schwertmannite was discovered in precipitates sampled from an AMD contaminated site at Steenkampskraal in the North Western Cape (Glendinning, 1997), creating a precedent for the existence of this mineral in South Africa. Therefore, it can be assumed that Fe concentrations in these waters are controlled by precipitation of jarosite, ferrihydrite, goethite and possibly schwertmannite.

Aluminium is present in high concentrations in the acid sulphate waters of the Blesbokspruit (Table 4.4 in Chapter 4). Nordstrom (1982) suggested that the mineral jurbanite $[Al(SO_4)(OH).5H_2O]$ may control aluminium concentrations. At low pH the waters may also be tending towards equilibrium with alunite $[(K_9Na)Al_3(SO_4)_2(OH)_6]$ (Table 6.5; and Figure 4.14 in Chapter 4) (Filipek *et al.*, 1987). However, no aluminium sulphate minerals were detected in the precipitate samples from the Blesbokspruit catchment, although small amounts of Al were detected in SEM-EDS and XRFS analyses of the precipitates. The suggestion by Nordstrom and Ball (1986) that Al behaves conservatively in waters with pH < 4.6 offers a possible explanation for the absence of aluminium sulphate mineral precipitation in the Blesbokspruit catchment.

6.3.3 Major and trace elemental composition of precipitates

The semi quantitative results of the major element analyses of the precipitates are summarized in Table 6.3.

Table 6.3 Results of the XRFS analysis for major elements in precipitates sampled in the Blesbokspruit catchment.

Elements/oxides in weight %	Precipitate P2	P2-3	P3	P9	P13	P15
SiO_2	2.1	35	20	6.5	62	46
TiO_2	0.02	0.42	0.28	0.12	0.33	0.18
Al_2O_3	4.3	7.4	6.7	2.9	3.1	1.6
Fe_2O_3	79	37	65	81	20	40
MgO	0.02	0.09	0.18	0.01	0.12	0.01
CaO	0.06	0.12	0.06	0.02	0.4	0.02
Na_2O	0.12	1.0	0.31	0.25	0.34	0.03
K_2O	0.06	2.01	0.61	0.83	0.59	0.1
BaO	0.003	0.03	0.02	0.01	0.01	0.01
P_2O_5	1.2	0.06	0.16	0.05	0.03	0.03
SO_3	9	11	6.5	8.5	5.3	6.3
Cl	0.22	0.08	0.1	0.1	0.05	0.08
H_2O	nd	nd	nd	nd	nd	nd
% orcanic C*	0.50	nd	nd	nd	nd	nd

* determined with the Walkley Black method; nd = not determined

The precipitates are Fe rich, and also contain high but variable concentrations of Si, Al and SO_3. The high Fe content is due to the precipitation of Fe oxyhydroxide, oxides and Fe sulphate minerals (Figures 6.7 and 6.8 and Table 6.3). The SiO_2 content of precipitates P3 (Table 6.3) is due to the presence of quartz and diatoms (Figure 6.5) (Drees *et al.*, 1989). The decrease in Fe_2O_3 and consequent increase in SiO_2 (Fig 6.10) content in the precipitates suggests a dilution of Fe_2O_3 by SiO_2 (Winland *et al.*, 1991). Although attempts were made to selectively sample the secondary precipitates, all samples contained clay and sand particles. Carlson and Schwertmann (1981) reported

that the sorption of dissolved silica to natural poorly ordered ferrihydrite suppressed the ordering of the ferrihydrite and also inhibited the transformation of ferrihydrite to goethite. The formation of Si−O−Fe bonds stabilizes ferrihydrite which may offer an explanation for the presence of ferrihydrite as the dominant mineral at the outwelling point (P2) (Figure 6.7).

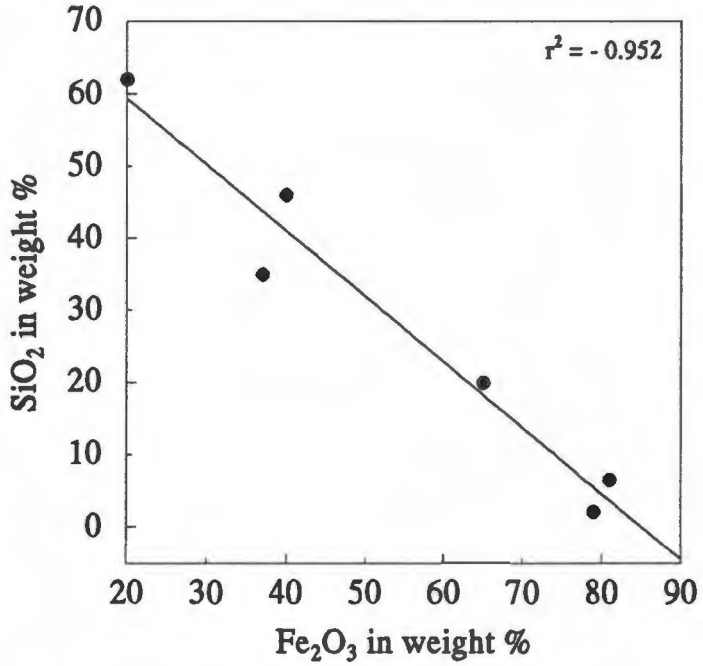

Figure 6.10 Plot of the relationship of Fe_2O_3 with SiO_2 in the Blesbokspruit precipitates. Note the strong negative correlation.

The SO_3 content in precipitate P2-3, P3, P13, P9 (Table 6.3) is either due to the presence of the metal sulphate minerals such as jarosite in P2-3, P3, P13 and P9 and gypsum in P13 (Figures 6.4, 6.7 and 6.8) or is coprecipitated as sulphate to the iron mineral surface (Winland *et al.*, 1991; Persson and Lövgren, 1996; Chapman *et al.*, 1983). The deposition of jarosite as the dominant mineral in precipitate P2-3 (Figure 6.7) explains the elevated potassium and sodium content in this sample (Table 6.3) (Chapman *et al.*, 1983). Positive correlations between SO_3 and K_2O (r_2 = 0.68), Na_2O (r_2 = 0.67) confirmed the precipitation of Na and K jarosite which explains the non-concervative behaviour of Na relative to Cl as discussed in Chapter 4 (Figure 4.12). Sulphate was used as an indicator for the presence of jarosite in the sediments. A plot of K_2O, Na_2O, SO_3 in the precipitates (Figure 6.11) shows fluctuations of K_2O, and Na_2O according to the proportions of jarosite in the samples (Figures 6.7 and 6.8). The low CaO content relative to the SO_3 content indicates trace amounts of gypsum present in the samples.

The presence of gypsum was confirmed by SEM analysis of precipitate P13 (Figure 6.4). The occurrence of phosphate in the precipitates can be due to the adsorption of phosphate to iron oxides (Schwertmann and Taylor, 1989).

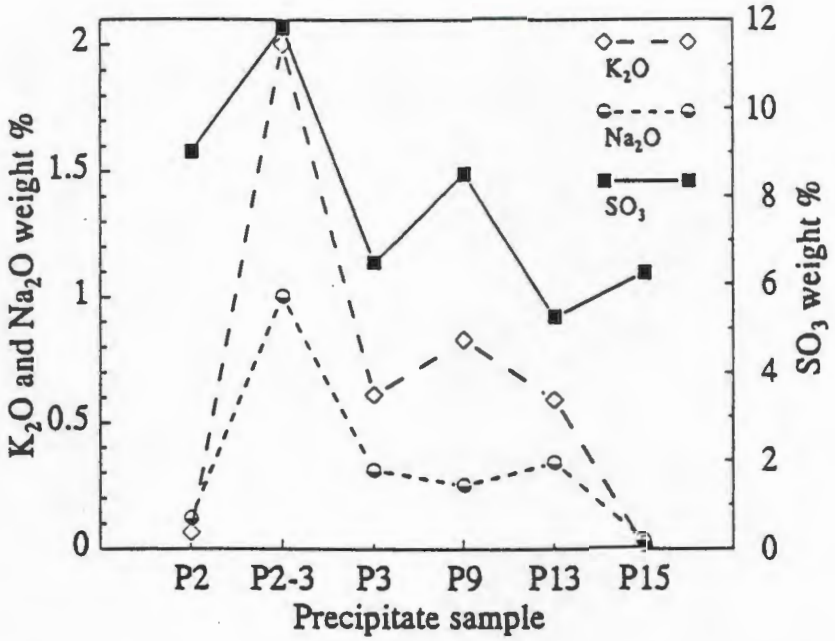

Figure 6.11 The plot of K_2O, Na_2O and SO_3 values in precipitates from the Blesbokspruit. Jarosite was detected in samples P2-3, P3, P9 and P13.

No aluminium minerals were detected in the precipitates, therefore, the high aluminium content of the precipitates can be due to adsorption of Al to iron hydroxide and oxide minerals in the precipitate and for the presence of aluminosilicate clay detrital matter (Chapman *et al.*, 1983; Winland *et al.*, 1991).

The quantitative results of trace element analyses of the precipitates are summarized in Table 6.4. Numerous studies have demonstrated that trace elements including metals adsorb to the surface of iron hydroxide and oxide minerals (Winland *et al.*, 1991; Schwertmann and Fitzpatrick, 1992; Millward and Moore, 1982; Johnson, 1986). Zinc, copper, nickel, manganese, chrome and lead are enriched (Table 6.4) in the precipitates in comparison to their concentrations in the associated waters (Table 4.4). The accumulation of Zn, Cu, Ni, Mn, Cr and Pb in the precipitates can be due to adsorption to iron oxyhydroxides (Millward and Moore, 1982; Schwertmann and Fitzpatrick, 1992; Milnes *et al.*, 1992). The higher trace element content of precipitate P2, P2-3, P9, and P13 in comparison with the trace element content of precipitate P2 and P15 (Table 6.4 and Figure 6.11) indicates that jarosite acts as

an important trace element accumulator.

Table 6.4 Results of the XRF spectrometry analysis for trace elements in precipitates sampled in the Blesbokspruit catchment.

Trace elements in mg/kg	Precipitate P2	P 2-3	P3	P9	P13	P15
Zn	17	44	53	34	18	8.5
Cu	9.4	20	50	39	14	12
Ni	<0.8	19	11	<0.8	15	7.1
V	800	62	123	263	198	178
Cr	69	112	570	104	93	81
Mn	37	149	276	34	178	54
Co	6.4	7.3	10	4.0	4.0	2.4
Mo	0.3	0.9	3.3	0.8	2.4	0.9
Rb	3.5	96	24	31	37	5.3
Pb	19	19	24	76	20	4.1
U	1.1	2.4	3.6	4.2	0.7	<0.9

The accumulation of V in precipitate P2 is due to the release of V from coal on oxidation of pyrite and the subsequent association of V with algae matter and Fe minerals covering the outwelling point (Edwards *et al.*,1995; Förstner and Wittmann, 1979). Molybdenum content of the precipitates was low (< 2.5 mg/kg) (Table 6.4). Molybdenum originates from coal and the associated shales. The oxidation of Mo containing minerals yields mainly molybdate (MoO_4^{2-}) and at pH <4.2 molybdate ions become protonated forming monomeric $HMoO_4^-$ and H_2MoO_4. Mobilised anions are readily co-precipitated by organic matter and Mo is strongly adsorbed on hydrous ferric oxides (Edwards *et al.*, 1995; Förstner and Wittmann, 1979).

A strong correlation between rubidium and K_2O (Figure 6.12) similar to the sediment Rb/K_2O correlation discussed in Chapter 5 (Figure 5.12) was noted in the precipitates. This is due to the ability of Rb to substitute for K in mineral structures (Heier and Billings, 1970). It was therefore not surprising to detect high Rb concentrations in the precipitates containing jarosite (P2-3, P3, P9, P15) An average K/Rb ratio of 173 was calculated for the precipitates. This

is higher than the average K/Rb ratio of 145 calculated for the sediments (Chapter 5, subsection 5.35).

The high Pb content of precipitate P9 suggests the possible sorption of Pb to goethite present in this sample (Schwertmann and Taylor, 1989). The accumulation of Pb in precipitate P9 has, however, no effect on the Pb concentration of the associated waters (Table 4.4).

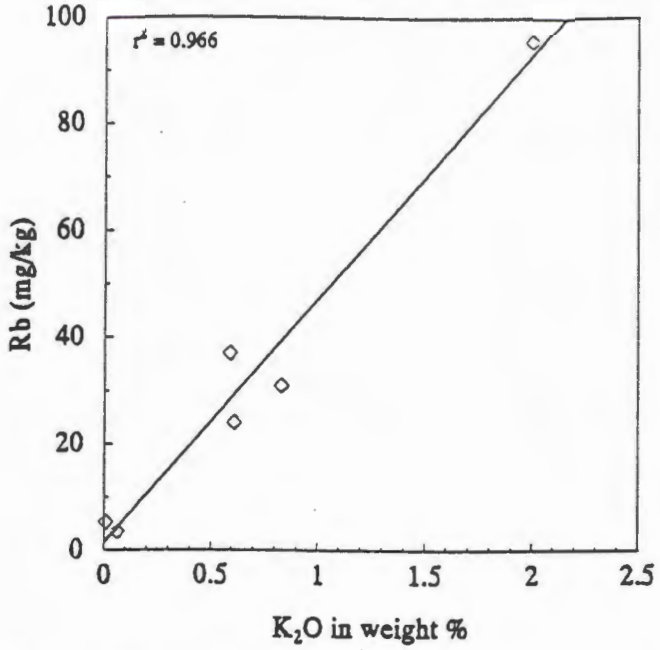

Figure 6.12 The Rb/K_2O correlation plot of precipitates from the Blesbokspruit catchment.

6.3.4 Mineral saturation

Mineral saturation indices for the water samples associated with the sampled precipitates were calculated, assuming iron as Fe^{3+}, using the MINTEQA2 speciation model as described in Chapter 4 (Subsection 4.2.2.11). The results are summarized in Table 6.5.

The calculated saturation indices for the water samples associated with the precipitates show that the waters are in approximate equilibrium with gypsum, jurbanite, cupricferite and alunite (sample W2, W13, W15). The waters are saturated with respect to nontronite, jarosite, goethite and quartz and undersaturated with respect to ferrihydrite and alunite (sample W3 and W9) (Table 6.5). The predictions of MINTEQA2 for the saturation indices compares well with the minerals found in the precipitates with the exception of ferrihydrite and goethite. Analyses of the precipitates indicate minor amounts of goethite in precipitates P9, P13 and P15 and no detectable goethite in the remaining precipitates (Figure 6.7). Ferrihydrite was, however,

present in precipitate P2 (Figure 6.7 (A)) although predicted as being undersaturated by the MINTEQA2 speciation model.

Table 6.5 Mineral saturation indices in water samples taken from the seepage area

Mineral name	Chemical formula	Saturation index				
		W2	W3	W9	W13	W15
GYPSUM	$CaSO_4.2H_2O$	-0.62	-0.55	-0.52	-0.62	-0.47
QUARTZ	SiO_2	1.0	1.2	0.99	1.3	1.2
JURBANITE	$AlOHSO_4$	0.060	-0.036	-0.034	0.35	0.28
ALUNITE	$(K,Na)Al_3(SO_4)_2(0H)_6$	-0.89	-1.6	-1.8	-0.096	-0.71
NA-NONTRONITE	$(Fe,Al)Si_2O_5(OH).nH_2O$	11	11	10	12	12
JAROSITE NA	$NaFe_3(SO_4)_2(OH)_6$	5.0	4.5	4.7	4.2	-0.59
JAROSITE K	$KFe_3(SO_4)_2(OH)_6$	7.1	6.7	6.7	6.2	5.9
JAROSITE H	$HFe_3(SO_4)_2(OH)_6$	4.6	3.9	4.6	3.9	7.9
FERRIHYDRITE	$5Fe_2O_3.9H_2O$	-1.6	-1.7	-1.9	-1.4	-1.3
GOETHITE	α-FeO(OH)	2.4	2.1	2.1	2.5	2.6
CUPRICFERITE		-0.074	-1.2	-0.84	0.21	0.3

Note: The water samples corresponding to the respective precipitate samples are: W2 = P2; W3 = P3; W9 = P9; W13 = P13; W15 = P15. Fe was entered as Fe^{3+}.

The massive precipitation of ferrihydrite and the possibility of a disordered schwertmannite phase on top of the outwelling point could explain the undersaturation of the sampled waters with respect to ferrihydrite. Caution should, however, be exercised in interpretation of saturation index data. Positive values of saturation do not necessarily indicate that a mineral is actively precipitating. The absence of suitable nucleation sites or slow crystallisation kinetics can prevent precipitation. Therefore, saturation index calculations only give a guide to those solids which might precipitate (Chapman *et al.*, 1983).

6.4 Conclusions

Electron images and EDS data of the precipitate samples suggest the presence of diatoms, gypsum, iron oxihydroxides or oxides and iron sulphates. The major elements in the different precipitate samples suggest the deposition of iron oxide or iron sulphate minerals with coprecipitation of other elements. Diffractograms of the individual precipitates identified the minerals quartz, ferrihydrite and jarosite and indicated the presence of minor amounts of the mineral goethite. The crystal morphology of precipitates P2 and P15 suggests the presence of schwertmannite which could however not be confirmed by XRD analysis. Trace element analysis of the precipitates suggested the accumulation of trace elements by adsorption and

coprecipitation to the iron oxide and iron sulphate minerals present in the precipitate.

Saturation index calculations of waters associated with the sampled precipitates from the Blesbokspruit catchment predict the precipitation of jarosite from these sulphate rich waters. Analyses of precipitates from the Blesbokspruit confirm the presence of jarosite in four of the six precipitate samples. No alumino sulphate or hydroxide minerals were detected in the precipitate samples which compares well with the equilibrium state of these minerals in the associated waters. The mineral gypsum, predicted to be in equilibrium with the solution, was however, identified in precipitate P13.

The precipitation of iron oxide and sulphate minerals from the acidic waters of the Blesbokspruit removes and immobilises dissolved iron from the associated waters and concurrently accumulates trace metals from these waters. The adsorption and coprecipitation of trace metals by ochreous precipitates in the Blesbokspruit has little effect on the trace element content of the associated waters. The low pH (pH 2.6 - 2.8) in the waters associated with the analyzed precipitates counteracts the adsorption of dissolved metals such as Pb to ochreous precipitates. Changes in environmental parameters such as pH, Eh, temperature, AMD flow rate and surface water run-off can affect the precipitation and dissolution of minerals and would be reflected in varying concentrations of specific elements in the Blesbokspruit waters.

Seasonal analysis (dry and wet cycle) of the Blesbokspruit catchment precipitates and the associated waters should be undertaken. This could determine seasonal variations in the formation of precipitates and coprecipitated trace elements. Further XRD analysis of precipitates P15 and P2 is recommended to determine the presence of schwertmannite in these precipitates.

Chapter 7

ANALYSIS OF ALGAE GROWING IN ACID MINE DRAINAGE

7.1 Introduction

The precipitation of minerals from acid mine drainage might be catalysed by abiotic or biotic processes. A good example is the mineral ferrihydrite which is formed by rapid precipitation from Fe-rich surface waters and is often associated with bacterial remains in the form of extracellular envelopes or encrustations (Bigham *et al.*,1992).

Many species of algae are known to tolerate AMD resulting from coal mining. Stevens *et al.* (1989) observed green algae (Chlorophyta) with rust-coloured or dark brown encrustations on their cell walls. Metallic components present in these encrustations were composed of the metals found in the surrounding AMD (Stevens *et al.*, 1989). Numerous authors (Brady *et al.*, 1994; Gale and Wixson, 1979; Stevens *et al.*, 1989; Crist. *et al.*, 1988) proposed that algae may play a role in metal attenuation in AMD. Filipek *et al.* (1987) described metal-organic interactions in aquatic environments contaminated with AMD. Varying amounts of metals were found in aquatic vegetation and algae (Schoonbee *et al.*, 1995; Stevens *et al.*, 1989). Some of this variability might be due to the different types of algae or might relate to the pH of the waters (Filipek *et al.*, 1987).

Different species of algae were present in the Blesbokspruit waters. Intensive algae growth was visible at the outwelling point and in the seepage area. Algae encrustations were visible as a spongy precipitate at the outwelling point and the seepage area. Algae were also seen in AMD collection ditches, AMD dams and the Blesbokspruit itself. The ability of these specific algae to interact with metals in their immediate habitat was, therefore, investigated. Although these studies were of a preliminary nature, they could give an indication of the effects of algae populations on metal rich solutions.

The objectives of the analyses were the following:

1) To determine the type of algae found at this specific AMD site.

2) To investigate interactions between dissolved metals and algae.

7.2 Materials and Methods

7.2.1 Sampling

Green coloured algae were collected from the outwelling point centre, and black coloured algae were collected from the edge of the outwelling point (Figure 7.1 and Figure 7.2). The algae were collected using a small shovel, placed in plastic jars and stored at room temperature. Algae were sensitive to anaerobic conditions in closed jars and were, therefore, stored in jars open to the atmosphere (Podge, 1997).

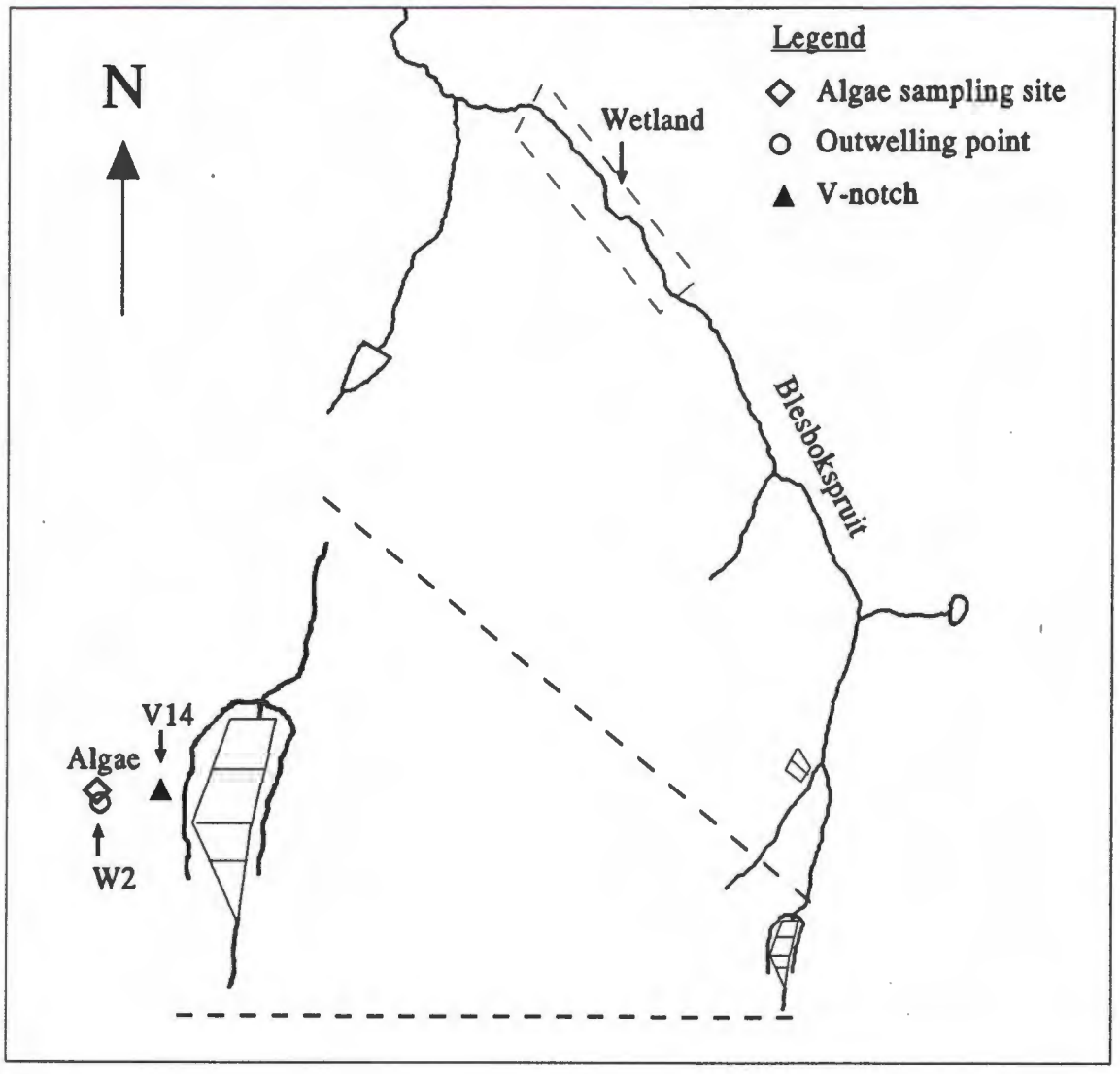

Figure 7.1 Algae were collected from the seepage area in close proximity to the outwelling point

(A)

(B)

Figure 7.2 (A) Algae sampling area at the outwelling point with clearly visible green and black algae. Rust-red encrustations are visible. (B) Algae in the Blesbokspruit (not sampled).

7.2.2 Analysis

7.2.2.1 Identification

Sample identification was undertaken by Mrs. J. Podge from the Department of Botany at the University of Cape Town, Dr. G.M. Lokhorst of the Rijksherbarium/Hortus Botanicus in Leiden (Netherlands) and Dr. D.M. John of the Department of Botany at the Natural History Museum in London. Initial identification of the two algae samples presented some problems due to the destruction of chloroplasts as a result of the transport in closed containers (Podge, 1996).

7.2.2.2 XRFS elemental analysis

X-ray fluorescence spectrometry (XRFS) was used to determine major and trace elements in the algae samples. This was done to give an indication of adsorbed or biomineralised elements.

Two algae samples were analyzed for major and trace elements using a Philips X'Unique II (1480/00/10) X-ray spectrometer. Powder briquettes were prepared by taking 8 g oven dried algae matter (- 300 mesh) and mixing with 2 grams of wax (Hoechst wax C) as a binding agent. No backing material was used and the mixture was pressed at approximately 10 tons pressure into 30 mm diameter powder briquettes. The samples required a dilution correction factor of 1.25 in the determination of the analyzed element concentrations.

The trace elements determined quantitavly were: Zn, Cu, Ni, V, Mn, Mo, Zr, Co, Cr, Pb, Y, Sr, Rb and Th (Appendix VI). Semi-quantitative major element determination using powder briquettes was done to give an indication of high, medium, or low levels of the respective element in the sample. The major elements determined were: SiO_2, TiO_2, Al_2O_3, Fe_2O_3, Na_2O, MnO, MgO, CaO, K_2O, BaO, SO_3, Cl and P_2O_5.

7.2.2.3 SEM analysis

Qualitative elemental analysis of two algae samples was done using scanning electron microscopy (SEM). This analysis generated electro optical and element areal and point distributions from the algae.

To examine the samples the Leica Stereoscan 440 SEM with a 3 lens system was used at a vacuum of 10^{-4} - 10^{-6} torr. A lanthanum hexaboride (LaB_6) crystal was used with a 15kV source giving 6-10 times more brightness than tungsten and better resolution. The maximum resolution with this instrument was 3nm. The instrument used secondary electrons for imaging, backscatter for atomic number determination, and X-rays for elemental analyses. Stevens *et al.* (1989) describe the use of SEM and energy dispersive spectroscopy (EDS), also known as X-ray micro analysis, in studies of metal accumulation in algae. Three types of analyses were done: 1) Image and size analyses; 2) point elemental analyses; 3) elemental scan analyses of a selected area.

Scanning electron microscopy analysis was done on the green and black algae sample. Samples were mounted on SEM stubs and frozen with liquid nitrogen. The specimens were then fractured and carbon coated (Stevens *et al.*, 1989). The fractured carbon coated filaments were then photographed and the cell wall, cytoplasm and background were analyzed for element content.

7.3 Results and discussion

7.3.1 Algae identification

Two algae species were identified. The green algae were of the genus *Mougeotia* and the black algae were of the genus *Microspora* (Podge, 1996).

The genus *Mougeotia* algae belong to the algae division Chlorophyta (green algae) and are found in the class Zygnematophyceae (van den Hoek *et al.*, 1995). The Zygnematophyceae are diverged from the green algae by loss of flagellate cells. Many of the commonest freshwater algae form part of this class. They are usually found as unbranched, unattached filaments of cylindrical cells (Pickett-Heaps, 1975). *Mougeotia* species algae were described in acid mine waters by Stevens *et al.* (1989) and Kepler (1988). Stevens *et al.* (1989) noted rust coloured encrustations containing iron and

sulphur on *Mougeotia* species. Kepler (1988) found that algae collected from natural and man-made wetlands receiving AMD contained populations of the genus *Mougeotia* which accumulated manganese and iron.

The algae belonging to the genus *Microspora* are known to tolerate acid mine waters and have been described in low pH environments with rust coloured smooth cylindrical iron and sulphur containing encrustations (Stevens, 1989). The *Microspora* belong to the algae division Chlorophyta and are found in the class Ulotrichales. The class Ulotichales have unbranched filaments with or without basal-distal differentiation. *Microspora* has bead-like chloroplast and a cell wall containing two overlapping sections (Prescott, 1984). The presence of *Mougeotia* and *Microspora* species algae in the AMD saturated seepage area suggested possible interactions of these algae species with elements in these high TDS waters.

7.3.2 SEM analysis of the algae

The transverse section of the *Mougeotia* sp. algae shows a ± 13 μm diameter algae cell with a 0.5 - 1 μm thick cell wall (Figure 7.3). A longitudinal section of the *Mougeotia* sp. algae shows the same (1 μm) thick cell wall and the filamentous nature of the algae (Figure 7.4).

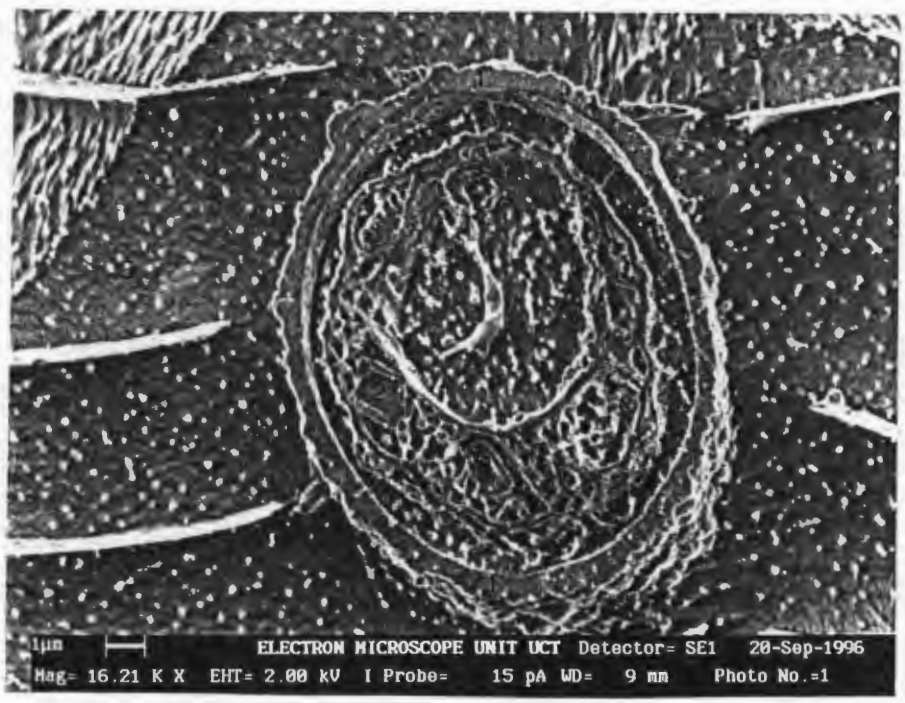

Figure 7.3 An SEM image of a transverse section of the *Mougeotia* sp. algae. [1 = cell wall; 2 = cytoplasm; 3 = surrounding material (background)] Bar = 1μm.

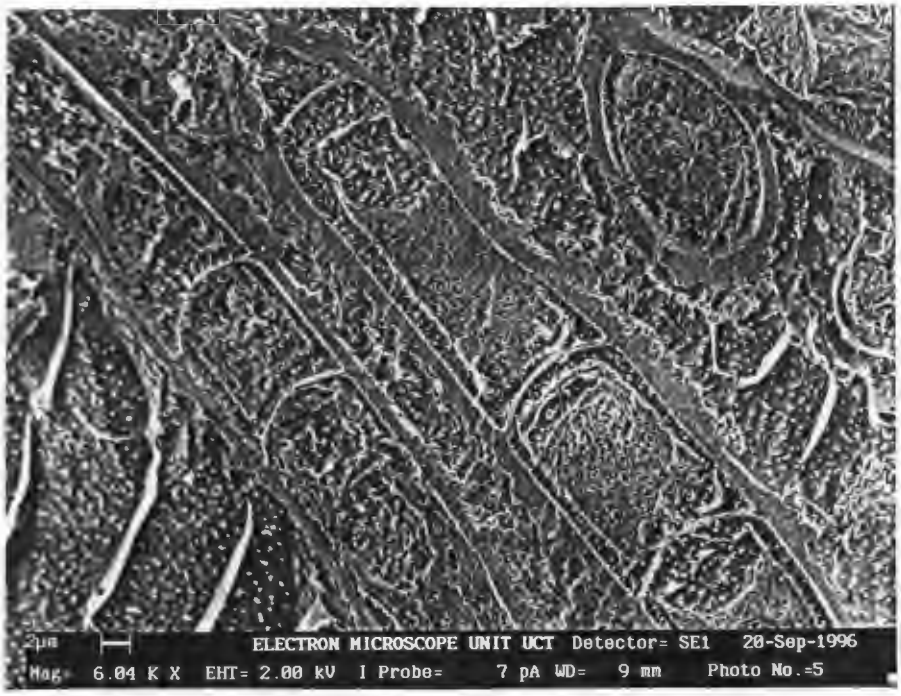

Figure 7.4 An SEM image of a longitudinal section of the *Mougeotia* sp. algae. Bar = 2μm

The transverse section of the *Microspora* sp. algae shows a ±6 μm diameter algae cell with 0.3 - 0.5 μm thick cell wall (Figure 7.5). The images of the two algae samples clearly demonstrate differences in cell size and cell wall thickness.

Figure 7.5 An SEM image of the transverse section of the *Microspora* sp. algae. [1 = cell wall; 2 = cytoplasms; 3 = surrounding material (background)] Bar = 1μm

Point elemental analysis of the cell wall, cytoplasm and the material surrounding the algae cells (background) was done to determine the intensities of different elements in these areas (Table 7.1). Qualitative X-ray analysis gave an indication of either high or low elemental concentrations in the cell wall, cytoplasm or background. The ratios of the Kα1 peak intensities were used to indicate relative elemental concentrations (EDS spectra derived from *Mougeotia* and *Microspora* sp. algae, Appendix V).

Table 7.1 Elements detected in algae samples

Sample description	A comparison of element Kα peak ratios in descending order of peak intensities*
Green algae: *Mougeotia* sp.	
Cell wall	O, Fe, S, Zn, Al (100 : 15 : 9 : 6 : 3)
Cytoplasm	O, Zn, S, P (100 : 5 : 3 : 3)
Background	O, S (100 : 2)
Black algae: *Microspora* sp.	
Cell wall	O, Fe, S, Zn, Al, Si (100 : 12 : 6 : 5 : 4 : 2)
Cytoplasm	O, Zn, S, Fe, K (100 : 4 : 3 : 1 : 1)
Background	O, S (100 : 2)

* > 50 = Major element (M); 50 – 10 = minor element (m); < 10 = trace element (t)

The presence of oxygen (O) as the major element in all three areas can be explained by the presence of water (H_2O) and organic matter in the samples. Trace amounts of sulphur (S) in all the areas analyzed can be due to the high concentration of sulphate in the aquatic environment of the algae and the presence of sulphur in thiol-compounds in organic matter. Both algae specimens contained minor amounts of Fe and trace amounts of Al and Zn in their cell walls (Table 7.1). The presence of Fe, Zn and Al in the cell walls of the algae has been described in the literature (Brady et al., 1994; Gale and Wixon, 1979; Deighton and Goodman, 1995). Trace amounts of Zn were detected in the cytoplasms of both algae species and *Microspora* sp. contained trace amounts of Fe in its cytoplasma. No Mn was detected in the analyzed cell compartments.

Several processes of metal removal by algae have been described. These include the

physical trapping of suspended mineral particles and subsequent chemical binding (chelation) to the numerous anionic sites within the cell walls of algae. The polymers which constitute the cell wall are rich in phosphoryl, carboxyl, aromatic and hydroxyl groups which bind cationic metals (Brady *et al.*, 1994). The presence of microorganisms that grow epiphytically on green algae filaments can result in mineral depositions on the algae cell walls (Stevens, 1989). Algae can accumulate metals by intracellular uptake which will contribute to the total accumulation of metals (Brady *et al.*, 1994). The X-ray micro analysis data of the cytoplasm, however, suggest no intracellular Fe uptake by *Mougeotia* sp. and low intracellular accumulation of Fe by *Microspora* sp. (Table 7.1). Both species accumulate Fe, Zn and Al in their cell walls and Zn in their cytoplasm.

The presence of metal encrustations on algae was noticed in SEM analysis of precipitate collected at the outwelling point (Figure 7.6). The encrustations appeared to form smooth rust coloured cylinders around single cells or algae filaments. Similar iron rich encrustations have been documented on *Microspora* sp. (Stevens, 1989).

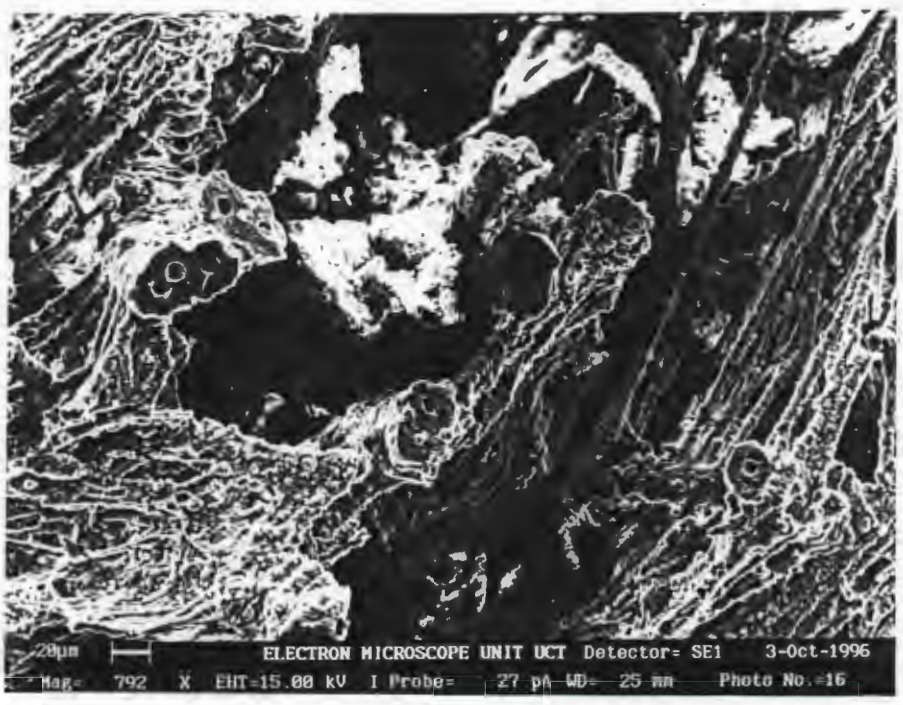

Figure 7.6 An SEM image of iron-rich encrustations on algae sampled as precipitate crust at the AMD outwelling point.

7.3.3 XRFS analysis of algae

Algae were analyzed for major and trace elements by XRFS. The results are summarised in Table 7.2.

Table 7.2 Semi-quantitative major and qualitative trace element analyses of algae from the seepage area in the Blesbokspruit catchment. An analysis of precipitate (P2) and water (W2) from the outwelling point was included to compare with the analysis of the algae from the same outwelling point.

Sample	Major elements in weight %											
	Fe_2O_3	TiO_2	BaO	CaO	K_2O	Cl	SO_3	P_2O_5	SiO_2	Al_2O_3	MgO	Na_2O
Green algae (*Mougeotia* sp.)	77	0.02	0.004	0.68	0.51	0.98	9.8	2.3	3.5	1.9	0.35	0.75
Black algae (*Microspora* sp.)	40	0.14	0.13	3.9	3.1	2.9	12	0.06	3.0	1.5	0.44	1.1
Precipitate P2	79	0.02	0.003	0.06	0.06	0.22	9	1.2	2.1	4.3	0.02	0.12

	Trace element concentrations in mg/kg algae												
	Zn	Cu	Ni	V	Cr	Mn	Co	Mo	Zr	Y	Sr	Rb	Th	Pb
Green algae (*Mougeotia* sp.)	91	52	9.0	797	81	221	13	0.4	7.1	17	4.9	14	2.0	4.3
Black algae (*Microspora* sp.)	230	14	63	79	337	789	33	0.5	17.1	22	33	165	2.3	6.5
Precipitate 2	17	9.4	<0.8	800	69	37	6.4	0.3	7	4.5	1.4	3.5	3.7	19
W2 (in mg/ℓ)*	2.74	0.96	1.77	nd	nd	11.5	nd	nd	nd	nd	nd	nd	nd	1.51

nd = not determined

* Water sample from outwelling point

High concentrations of Fe_2O_3 were detected in both algae samples (Table 7.2). The *Mougeotia* species algae contain 77 weight % Fe_2O_3 and the *Microspora* species 40 weight % Fe_2O_3. This suggests that *Mougeotia* sp. accumulate nearly double the amount of Fe_2O_3 than *Microspora* sp. (Table 7.2). *Microspora* sp. were found to contain 6 fold higher CaO and K_2O concentrations than *Mougeotia* sp. (Table 7.2). X-ray fluorescence spectrometry of *Mougeotia* sp. showed an approximately 40 fold higher P_2O_5 concentration in these algae in comparison to *Microspora* sp.

Ghiorse and Ehrlich (1992) describe the ability of microorganisms, including algae and bacteria, to promote iron and manganese precipitation. The high concentrations of Fe_2O_3 in these algae suggests that the algae participate in either passive or active biomineralisation of Fe from the surrounding Fe-rich acidic waters. This corresponds well with the presence of Fe detected in the cell walls of both algae species. The mineral ferrihydrite was the dominant mineral found on XRD analysis of precipitate crust from the algae covered outwelling point (Figure 5.7(A) in Chapter 5). Schwertmann and Fitzpatrick (1992) describe microorganism assisted abiotic formation of ferrihydrite in surface environments. In the case of filamentous algae non enzymatic oxidation of Fe^{2+} and Mn^{2+} may be the result of a localized rise in pH resulting from CO_2 consumption and the production of O_2 during photosynthesis. These reactions take place in algae mats which retain the oxidation products precipitated in the form of Fe and Mn minerals. This oxidation might encrust the microorganisms responsible for their formation (Schwertmann and Fitzpatrick, 1992). The very small and poorly ordered crystals of ferrihydrite generate a large surface area making this phase highly reactive and many environmentally important solutes such as heavy metals adsorb on the surface of these particles (Schwertmann and Fitzpatrick, 1992; Förstner and Wittmann, 1979).

The major elements in the algae samples were compared to the major elements detected in the outwelling point precipitate (Table 7.2). Similarities in concentrations Fe_2O_3, S, BaO and TiO_2 were evident from the comparison of the *Mougeotia* sp. algae with the precipitate. *Microspora* sp. major element composition differed considerably from that of the precipitate. This could be due to the sampling of *Microspora* on the edge of the outwelling point or different metal accumulation mechanisms.

Deighton and Goodman (1995) describe the ability of acid tolerant algae to accumulate Al in their cytosol as an enzyme activator and in their cell surface. Aluminium oxide concentration in the algae samples (Table 7.2) can be due to either adsorption of Al to the already present precipitate or to the accumulation of Al due to the increased availability of the metal at low pH (Mcbride, 1994).

Large differences in trace element concentrations, with the exception of Mo, Nb, U, Y, Th and Pb, were noticed on comparison of the trace element data of the two algae species (Table 7.2). Both species contained high concentrations of Zn, Cr, V, and Mn (Table 7.2).

High concentrations Zn were detected in both algae species with a 2.5 fold increase in Zn concentration in *Microspora* sp. (Table 7.2). Most coals have Zn concentrations in the

range of 5-300 ppm which can be mobilised as a result of pyrite oxidation (Swaine, 1990). The high concentrations Zn detected in the algae indicate an accumulation of Zn by algae matter from acidic waters containing low concentrations of Zn (Table 4.4, Sample W2). Zinc is present as Zn^{2+} in solutions with pH < 7.7 and can, therefore, adsorb to negatively charged algae cell walls or coprecipitate with iron minerals (Kiekens, 1995; Förstner and Wittmann, 1979). Zinc plays essential metabolic roles in plants and is relatively active in biochemical processes. Zinc was detected in the cell walls and cytoplasm of both algae species (Table 7.1) and the values determined by XRFS for both algae sp. (Table 7.2) fall within the range of 65 to 350 ppm of grass grown in old mining areas (Kabata-Pendias and Pendias, 1985). Zinc-copper antagonistic interactions have been observed in plants in which the uptake of one element was competitively inhibited by the other (Kabata-Pendias and Pendias, 1985). This antagonistic interaction was seen on comparing Zn/Cu ratios of the two algae species. The Zn/Cu ratio of *Mougeotia* sp. and *Microspora* sp. were 1.7 and 16.4, respectively (from Zn and Cu values in Table 7.2). This data suggests that the uptake of Zn inhibits the uptake of Cu in *Microspora* sp. algae which may indicate the same carrier sites in adsorption mechanisms of both metals in this algae species (Kabata-Pendias and Pendias, 1985).

Microspora sp. algae have 4 times higher Cr concentrations than *Mougeotia* sp. (Table 7.2). Most coals have Cr values in the range 80 - 340 ppm (Swaine, 1990). Brady *et al.* (1994) and Förstner and Wittmann (1979) documented chrome accumulation by algae with 0.45 ± 0.38 ppm Cr detected in *Ulva* sp. green algae. The presence of high concentrations of chrome associated with the algae can be due to adsorption of Cr to algae cell walls or coprecipitation with Fe minerals (Schwertmann and Fitzpatrick, 1992).

Both algae samples contained high concentrations manganese with 3.5 fold higher concentrations of Mn in *Microspora* sp. (Table 7.2). Accumulation of Mn in algae was documented by Filipeck *et al.* (1987), Mann *et al.* (1992) and Brady *et al.* (1994). Manganese is an abundant metal in the earth's crust and concentrations in coal range from 5-300 ppm (Swaine, 1990). Skinner and Fitzpatrick (1992) suggest that microorganisms are involved in the biomineralization of Mn. The high concentration of Mn in the black algae (*Microspora* sp.) could be due to either internal or external biomineralization of Mn. Adsorption and coprecipitation of Mn to algae cell walls and Fe minerals could be another reason for high Mn concentrations in the algae.

Very high vanadium concentrations were detected in *Mougeotia* sp. algae (Table 7.2). Precipitate from the outwelling point contained similar V concentrations to those detected in *Mougeotia* sp. algae (Table 7.2). Vanadium is ubiquitous in the lithosphere

and most coals have V values in the range 2-100 ppm (Swaine, 1989). The uptake of V by plant roots was found to be highly dependant on pH. Vanadium occurs as VO^{2+} under acidic conditions such as those found in the Blesbokspruit waters. This species (VO^{2+}) is more readily adsorbed by plant roots than VO_3^- and HVO_4^{2-} which are the predominant V species in neutral and alkaline solutions (Kabata-Pendias and Pendias, 1985).High vanadium values can be due to V being an essential micronutrient for certain green algae (Arnon and Wessel, 1953) and the presence of Al and ferric ions which can cause precipitation of V. Vanadium (III) has a similar ionic radius to Fe (III) and may replace it in Fe minerals resulting in accumulation of V in Fe minerals (Edwards *et al.*, 1995).

The rubidium content of *Mougeotia* sp. is lower than the reported Rb range of 25 to 250 ppm (in dry ash of algae), whereas *Microspora* sp. Rb values fall into the reported range (Heier and Billings, 1970). Rubidium apparently is easily taken up by plants, as are other monovalent cations. It may partly substitute for K sites, but cannot substitute for K metabolic roles, therefore, in high concentrations, it is toxic to plants (Kabata-Pendias and Pendias, 1985; Bennet, 1993). Green algae (*Mougeotia* sp.) had a K/Rb ratio of 320 and the K/Rb ratio of black algae (*Microspora* sp.) was 155. The fact that rubidium competes with K in adsorption processes (Heier and Billings, 1970) and the presence of K in the cytoplasm of *Microspora* sp. (Table 7.1) might explain the lower K/Rb ratio in these algae. No toxicity symptoms were detected in the algae at the outwelling point and further downstream in the Blesbokspruit. The difference in K/Rb ratios can also indicate different metal accumulation mechanisms, or different rates of metal accumulation of the two algae species.

The available data indicates that trace metals are accumulated in algae growing in the the acidic waters (W2) welling out of the underground mine workings. The Zn, Cu, Ni, Mn, and Pb content of both algae species is enriched with respect to the concentrations of these elements in the waters sampled at the outwelling point (Table 7.2). The data in Table 7.2 suggests some similarities between the major and trace metal content of the algae and the ferrihydrite-rich precipitate (P2) formed as algae encrustations at the outwelling point. Similar Fe_2O_3, TiO_2, SO_3, Cr, Mo, Zr and V concentrations appear for *Mougeotia* sp. algae and precipitate P2. These similarities may indicate that *Mougeotia* sp. algae could be the primary algae species involved in the formation of the outwelling point precipitate.

7.4 Conclusion

Visually and physiologically different algae were collected from the low pH, metal rich, AMD outwelling point in the Blesbokspruit catchment. Differences in the major and trace element concentrations in the two algae species confirm two different algae species and suggest two different element accumulation mechanisms.

The analysis of fresh algae cell walls and cytoplasm showed accumulation of Fe, Zn and Al in the cell walls which correlates with the presence of high concentrations of Fe_2O_3, Zn and Al_2O_3 in whole cell XRFS analysis. The presence of iron rich encrustations on dead algae matter suggest metal deposition mechanisms on cell wall material. The biochemical pathway of these mechanisms is unknown. Metal deposition in the form of iron precipitates (encrustations), such as ferrihydrite, can result in the coprecipitation of different elements (metals). The presence of a build up of precipitate at the outwelling point suggests continuous deposition of precipitate in the presence of dead encrusted and living algae.

The ability of algae to grow in an acidic environment containing high concentrations of dissolved salts, and the accumulation of metals by these algae populations, suggests that metal encrusting algae might play a role in metal removal from AMD. Ultimately, the significance of these algae in the treatment of AMD will depend on metal removal efficiencies and algae density. However, the available data suggest that these algae can, to a certain extent, attenuate the concentration of metals in these waters.

Further and more extensive investigations concerning metal uptake by the algae species growing in the Blesbokspruit catchment can be recommended. A more quantitative analysis of metal accumulation by the same species of algae from different sampling sites in the Blesbokspruit catchment may give a better indication of the metal accumulating ability of these organisms.

Chapter 8

SUMMARY AND RECOMMENDED FUTURE WORK

8.1 Summary

Weathering of sulphide minerals exposed to the atmosphere in collapsed and abandoned underground coal mine workings in the Witbank area (R.S.A.) results in the generation of acid mine drainage. The Blesbokspruit catchment collects and drains such acidic waters originating in the surrounding abandoned coal mines. The catchment contains AMD seepage points, AMD drainage ditches, AMD retention dams, a small wetland and inflow from an uncontaminated tributary downstream of the wetland.

Oxidation of pyrite in the underground workings results in the formation of high concentrations of dissolved iron and sulphate, high acidity and low pH. Algae and orange Fe precipitates are ubiquitous at the outwelling point, seepage area and drainage ditches. Yellowish efflorescences were noted on the edges of some AMD retention dams. A 50% reduction of the stream acidity and TDS occurred in the wetland, with only minor changes in acidity, pH and TDS after inflow of unbuffered clean waters from an uncontaminated tributary.

Water, sediment, precipitate and algae were sampled in the Blesbokspruit catchment. Twenty one water samples were collected from: 1) the AMD outwelling point and seepage area; 2) the AMD collection ponds and drainage ditches; 3) the contaminated Blesbokspruit stream; and 4) an uncontaminated tributary. Sediments were taken from: 1) the AMD outwelling point; 2) the AMD retention ponds; 3) the Blesbokspruit streambed; and 4) the wetland in the Blesbokspruit catchment. Ochreous precipitates were visible in the Blesbokspruit catchment. Precipitates were, therefore, collected from the outwelling point and seepage area, from one AMD retention pond, and the AMD drainage ditches. Algae were ubiquitous in the Blesbokspruit catchment. Dense algae growth occurred at the outwelling point and two algae samples were, therefore, collected from this site.

All the water samples were analyzed for pH, acidity and Eh, anion and total elemental content. The top horizons of the sediment samples were analyzed for exchangeable acidity,a exchangeable cations, % organic carbon and sediment cation exchange capacity. Sediment mineralogy and major and trace element content were determined with XRD

and XRFS, respectively. Scanning electron microscopy and EDS were used for electro-optical and elemental analysis of the precipitate samples. Precipitate mineralogy was determined with XRD and major and trace element content with XRFS. The sampled algae species were identified and their major and trace element content was determined by XRFS analysis.

The analysis of water samples from the upper Blesbokspruit shows that these low pH waters are highly enriched with sulphate, chloride, aluminium, sodium, calcium, magnesium, iron, manganese and lead. The water would, therefore, be unsuitable for domestic, agricultural and recreational purposes. Fluctuations in metal concentrations in the Blesbokspruit waters suggests changes in metal mobility occurring as a result of metal attenuation mechanisms such as dilution, dissolution-precipitation and adsorption. Calculated speciation of the metal-rich Blesbokspruit waters indicated that the minerals jarosite and goethite could precipitate from these waters.

Electron images and EDS data of the precipitate samples suggest the presence of diatoms, iron oxihydroxides or oxides and iron sulphates and gypsum. Jarosite and goethite were indeed detected in precipitates associated with the Blesbokspruit waters. The presence of large quantities of the mineral ferrihydrite (calculated as being undersaturated) at the algae-covered outwelling point suggest an algae/microorganism mediated iron precipitation mechanism at this site. The pincushion crytal morphology of precipitates P15 and P2 closely resembles the crystal morphology of schwertmannite. Schwertmannite may thus be present at the outwelling point and in AMD drainage ditch W15 although its characteristic XRD lines were not detected. Therefore, the available data suggest that iron mobility in the acidic Blesbokspruit waters is controlled by dissolution/precipitation mechanisms. Sorption of trace elements and sulphate by the precipitates occurs but it has not affected the concentrations of these elements in the associated waters.

The mineralogy of the Blesbokspruit sediments indicates the presence of clay minerals (kaolinite, mica and feldspar) which are potential source of cations. Outwelling AMD seeps through the clay rich surface of the seepage area and is collected in AMD retention ponds constructed from the local clay rich soil. The dissolution of clay minerals in the seepage area and AMD retention ponds, by the acidic waters, increases the already elevated Al concentration and acidity of the Blesbokspruit waters. This results in the absence of fish and amphibian life forms in the upper Blesbokspruit catchment. However, no alumino-sulphate or hydroxy mineral phases were detected in the associated sediments and precipitates, which corresponded well with the predicted undersaturated

state of alumino-sulphate and hydroxy minerals in these acidic waters. Reduction of the Al concentration after passing through a small wetland and as result of inflow from an uncontaminated water tributary suggests dilution and adsorption as Al attenuation mechanisms in the Blesbokspruit.

The attenuation of Zn, Cu, Ni and Mn concentrations in the waters flowing through the wetland correlated well with an increase in the concentrations of these elements in the wetland sediment suggesting the immobilization of Zn, Cu, Ni and Mn by adsorption mechanisms. The high organic carbon content of the wetland sediments, although partly saturated by aluminium, provides enough sorption capacity to attenuate trace metal concentrations. The low pH waters downstream of the wetland contain dissolved Al, Fe, Mn and Pb concentrations which are higher than their allowed target water quality values, indicating that not all elements were removed by sorption in the wetland. However, toxic concentrations of lead and elevated concentrations of Al, Fe and Mn remained in the Blesbokspruit.

Algae are ubiquitous in the acid waters, and analysis of two algae species sampled at the algae–precipitate–covered outwelling point suggest that algae material catalyses the precipitation of ferrihydrite at this specific site. Two different algae species (*Mougeotia* and *Microspora* sp.) were identified. Minor amounts of Fe and trace amounts of Zn and Al were detected in the cell walls of both algae species indicating the presence of metal accumulating mechanisms. The V, Cr, Zn and Mn content of whole algae indicated accumulation of these elements by the algae, however, accumulation of these metals had a minimal effect on their concentrations in the associated waters.

The hypothesis stated at the beginning of this thesis is thus partly supported by the data reported in the thesis. The precipitation of secondary minerals affected only the mobility of dissolved iron whereas adsorption to organic matter in the wetland played a major role in reducing aluminium and trace element quantities in the Blesbokspruit.

8.2 Suggested future work and recommendations

The data presented in this thesis suggest certain topics on which additional work should be done to gain a better understanding of the metal mobility in the Blesbokspruit catchment. These topics are:

1. Analysis of the Blesbokspruit waters downstream of the wetland up to the confluence with the Klipspruit. This would give an indication of changes in pH , acidity, TDS, and especially Al and Pb in the downstream regions of the Blesbokspruit.
2. Seasonal analysis of Blesbokspruit waters and associated precipitates could detect possible seasonal fluctuations of metal attenuating mechanisms.
3. The quantitative evaluation of algae metal accumulation mechanisms and the applicability of this data to the use of algae as metal scavengers from acidic metal-rich solutions.
4. Further investigation of the precipitates P2 and P15 to prove the presence of schwertmannite in these precipitates

The construction of small artificial wetlands either downstream or upstream of the existing wetland is recommended. These wetlands will further attenuate metal concentrations and increase the water quality of the Blesbokspruit waters. The liming of the Blesbokspruit waters may be another alternative in immobilising metallic elements in these waters. The analysis of water, sediment and precipitate samples from rivers in the Olifants river catchment area such as the Riet, Steenkool, Klein Olifants, and upper Olifants and their smaller tributaries is recommended. This will give an indication of the coal mining related contamination of the greater Olifants River catchemnt.

8 REFERENCES

Allison J.D., Brown D.S., and Novo-Gradac K.J. (1991) *MINTEQA2/PRODEFA2, A Geochemical Assessment Model for Environmental Systems (EPA/600/3-91/021)*, United States Environmental Protection Agency, Athens, GA.

Alpers C.N., Blowes D.W., Nordstrom D.K., and Jambor J.L. (1994) Secondary minerals and acid mine water. In: Jambor J.L. and Blowes D.W. (Eds.) *Short Course Handbook on Environmental Geochemistry of Sulfide Mine-Wastes*, Mineralogical Association of Canada, pp. 59 - 102.

Arnon D.J. and Wessels G. (1953) Vanadium as an essential element for green plants, *Nature*, 172, 1039 – 1040.

Becker B., Graff M., and Naveke R. (1993) Initiation of bacterial sulphate reduction in acidic overburden dumps. *SA Mining, Gold and Base Minerals*, August, 45 - 46.

Bennet W.F. (1993) Plant nutrient utilization and diagnostic plant symptoms. In: Nutrient *Deficiencies & Toxicities in Crop Plants*, APS Press, The American Phytopathological Society, Minnesota, pp. 1 – 7.

Bennetts R. (1992) Mastering the monoliths. *SA Mining, Gold and Base Minerals*, June, 15 - 21.

Bigham J.M., Schwertmann U. and Carlson L. (1992) Mineralogy of precipitates formed by the biogeochemical oxidation of Fe(II) in mine drainage. In: Skinner H.C.W. and Fitzpatrick R.W. (Eds.) *Biomineralization Processes of Iron and Manganese*, Catena Supplement 21, pp. 219 - 232.

Bigham J.M. (1994) Mineralogy of ochre deposits formed by sulphide oxidation. In: Jambor J.L. and Blowes D.W. (Eds.) *Short Coarse Handbook on Environmental Geochemistry of Sulfide Mine-Wastes*, Mineralogical Association of Canada, pp. 103 - 131.

Bosch C. (1990) Distribution and Inhibition Of Iron - Oxidizing Bacteria in Relation to Acid Drainage from Gold and Coal Mine Dumps in the South Eastern Transvaal, In: *M.Sc. Thesis*, University of Stellenbosch.

Bouska V. (1981) Mineralogy of coal seams and Contents of chemical elements in coals and coal ashes. In: *Geochemistry of Coal*, Elsevier Scientific Publishing Company, Amsterdam, pp. 164 - 188.

Brady D., Letebele B., Duncan J.R. and Rose P.D. (1994) Bioaccumulation of metals by *Scenedesmus*, *Selenastrum* and *Chlorella* algae, *Water SA*, 20, 213 - 218.

Bullock S., Bell F.G. and Marsh C.A. (1996) The environmental impacts associated with a coal mine in the Witbank coal field. *Personal communications*.

Carlson L. and Schwertmann U. (1981) Natural ferrihydrites in surface deposites from Finland and their association with silica, *Geochim. Cosmochim. Acta*, 45, 421 - 429.

Chapman B. M., Jones D.R. and Jung R.F. (1983) Processes controlling metal ion attenuation in acid mine drainage streams, *Geochim. Cosmochim. Acta*, 47, 1957 - 1973.

Crist R.H., Oberholser K., Schwartz D., Marzoff J., Ryder D. and Crist D.R. (1988) Interactions of metals and protons with algae, *Environ. Sci. Technol.*, 22, 755 - 760.

Deighton N. and Goodman B.A. The speciation of metals in biological systems. In: Ure A.M. and Davidson C.M. (Eds.) *Chemical Speciation in the Environment*, Blackie Academic & Professional, London, pp. 307 - 331.

Department of Water Affairs and Forestry (1995) Geohydrological Assessment of old Mine Workings in the Blesbokspruit Catchment. In: *Report no.: 2938/1023/1/E, Water Quality Management Series*, May.

Department of Water Affairs and Forestry (1994) The proposed water pollution control works at abandoned coal mines in the Witbank and Ermelo districts. In: *Department of Water Affairs and Forestry Report*, Director-General: Water Affairs and Forestry (Branch: Water Affairs), pp. 1 - 17.

Department of Water Affairs and Forestry (1996) *South African Water Quality Guidelines*, Volumes 1 - 7.

Doner H. and Lynn W.C. (1989) Carbonate, halide, sulfate and sulfide minerals. In: Dixon J.B. and Weed S.B. (Eds.) *Minerals in Soil Environments (2nd Edition)*, Soil Science Society of America, Madison, Wisconson, pp. 279 - 323.

Drees R.L., Wilding L.P., Smeck N.E. and Senkayi A.L. (1989) Silica in soils: Quartz and dissolved silica polymorphs. In: Dixon J.B. and Weed S.B. (Eds.) *Minerals in Soil Environments (2nd Edition)*, Soil Science Society of America, Madison, Wisconson, pp. 913 - 931.

Drever J.I. (1988) Redox equilibria. In: *The Geochemistry of Natural Waters (2nd ed.)*, Prentice Hall, New Jersey, pp. 281 - 308.

Duncan A.R., Erlank A.J. and Betton P.J. (1984) Analytical techniques and database descriptions, *Spec. Publ. geol. Soc. S. Afr.*, 13, Appendix 1, 389 - 395.

Edwards R., Lepp N.W. and Jones K.C. (1995) Other less abundant elements of potential environmental significance. In: Alloway B.J. (Ed.) *Heavy Metals in Soils*, Blackie Academic & Professional, London, pp. 306 - 351.

Elsokkary I.H. (1992) Trace metals in the sediments and waters: Case study from Egypt. In: Vernet J.-P. (Ed.) *Impact of Heavy Metals on the Environment*, Elsevier, Amsterdam, pp. 355 - 379.

Evangelou V.P. and Zhang Y.L. (1995) A Review: Pyrite oxidation mechanisms and acid mine drainage prevention, *Crit. Rev. Environ. Sci. Technol.*, 25, 149 - 199.

Evans L.J. (1989) The chemistry of metal retention by soils, *Environ. Sci. Technol.*, 23, 1046 - 1056.

Falcon R.M.S. and Snyman C.P. (1986) Composition of coal. In: *An Introduction To Petrography: Atlas of the Petrographic Constituents in the Bituminous Coals of Southern Africa*, The Geological Society of South Africa, Johannesburg, pp. 1 - 27.

Filipek L., Nordstrom D.K. and Ficklin W.H. (1987) Interaction of acid mine drainage with waters and sediments of the West Squaw Creek in the West Shasta Mining District, California, *Environ. Sci. Technol.*, 21, 388 - 396.

Förstner U. and Wittmann G.T.W. (1979) *Metal Pollution in the Aquatic Environment*, Springer Verlag, Berlin.

Gale N.L. and Wixon B.G. (1979) Removal of heavy metals from industrial effluent by algae. In: *A Society for Industrial Microbiology Symposium: Biological Recovery of Metals from Wastewater.*, 20, pp. 259 – 273.

Garrels R.M. and Christ (1965) Measurement of Eh and pH. In: *Solutions Minerals and Equilibria*, Freeman Cooper & Company, California, pp. 122 - 144.

Gee G.W. and Bauder J.W. (1986) Particle-size analysis. In: Klute A. (Ed.) *Methods of Soil Analysis Part 1 - Physical and Mineralogical Methods*, Soil Science Society of America, Madison, Wisconson, pp. 383 - 409.

Ghiorse W.C. and Ehrlich H.L. (1992) Microbial biomineralization of iron and manganese. In: Skinner H.C.W. and Fitzpatrick R.W. (Eds.) *Biomineralization Processes of Iron and Manganese*, Catena Supplement 21, pp. 75 - 99.

Glendinning J. (1997) Factors influencing the mobility of uranium, thorium and rare earth elements at the Steenkampskraal monazite mine. North Western Cape, In: *M.Sc. Thesis*, University of Cape Town.

Gould W.D., Bechard G. and Lortie L. (1994) The Nature and Role of Microorganisms in the Tailings Environment. In: Jambor J.L. and Blowes D.W. (Eds.) *Short Coarse Handbook on Environmental Geochemistry of Sulfide Mine-Wastes*, Mineralogical Association of Canada, pp. 103 - 131.

Hattingh L. (1996) Water just as valuable as gold. *The Argus*, June 17, pp. 7.

Heier K.S. and Billings G.K. (1970) Rubidium. In: Wedepohl K. (Ed.) *Handbook of Geochemistry II-2*, Springer-Verlag, Berlin, pp. [37-B-1] - [37-N-1].

Heinrich K.F.J. (1986) Mass adsorption coefficients for electron probe microanalysis. In: Brown J.B. and Packwood R.H. (Eds.) *Proc. 11th Int. Congress on X-ray Optics and Microanalysis*, London, Canada.

Horowitz A.J., Elrick K.A. and Callender E. (1988) The effect of mining on the sediment-trace element geochemistry of cores from the Cheyenne river arm of lake Oahe, South Dakota, U.S.A., *Chemical Geology*, 67, 17 - 33.

Hsu P. (1989) Aluminium oxides and oxyhydroxides. In: Dixon J.B. and Weed S.B. (Eds.) *In: Minerals in Soil Environments (2nd Edition)*, Soil Science Society of America, Madison, Wisconson, pp. 331 - 371.

Jenkinson D.S. (1988) Soil organic matter and its dynamics. In: Wild A. (Ed.) *Russel's Soil Conditions and Plant Growth*, Longman Scientific & Technical, New York, pp. 564 - 608.

Jambor J.L. (1994) Mineralogy of sulfide-rich tailings and their oxidation products. In: Jambor J.L. and Blowes D.W. (Eds.) *Short Coarse Handbook on Environmental Geochemistry of Sulfide Mine-Wastes*, Mineralogical Association of Canada, pp. 59 - 102.

Johnson C.A. (1986) The regulation of trace element concentrations in river and estuarine waters contaminated with acid mine drainage: the adsorption of Cu and Zn on amorphous Fe oxyhydroxides, *Geochim. Cosmochim. Acta*, 50, 2433 - 2438.

Johnson C.A. and Thornton I. (1987) Hydrogeological and chemical factors controlling the concentrations of Fe, Cu, Zn, and As in a river system contaminated by acid mine drainage, *Wat. Res.*, 21, 359 – 365.

Kabata-Pendias A. and Pendias H (1985) *Trace Elements in Soils and Plants*, CRC Press Inc., Boca Raton, Florida, pp. 33 - 66.

Karathanasis A.D., Evangelou V.P. and Thompson Y.L. (1988) Aluminium and iron equilibria in soil solutions and surface waters of acid mine watersheds, *J. Environ. Qual.*, 17, 534 - 542.

Karlsson S., Allard B. and Håkansson K. (1988) Chemical characterization of stream-bed sediments receiving high loadings of acid mine effluents, *Chemical Geology*, 67, 1 - 15.

Kelly M. (1988) Acid mine drainage in the aquatic environment. In: *Mining and the Freshwater Environment*, Elsevier Applied Science, London, pp. 33 - 42.

Kennedy J.A. and Powell H.K. (1986) Colorimetric determination of Al(III) with Chrome Azurol S and the reactivity of hydrolysed Al species, *Anal. Chim. Acta.*, 18, 329 - 333.

Kepler D.A. (1988) An overview of the role of algae in the treatment of acid mine drainage. In: *Proceedings of a conference sponsored by The American Society for Surface Mining and Reclamation: Mine Drainage and Surface Mine Reclamation*, Vol I: Mine Water and Mine Waste, Bureau of Mines Information Circular, United States Department of the Interior, pp. 286 - 290.

Kiekens L. (1995) Zinc. In: Alloway B.J. (Ed.) *Heavy Metals in Soils*, Blackie Academic & Professional, London, pp. 284 - 303.

Krauskopf K.B. Distribution of the elements. In: *Introduction to Geochemistry*, McGraw-Hill Book Company, New York, pp. 577 - 598.

Kunze G.W. and Dixon J.B. (1986) Pretreatment for mineralogical analysis. In: Klute A. (Ed.) *Methods of Soil Analysis Part 1 - Physical and Mineralogical Methods*, Soil Science Society of America, Madison, Wisconson, pp. 91 - 99.

Lumsdon D.G. and Evans L.J. (1995) Predicting chemical speciation and computer simulation. In: Ure A.M. and Davidson C.M. (Eds.) *Chemical Speciation in the Environment*, Blackie Academic & Professional, London, pp. 86 - 131.

Lundgren D.G. and Silver M. (1980) Ore leaching by bacteria, *Ann. Rev. Microbiol.*, 34, 263 - 283.

Mann H., Tazaki K., Fyfe W.S. and Kerrich R. (1992) Microbial accumulation of iron and manganese in different aquatic environments: An electron optical study. In: Skinner H.C.W. and Fitzpatrick R.W. (Eds.) *Biomineralization Processes of Iron and Manganese*, Catena Supplement 21, pp. 102 - 115.

McBride M.B. (1994) *Environmental Chemistry of Soils*, Oxford University Press, New York.

McGrath S.P. (1995) Chromium and nickel. In: Alloway B.J. (Ed.) *Heavy Metals in Soils*, Blackie Academic & Professional, London, pp. 152 - 174.

McKenzie R.M. (1989) Manganese oxides and hydroxides. In: Dixon J.B. and Weed S.B. (Eds.) *In: Minerals in Soil Environments (2nd Edition)*, Soil Science Society of America, Madison, Wisconson, pp. 439 – 461.

McLean E.O. (1982) Soil pH and lime requirement. In: Page A.L. (Ed.) *Methods of Soil Analysis (Part 2: Chemical and Microbiological Properties)*, Soil Science Society of America, Madison, Wisconson, pp. 199 - 223.

Millward G.E. and Moore R.M. (1982) The adsorption of Cu, Mn, and Zn by iron oxyhyroxides in model estuarine solutions, *Water Res.*, 16, 981 - 985.

Milnes A.R., Fitzpatrick R.W., Self P.G., Fordham A.W. and McLure S.G. (1992) Natural iron precipitates in a mine retention pond near Jaribu, Northern Territory, Australia. In: Skinner H.C.W. and Fitzpatrick R.W. (Eds.) *Biomineralization Processes of Iron and Manganese*, Catena Supplement 21, pp. 233 - 261.

Munsell (1992) *Munsell Soil Colour Charts*, Macbeth Color, New York.

Murray K. and Wade P. (1996) Checking anion – cation charge balance of water quality analyses: Limitations of the traditional method for non – potable waters, *Water SA*, 22, 27 - 32.

Nelson D.W and Sommers L.E. (1982) Total carbon, organic Carbon, and organic matter. In: Page A.L. (Ed.) *Methods of Soil Analysis (Part 2: Chemical and Microbiological Properties)*, Soil Science Society of America, Madison, Wisconson, pp. 539 - 577.

Nordstrom D.K. (1982) The effect of sulfate on aluminium concentrations in natural waters: some stability relations in the system Al_2O_2-SO_3-H_2O at 293K, *Geochim. Cosmochim. Acta*, 46, 681 - 692.

Nordstrom D.K. and Ball J.W. (1986) The geochemical behaviour of aluminium in acidified surface waters, *Science*, 232, 54 - 56.

Nordstrom D.K. and Munoz J.L. (1994) *Geochemical Thermodynamics*, Blackwell Scientific Publications, Boston.

Pettijohn F.J. (1975) The texture of sediments. In: *Sedimentary Rocks*, Harper & Row Publishers, New York, pp. 30 - 35.

Persson P. and Lövgren L. (1996) Potentiometric and spectroscopic studies of sulfate complexation at the goethite-water interface, *Geochim. Cosmochim. Acta*, 60, 2789 - 2799.

Pickett-Heaps J.D. (1975) *Green Algae*, Sinauer Associates Inc. Publishers, Sunderland, Massachusetts, pp. 167 - 467.

Pierzynski G.M., Thomas J.T., and Vance G.F. (1994) Trace Elements. In: *Soils and Environmental Quality*, Lewis Publishers, Boca Raton. pp. 167 - 184.

Plummer C.C and McGeary D. (1979) Geological resources. In: *Physical Geology*, Wm. C. Brown Company Publishers, Dubuque, pp. 417 - 442.

Podge J. (1996) *Personal communications*, Botany Department, University of Cape Town, Cape Town, South Africa.

Potts P.J. (1987) Inductively coupled plasma – atomic emission spectroscopy. In: *A Handbook of Silicate Rock Analysis*, Blackie Academic & Professional, London, pp. 153 - 189.

Prescott G.W. (1984) *The Algae: A Review*, Otto Koeltz science Publishers, Koenigstein, Germany, pp. 37 – 135.

Pulford I.D. (1991) A review of methods to control acid generation in pyritic coal mine wastes. In: Davies M.C.R. (Ed.) *Land Reclamation: An End to Dereliction?*, Elsevier Applied Science, pp. 269 - 278.

Rhoades J.D. (1982) Cation exchange capacity. In: Page A.L. (Ed.) *Methods of Soil Analysis (Part 2: Chemical and Microbiological Properties)*, pp. 149 - 157.

Schoonbee H.J., Adendorf A, De Wet L.M., De Wet L.P.D., Fleischer C.L., van der Merwe C.G., van Eeden P.H. and Venter A.J.A. (1995) The occurrence and accumulation of selected heavy metals in fresh water ecosysytems affected by mine and industrial polluted effluent. In: *Report to the Water Research Commision*, Report No. 312/1/96, pp 41 - 87.

Schwertmann U. and Fitzpatrick R.W. (1992) Iron minerals in surface environments. In: Skinner H.C.W. and Fitzpatrick R.W. (Eds.) *Biomineralization Processes of Iron and Manganese*, Catena Supplement 21, pp. 7 - 30.

Schwertmann U. and Taylor R.M. (1989) Iron oxides. In: Dixon J.B. and Weed S.B. (Eds.) *Minerals in Soil Environments (2nd Edition)*, Soil Science Society of America, Madison, Wisconson, pp. 379 - 438.

Singer P.C. and Stumm W. (1970) Acid mine drainage: The rate-limiting step, *Science*, 167, 1121 - 1123.

Skinner H.C.W and Fitzpatrick R.W. (1992) Iron and manganese biomineralization. In: Skinner H.C.W. and Fitzpatrick R.W. (Eds.) *Biomineralization Processes of Iron and Manganese*, Catena Supplement 21, pp. 1 - 7.

Smith K.A. and Paterson J.E. (1995) Manganese and cobalt. In: Alloway B.J. (Ed.) *Heavy Metals in Soils*, Blackie Academic & Professional, London, pp. 224 - 242.

Span D., Dominik J., Loizeau J.-L., Thomas R.L. and Vernet J.-P. (1992) Dynamic processes in relation to heavy metal distributions in surficial sediments: The example lake Geneva. In: Vernet J.-P. (Ed.) *Impact of Heavy Metals on the Environment*, Elsevier, Amsterdam, pp. 381 - 396.

Sposito G. (1989) *The Chemistry of Soils*, Oxford University Press, New York, pp.209 -223.

Standard Methods (1985) *Standard Methods for the Examination of water and Wastewater (16th edition)*, American Public Health Association, Washington DC.

Stevens S.E., Dionis K. and Stark L.R. (1989) Manganese and iron encrustations on green algae living in acid mine drainage. In: Hammer D. (Ed.) *Constructed Wetlands for Wastewater Treatment. (Municipal, Industrial and Agricultural)*, Lewis Publishers INC., Michigan, pp. 765 - 773.

Stumm W. and Morgan J.J. (1970) *Aquatic chemistry: An introduction emphasising chemical equilibria in natural waters.* John Wiley and Sons, New York.

Swaine D.J. (1990) *Trace Elements in Coal*, Butterworths, London, pp. 77 - 178.

Thomas G.W. (1982) Exchangeable cations. In: Page A.L. (Ed.) *Methods of Soil Analysis (Part 2: Chemical and Microbial Properties)*, pp. 159 - 165.

Ure A.M. and Davidson C.M. (1995) Introduction to speciation. In: Ure A.M. and Davidson C.M. (Eds.) *Chemical Speciation in the Environment*, Blackie Academic & Professional, London, pp. 86 - 131.

Van Grieken R. and Xhoffer C. (1992) Microanalysis of individual environmental particles, *J. Ana. A. Spect.*, 7, 81 -87.

Van Hoek C., Mann D.G. and Jahns H.M. (1995) Chlorophyta: Class 10. Zygnematophyceae. In: Algae, *An Introduction to Phycology*, Cambridge University Press, Cambridge, pp. 460 - 465.

Verster E., van Deventer P.W., and Ellis F. (1992) Soils and associated materials of some pan floors and margins in Southern Africa: A Review, *SA Geographer*, 19, 35 - 47.

Winland R.L., Triana S.J. and Bigham J.M. (1991) Chemical composition of ochreous precipitates from Ohio coal mine drainage, *J. Environ. Qul.*, 20, 452 - 460.

Willis J. (1996) High performance ion chromatography (HPIC), *Personal Communications*, pp. 1 - 5.

Willis J. (1996) Instrumental parameters and data quality for routine major and trace element determinations by WDXRFS, *Personal Communications*.

Yariv S. and Cross H. (1979) Formation of aqueous solutions and suspensions of hydrophobic colloids. In: *Geochemistry of Colloid Systems For Earth Scientists*, Springer Verlag, Berlin, pp. 157 - 201.

Appendix I

Rainfall and V–notch flow data

Table A I.1 Seasonal rainfall data for the years 86/93 (Witbank) (DWAF,1995).

Summer

Year	Min. rainfall in mm	Max. rainfall in mm	Mean. rainfall in mm
86/87	5.8	154	102
87/88	67	221	112
88/89	48	218	109
90/91	7.0	170	90
91/92	7.1	351	128
92/93	4.0	111	64
93/94	0.0	112	45

Winter

Year	Min. raifall in mm	Max. rainfall in mm	Mean. rainfall in mm
87	0.0	39	15
88	1.0	42	12
89	0.0	59	21
90	0.0	112	27
91	0.0	21	7.9
92	0.0	22	8.3
93	0.0	13	2.7

Table A I.2 Blesbokspruit average minimum and maximum V-notch flow data for the period September 1986 to April 1994 (DWAF, 1995).

V-notch 11	
	Flow of water (m^3/day)
Minimum	12
Maximum	590
V-notch 12	
	Flow of water (m^3/day)
Minimum	10
Maximum	938
V-notch 13	
	Flow of water (m^3/day)
Minimum	1
Maximum	225

Appendix II

Water analysis

Analysis of waters from the Blesbokspruit catchment. Instrumental parameters, calculations, additional tables and accuracy and precision determinations.

A II.1 Laboratory pH and EC determination of water samples

Table A II.1 pH and EC repeat analysis.

Sample No.	Field pH	Field EC mS/cm	Lab pH 1	Lab pH 2	Lab pH 3	Mean pH	Std Dev.	Lab EC 1 mS/cm	Lab EC 2 mS/cm	Lab EC 3 mS/cm	EC Mean mS/cm	EC Std Dev.
W4	3.6	0.65	3.51	3.55	3.54	3.53	0.02	0.84	0.84	0.84	0.84	0.00
W1	2.9	3.66	2.57	2.57	2.56	2.57	0.01	3.57	3.57	3.57	3.57	0.00
W2	3.1	3.92	2.71	2.74	2.74	2.73	0.02	3.72	3.70	3.70	3.71	0.01
W3	2.7	3.75	2.67	2.60	2.60	2.62	0.04	3.73	3.72	3.73	3.73	0.01
W5	2.4	3.78	2.75	2.75	2.75	2.75	0.00	3.30	3.27	3.29	3.29	0.02
W6	2.5	4.44	2.69	2.70	2.71	2.70	0.01	3.91	3.91	3.89	3.90	0.01
W7	2.4	4.02	2.68	2.68	2.68	2.68	0.00	3.65	3.6	3.64	3.63	0.03
W8	2.3	4.12	2.65	2.65	2.66	2.65	0.01	3.65	3.64	3.63	3.64	0.01
W9	2.2	3.80	2.61	2.60	2.61	2.61	0.01	3.79	3.79	3.77	3.78	0.01
W11	2.5	3.12	2.71	2.71	2.71	2.71	0.00	3.09	3.08	3.08	3.08	0.01
W12	2.6	3.89	2.91	2.91	2.91	2.91	0.00	3.50	3.51	3.50	3.50	0.01
W13	2.6	4.14	2.79	2.79	2.80	2.79	0.01	3.74	3.71	3.73	3.73	0.02
W15	2.6	4.57	2.67	2.66	2.66	2.66	0.01	4.36	4.39	4.38	4.38	0.02
W14	2.5	3.30	2.80	2.79	2.78	2.79	0.01	3.17	3.18	3.14	3.16	0.02
W16	2.9	5.33	2.91	2.92	2.92	2.92	0.01	4.75	4.74	4.75	4.75	0.01
W17	2.9	3.37	2.81	2.80	2.80	2.80	0.01	3.29	3.32	3.30	3.30	0.02
W18	2.9	3.43	2.82	2.82	2.82	2.82	0.00	3.34	3.22	3.35	3.30	0.07
W19	2.6	1.85	3.05	3.05	3.05	3.05	0.00	1.66	1.66	1.65	1.66	0.01
W20	6.4	0.361	7.32	7.39	7.38	7.36	0.04	0.33	0.33	0.33	0.33	0.00
W21	6.0	0.257	7.36	7.29	7.28	7.31	0.04	0.23	0.23	0.23	0.23	0.00
W22	3.0	1.34	3.17	3.17	3.16	3.17	0.01	1.25	1.26	1.26	1.26	0.01

A II.2 Theoretical total dissolved salt calculation

The TDS of the solution was calculated from the sum of the base metal ion and the anion concentration in each sample. The TDS calculation is shown below (McBride, 1994):

$$TDS\ (mg/litre) = EC(mS/cm) \times 640$$

A II.3 Determination of anions using high performance ion chromatography (HPIC)

Table A II.2 The dilution (with Milli-Q) of waters sampled in the Blesbokspruit catchment.

Sample No.	Dilution factor
W4	27 fold
W1	120 fold
W2	160 fold
W3	120 fold
W5	120 fold
W6	120 fold
W7	120 fold
W8	120 fold
W9	120 fold
W11	120 fold
W12	120 fold
W13	120 fold
W15	135 fold
W14	120 fold
W16	200 fold
W17	120 fold
W18	120 fold
W19	60 fold
W20	12 fold
W21	9 fold
W22	20 fold

Repeated runs of the following samples were made to ensure precision of the instrument.

Table A II.3 Sample repeats for HPIC precision.

Sample No.	SO_4^{2-} mg/ℓ	Cl^- mg/ℓ	NO_3^- mg/ℓ	Repeat No.
W12	1086	245	BDL*	1
	1077	238	BDL	2
	1045	243	BDL	3
	1069	241	BDL	4
	1072	247	BDL	5
Mean	1070	243	--	
S.D.#	15.3	3.6	--	
RSD(%)$	1.4	1.5	--	
W4	284	111	BDL	1
	280	107	BDL	2
Mean	282	109	--	
S.D.	2.8	2.8	--	
RSD(%)	1.0	2.6	--	
W9	1470	552	BDL	1
	1468	550	BDL	2
Mean	1469	551	--	
S.D.	1.4	1.4	--	
RSD(%)	0.1	0.3	--	
W17	1512	299	BDL	1
	1511	297	BDL	2
Mean	1511	298	--	
S.D.	0.71	1.41	--	
RSD(%)	0.05	0.47	--	

* BDL below detection limit

Detection limit of the system was in the ppb range (Willis, 1996).

S.D. Standard Deviation

$ RSD(%) Relative Standard Deviation

Accuracy of the instrument was determined by analysis of standard solutions with known concentrations (Table A II.3)

Table A II.4 Standards and a blank (MilliQ water) were analyzed for anion content with HPIC.

Anion conc. in mg/ℓ					
SO_4^{2-}	Cl^-	NO_3^-	NO_2^-	PO_4^{3-}	Br^-
(0)*	(0)	(0)	(0)	(0)	(0)
BDL**	BDL	0	0	0	0
(1)*	(0.9)	(0.5)	(0.5)	(0.5)	(0.25)
0.97	0.91	0.51	0.48	0.45	0.25
(2)*	(1.9)	(1.0)	(1.0)	(1.0)	(0.5)
2.1	2.0	1.0	1.1	1.1	0.52
(5)*	(4.7)	(2.5)	(2.5)	(2.5)	(1.25)
4.2	3.9	2.1	2.1	2.1	1.0
(10)*	(9.4)	(5.0)	(5.0)	(5.0)	(2.5)
10.0	9.3	5.0	5.0	5.2	2.5

* Values in brackets are standard concentrations made from standards (Merck AR chemicals, Dionex 5 Anion Standards).

** Below Detection Limit

A II.4 Acidity determination

Table A II.5 Acidity determination sample repeats and standard titration

Sample No.	Acidity in mM	Repeats
W1	17.4	1
	18.7	2
	17.3	3
	18.8	4
Mean	18.3	
S.D.[#]	1.16	
RSD(%)[$]	6.33	
W22	7.51	1
	7.40	2
	8.27	3
	7.46	4
Mean	7.66	
S.D.	0.41	
RSD(%)	5.34	
Std. 25 mM HCl	26.9	

[#] S.D. Standard Deviation

[$] RSD(%) Relative Standard Deviation

A II.5 Silica determination

All samples were done in duplicate and the mean value was used in the presented data. Standard curves were prepared for the three silica determination experiments (Figure A II.1).

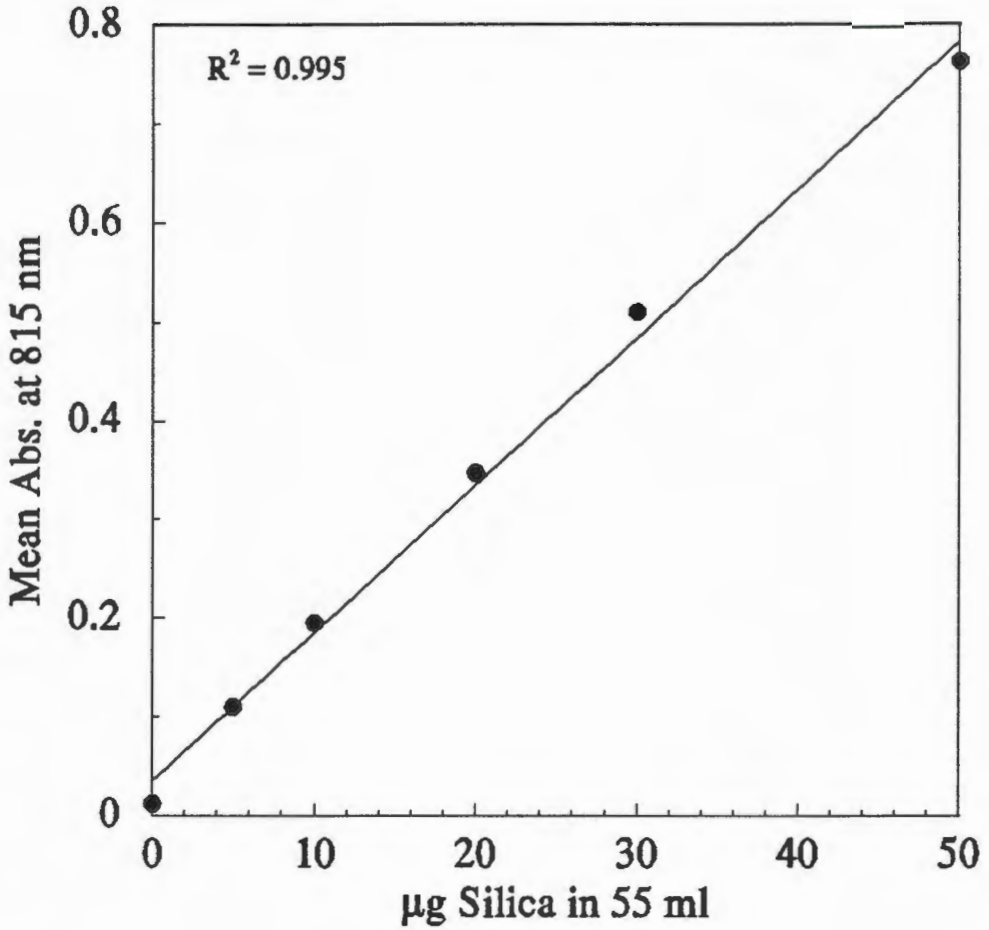

Figure A II.1 Standard curve for the silica determination.

A II.6 Aluminium determination

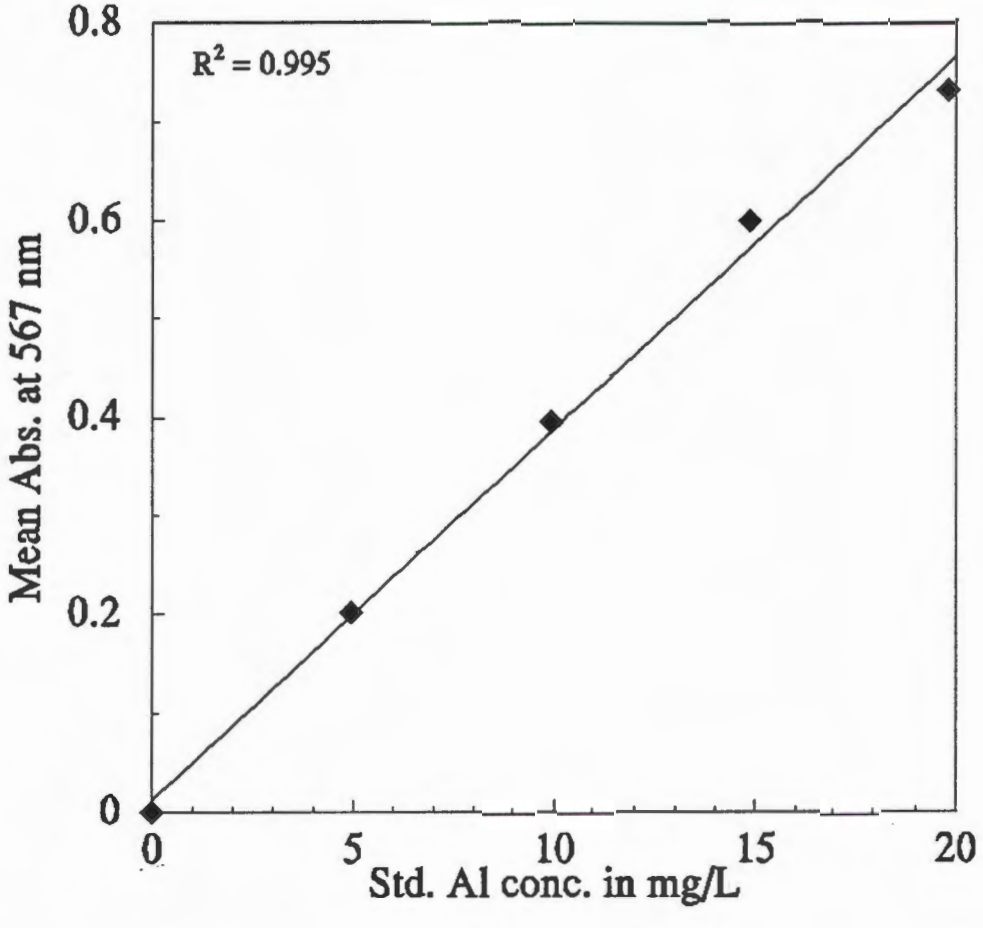

Figure A II.2 Standard curve for aluminium determination.

A II.8 Fluoride determination

Table A II.6 Fluoride hidden standard analysis (all repeats are in mg/ℓ)

Repeat	Sample No. W (0.1)*	W (1.0)	W (10.0)
1	0.11	1.11	9.56
2	0.11	1.13	9.89
3	0.10	1.14	10.2
Mean (mg/ℓ)	0.11	1.13	9.88
S.D.#	0.01	0.02	0.32
RSD(%)$	9.1	1.8	3.2

* Values in brackets are the standard concentrations in mg/ℓ

S.D. Standard Deviation

$ RSD(%) Relative Standard Deviation

A II.8 Eh determination

The Eh of the AMD samples was determined using a M21Pt metal electrode (Radiometer, Copenhagen) together with the standard Ag/AgCl reference electrode. The cell was calibrated in a solution of ferrous and ferric ammonium sulphate, each at a concentration of 100 mM in 1M H_2SO_4 (redox buffer). The accepted value for Eh in this buffer is 430 mV at 298 K (McBride, 1994). The redox buffer value for this determination was 432 mV at 293 K. All samples were analyzed once, and the Eh value was corrected for the Eh of the saturated calomel electrode (244 mV) (Garrels and Christ, 1965).

A II.9 ICP - AES analysis of element concentrations

General parameters of the Jobin Yvon 70C combined simultaneous/sequential ICP spectrometer are the following:

Power:	1kW
Pressure -Ar gas:	3.4 bar
R.F.:	27.12 MHz
Sample uptake:	2.0 ml/min
Observation height:	14 mm above coil
Aerosol gas flow (Ar):	0.4 L/min and 0.8 L/min (Na & K)
Plasma gas flow (Ar):	0.1 L/min
Coolant gas flow (Ar):	16 L/min

General detection limits for the technique have been described in the literature (Potts, 1987).

All water samples were analyzed by ICP-AES and standard deviation and relative standard deviations were reported for each sample (Table A II.7).

Table A II.7 Standard deviations and relative standard deviations (RSD) of one water sample as an example of ICP-AES analyses.

Sample	Element	Concentration in ppm	Standard deviation	RSD
W16	Na	73.4	0.014	0.20
	K	1.1	0.016	1.50
	Ca	359	0.038	0.10
	Mg	277	0.009	0.03
	Fe	10.2	0.009	0.85
	Al	240	0.042	0.17
	Mn	79.5	0.002	0.03
	Si	39.4	0.012	0.31
	Zn	10.4	0.003	0.27
	Ni	4.7	0.000	0.00
	Cu	1.1	0.000	0.11
	Pb	2.2	0.002	0.77

Appendix III

Sediment analysis

A III.1 Sediment pH

A summary of sediment pH means, standard deviations and % relative standard deviations for the analyzed sediment samples (Table A III.1).

Table A III.1 Mean values, standard deviations and %RSD values for duplicate analysis of sediment pH.

Sample No.	Mean H_2O pH	Std.* Dev.	%RSD#	Mean $CaCl_2$ pH	Std. Dev.	%RSD
S2L	3.5	0.01	0.3	3.4	0.02	0.5
S5T	3.0	0.04	1.3	3.1	0.01	0.3
S6T	3.0	0.04	1.3	2.8	0.01	0.4
S7T	2.9	0.01	0.3	2.7	0.00	0.0
S8T	2.6	0.01	0.4	2.5	0.03	1.2
S11T	3.4	0.01	0.3	3.4	0.01	0.3
S12T	3.1	0.03	1.0	3.0	0.03	1.0
S13T	3.7	0.01	0.3	3.6	0.02	0.6
S14T	3.2	0.00	0.0	3.1	0.01	0.3
S19T	3.0	0.02	0.6	2.9	0.01	0.3
S22T	3.8	0.01	0.3	3.7	0.02	O.5

* Standard deviation
# % Relative standard deviation

A III.2 Sediment % organic carbon

A summary of sediment % organic carbon means, standard deviations and % relative standard deviations for the analyzed sediment samples (Table A III.2).

Table A III.2 Mean values, standard deviations and %RSD values for duplicate analysis of sediment % organic carbon.

Sample No.	Mean % organic carbon	Std.* Dev.	%RSD#
S2L	2.6	0.05	1.9
S5T	0.3	0.01	3.3
S6T	0.5	0.03	6.0
S7T	0.5	0.02	4.0
S8T	0.6	0.01	1.6
S11T	1.8	0.11	6.1
S12T	0.5	0.08	16
S13T	0.9	0.03	3.3
S14T	0.7	0.04	5.7
S19T	9.5	0.00	0.0
S22T	3.9	0.03	0.7

* Standard deviation
# % Relative standard deviation

Table A III.3 Correlation matrix associating trace elements concentrations in the sediments with possible controlling variables

SiO_2															
Al_2O_3	-.93*														
Fe_2O_3	-.20	-.05													
K_2O	-.07	.70*	-.09												
SO_3	-.92*	-.06	.99*	-.07											
O.C.	-.06	-.09	.03	.12	.08										
Zn	.05	.20	-.16	.16	-.13	.34									
Cu	.05	.44	-.31	.49	-.31	.53	.42								
Ni	-.59*	-.18	.64*	-.36	.67*	.59*	.15	.01							
V	-.87*	-.03	.92*	-.27	.93*	.12	-.16	-.30	.81*						
Cr	.24	.05	-.38	.47	-.37	.06	.09	.50	-.45	-.52					
Mn	.51	-.03	-.60*	.10	-.60*	.50	.49	.74*	-.03	-.55	.44				
Co	.12	.17	-.19	.29	-.13	.89*	.63*	.61*	.41	-.09	.05	.62*			
Rb	.00	.73*	-.18	.99*	-.16	.13	.13	.54	-.40	-.33	.49	.12	.30		
Pb	-.16	.32	-.01	.21	0.2	-.10	.02	.36	-.09	.06	.27	-.03	-.08	.29	
U	-.06	.43	-.20	.59*	-.19	.67*	.40	.92*	.07	-.22	.51	.60*	.69*	.62*	.28
	SiO_2	Al_2O_3	Fe_2O_3	K_2O	SO_3	O.C.	Zn	Cu	Ni	V	Cr	Mn	Co	Rb	Pb

* marked correlations are significant at $p < 0.05$

Appendix IV

Precipitate energy dispersive spectra

A IV.1 SEM energy dispersive spectra of precipitate P2 (outwelling point).

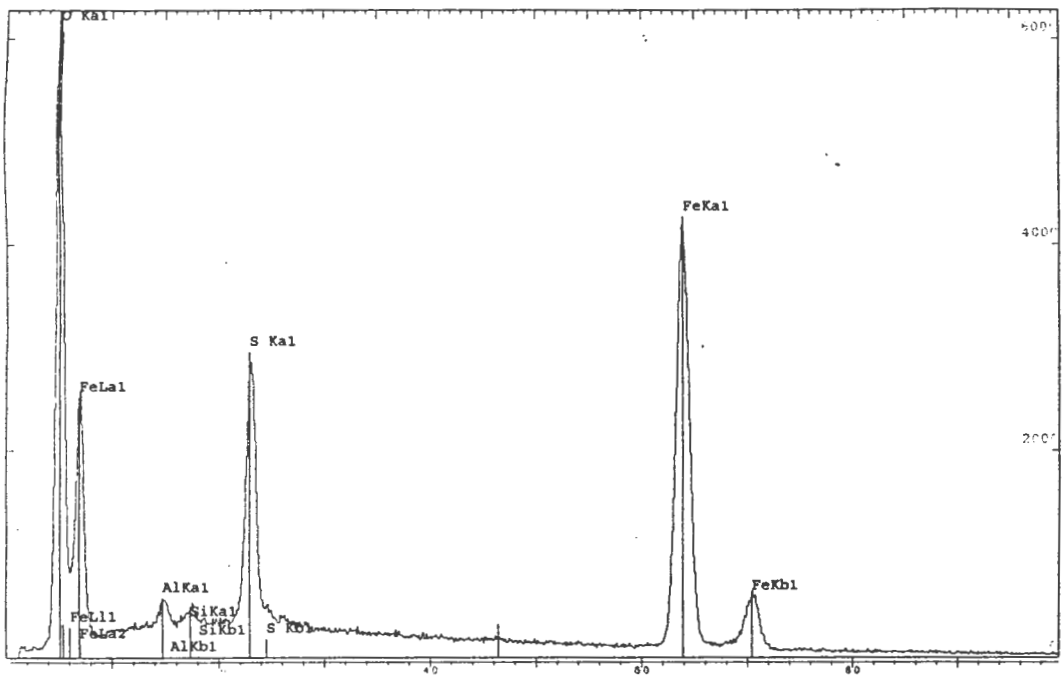

Figure A IV.1 P2 encrustation EDS spectrum. (Range: 20 keV, Total counts = 345931)

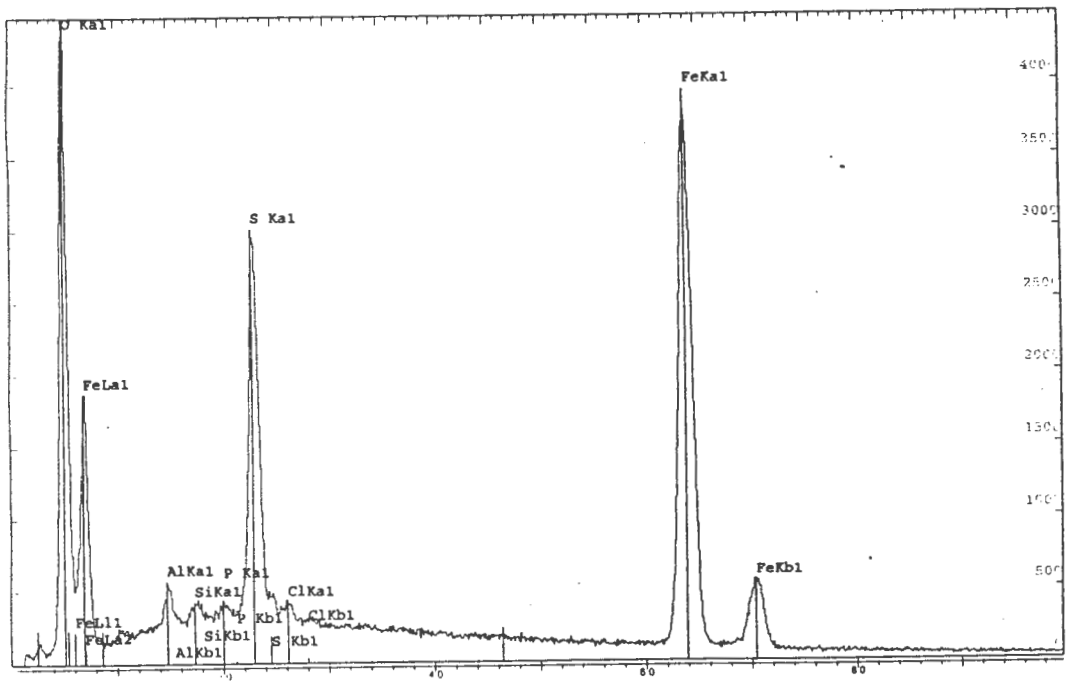

Figure A IV.2 P2 total area EDS spectrum. (Range: 20 keV, Total counts = 301590)

A IV.2 SEM energy dispersive spectra of precipitate P3 (V-notch 14).

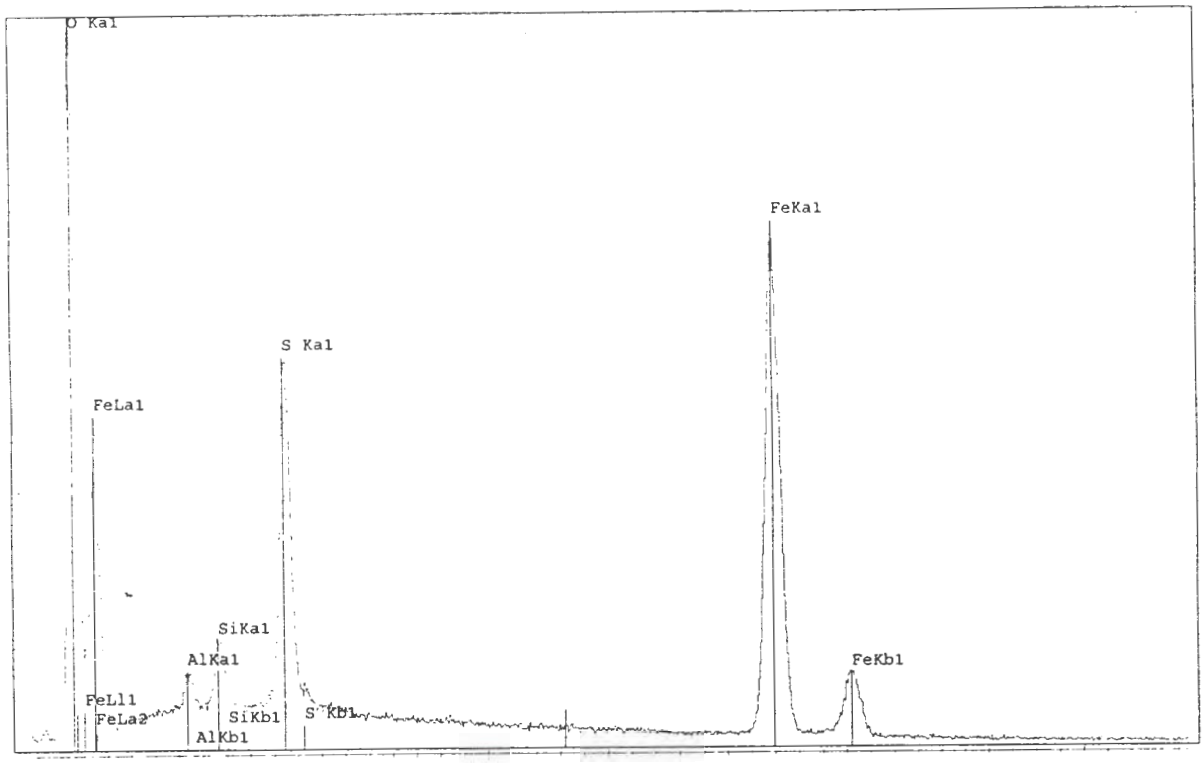

Figure A IV.3 P3 conglomerate EDS spectrum. (Range: 20 keV, Total counts = 233250)

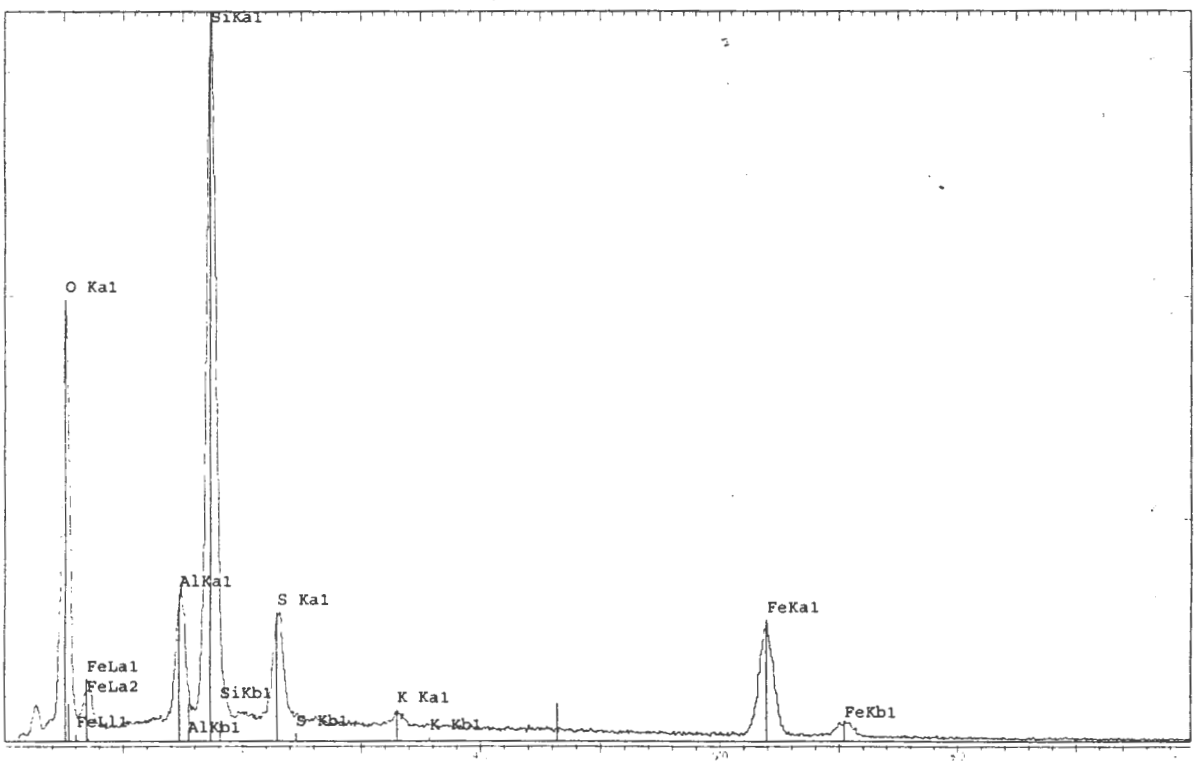

Figure A IV.4 P3 spindle shapes EDS spectrum. (Range: 20 keV, Total counts = 327586)

A IV.3 SEM energy dispersive spectra of precipitate P13 (AMD dam 6).

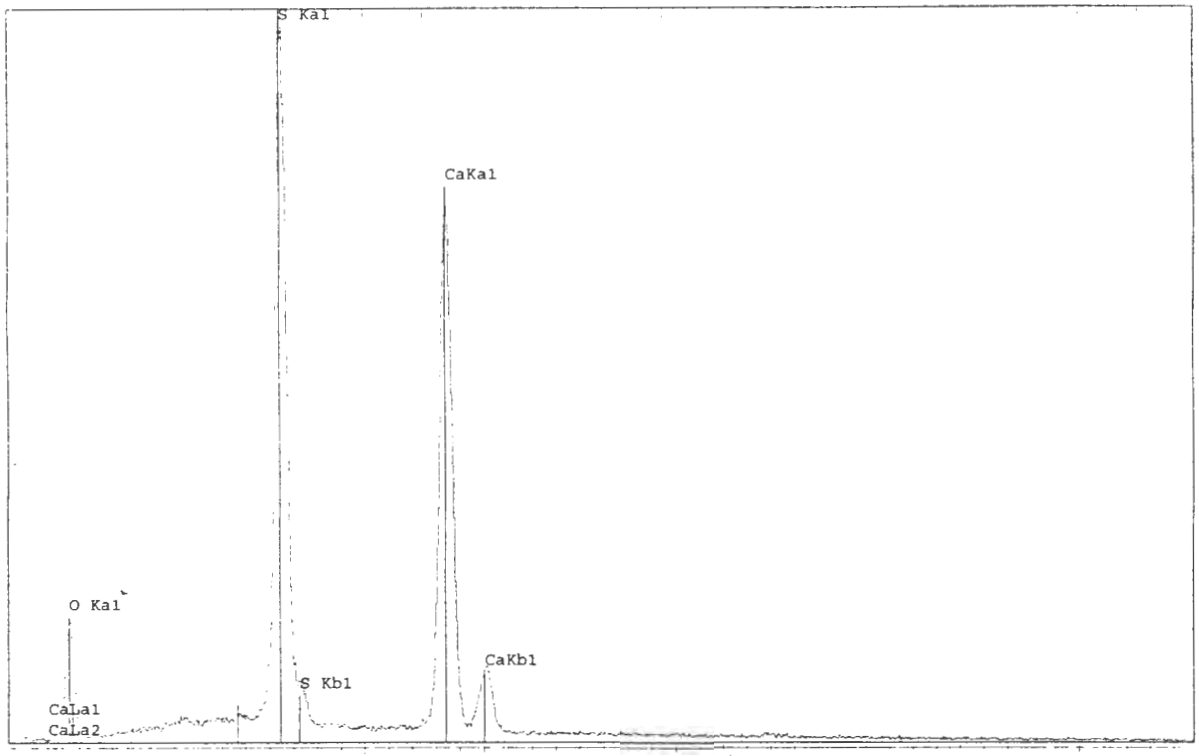

Figure A IV.5 P13 needles structure EDS spectrum. (Range: 20 keV, Total counts = 183732)

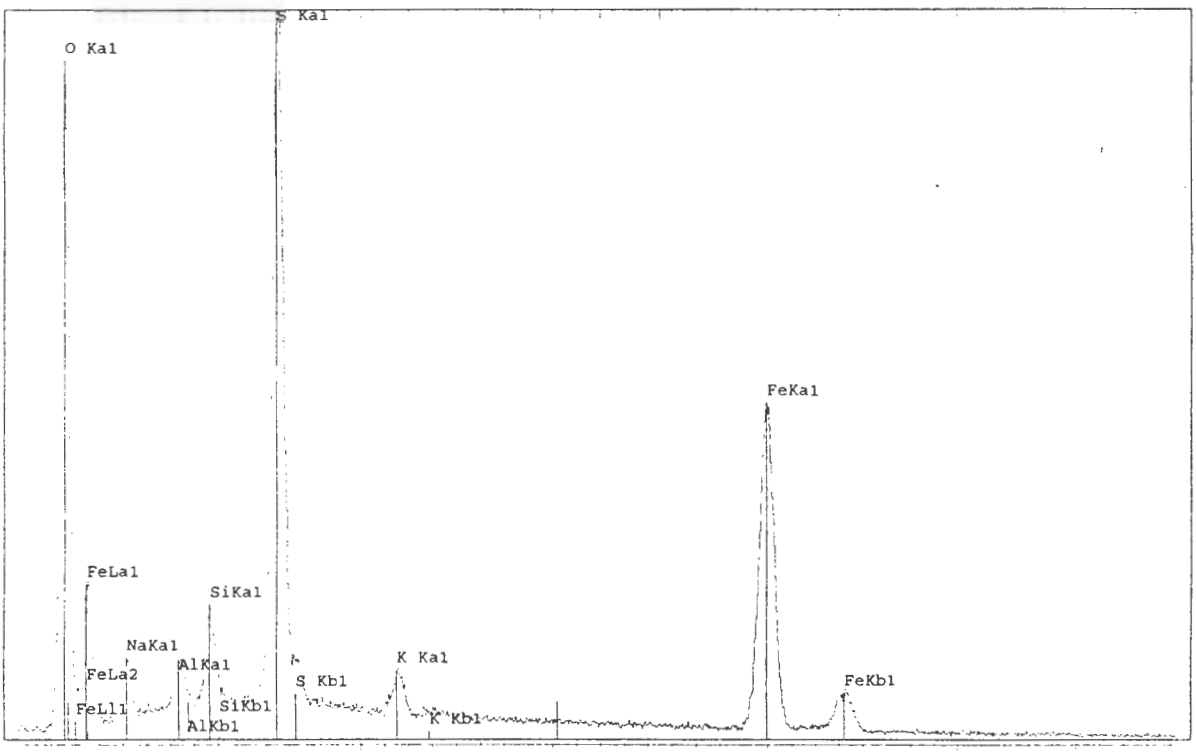

Figure A IV.6 P13 pseudo cubic structure EDS spectrum. (Range: 20 keV, Total counts = 215727)

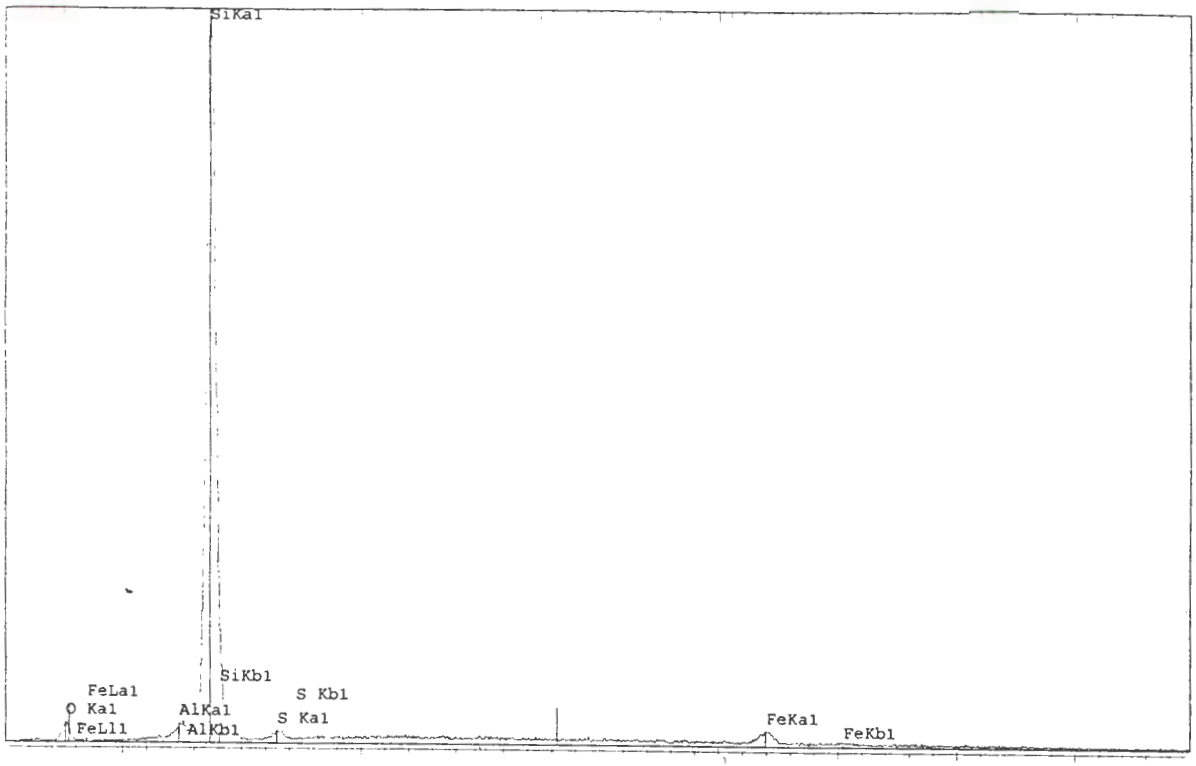

Figure A IV.7 P13 rounded feature EDS spectrum. (Range: 20 keV, Total counts = 28631)

A IV.4 SEM energy dispersive spectra of precipitate P15 (AMD ditch).

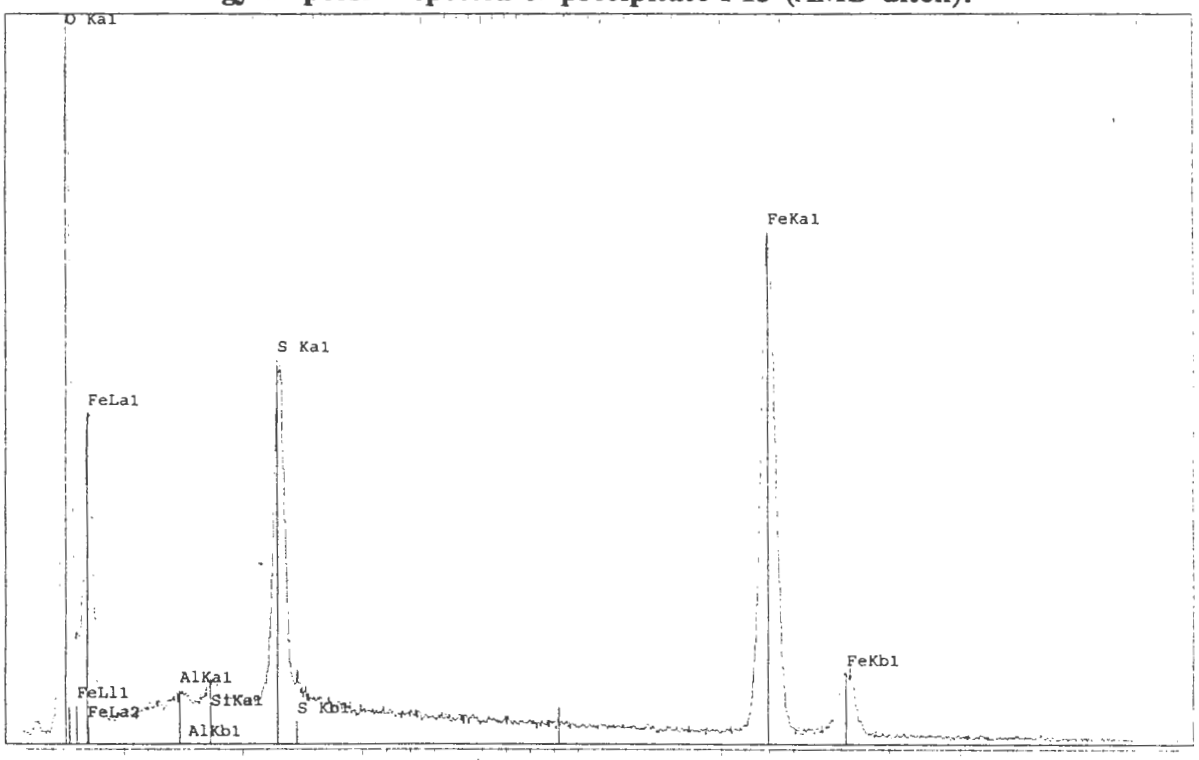

Figure A IV.8 P15 pin cushion structure EDS spectrum. (Range: 20 keV, Total counts = 83512)

Appendix V

Algae energy dispersive spectra

A V.1 SEM energy dispersive spectra of *Mougeotia* sp. algae

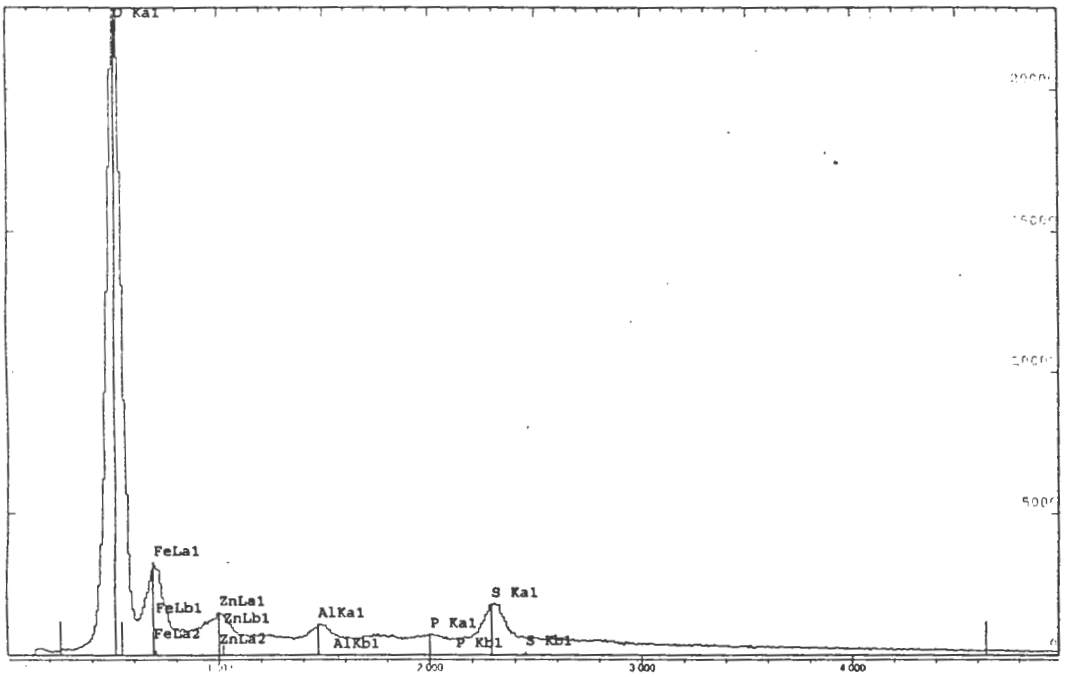

Figure A V.1 *Mougeotia* sp. cell wall EDS spectrum. (Range: 20 keV, Total counts = 467726)

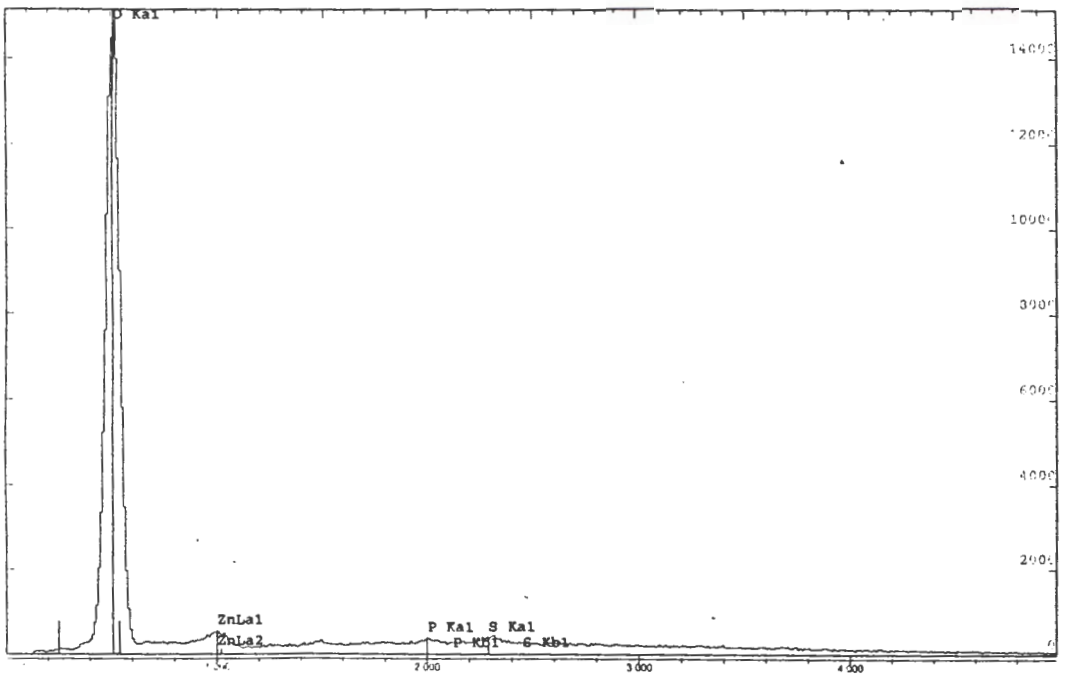

Figure A V.2 *Mougeotia* sp. cytoplasm EDS spectrum. (Range: 20 keV, Total counts = 217437)

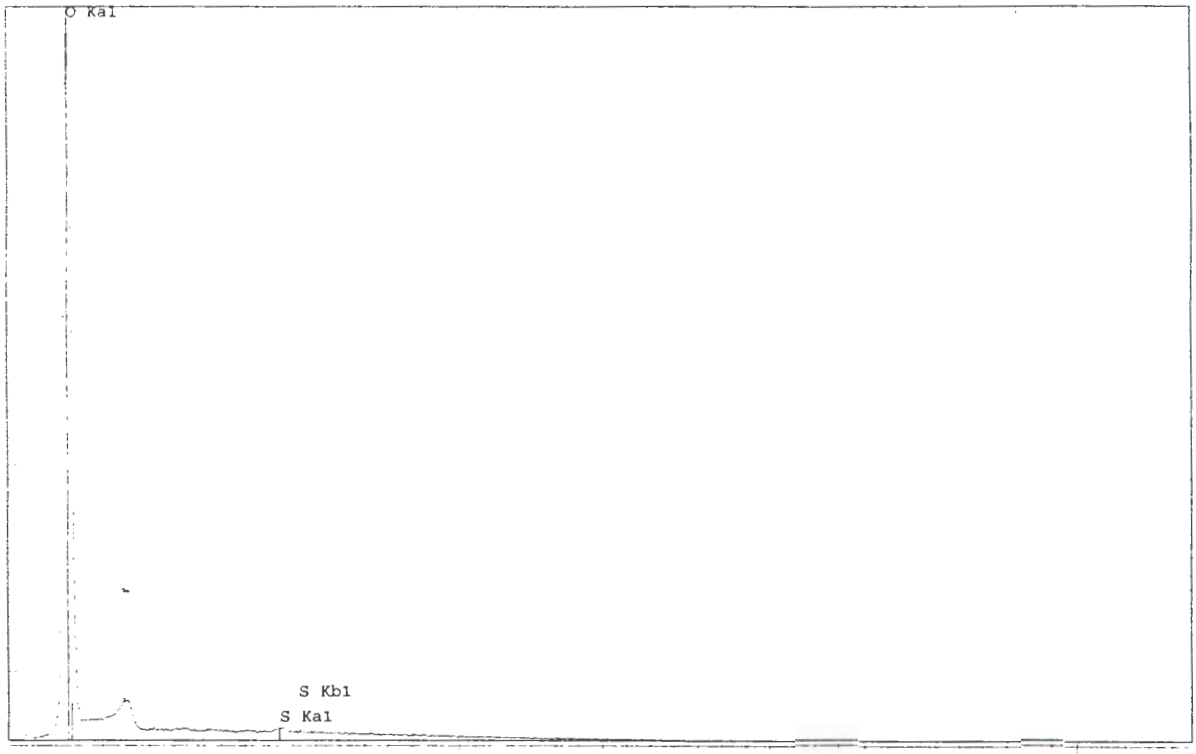

Figure A V.3 *Mougeotia* sp. backround EDS spectrum. (Range: 20 keV, Total counts = 217437)

A V.2 SEM energy dispersive spectra of *Microspora* sp. algae

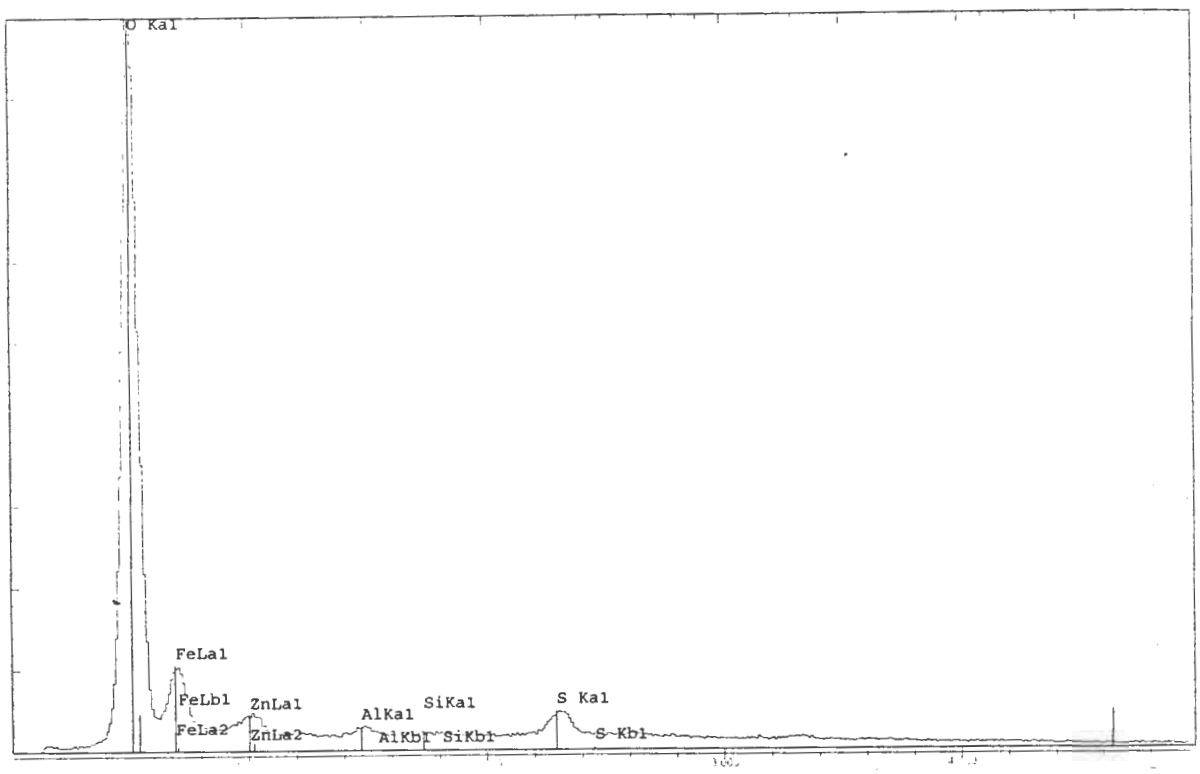

Figure A V.4 *Microspora* sp. cell wall EDS spectrum. (Range: 20 keV, Total counts = 313983)

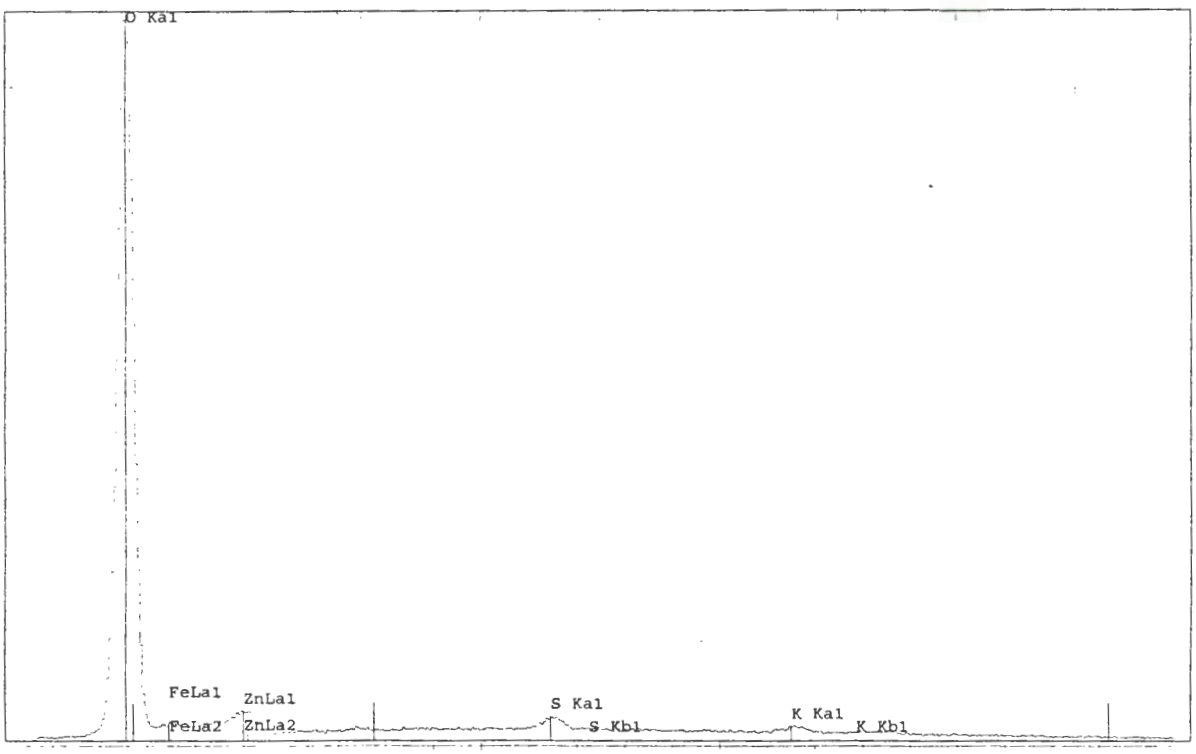

Figure A V.5 *Microspora* sp. cytoplasm EDS spectrum. (Range: 20 keV, Total counts = 226009)

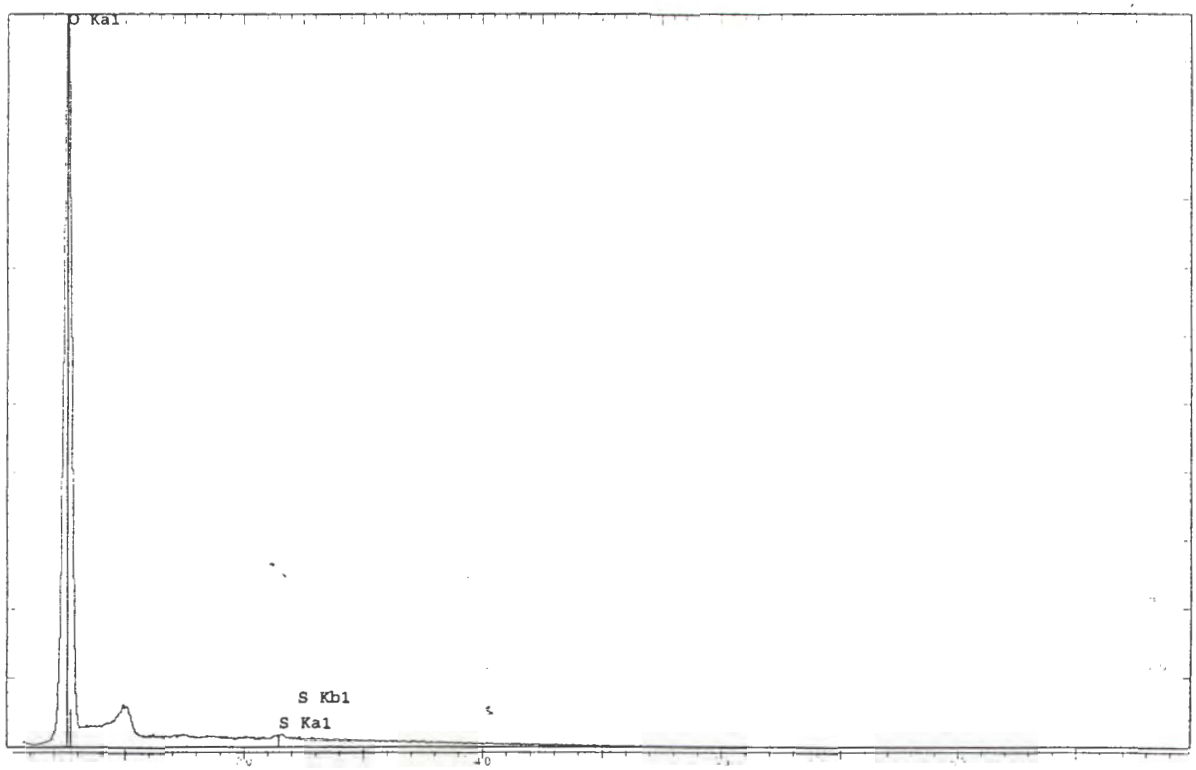

Figure A V.6 *Microspora* sp. backround EDS spectrum. (Range: 20 keV, Total counts = 285226)

Appendix VI

INSTRUMENTAL PARAMETERS AND DATA QUALITY FOR ROUTINE TRACE ELEMENT DETERMINETAIONS BY WDXRFS

TRACE ELEMENTS

Trace elements are determined on powder briquettes using a series of x-ray tubes. Analytical conditions are listed in Tables 2 and 3.

Table A VI.1 X-ray tubes and tube and x-ray path settings for the determination of trace elements using a Siemens SRS303AS and Philips PW1480 WDXRF spectrometer.

Spectrometer	Element/line	X-ray tube		X-ray path
		Target	kV - mA	
SRS303AS	RhKαC	Rh	60 45	Vacuum
SRS303AS	MoKα	Rh	60 45	Vacuum
SRS303AS	NbKα	Rh	60 45	Vacuum
SRS303AS	ZrKα	Rh	60 45	Vacuum
SRS303AS	Y Kα	Rh	60 45	Vacuum
SRS303AS	SrKα	Rh	60 45	Vacuum
SRS303AS	U $L\alpha_1$	Rh	60 45	Vacuum
SRS303AS	RbKα	Rh	60 45	Vacuum
SRS303AS	Th $L\alpha_1$	Rh	60 45	Vacuum
SRS303AS	Pb $L\beta_1$	Rh	60 45	Vacuum
PW1480	ZnKα	Au	60 45	Vacuum
PW1480	CuKα	Au	60 45	Vacuum
PW1480	NiKα	Au	60 45	Vacuum
PW1480	CoKα	W	50 55	Vacuum
PW1480	MnKα	W	50 55	Vacuum
PW1480	CrKα	W	50 55	Vacuum
PW1480	V Kα	W	50 55	Vacuum
PW1480	Ba $L\alpha_1$	Cr	50 55	Vacuum
PW1480	ScKα	Cr	50 55	Vacuum

Table VI.2 Instrumental conditions for determination of trace elements using a Siemens SRS303AS and Philips PW1480 WDXRF spectrometer.

Element /line	Collimator	Crystal	Detector	PHS LWL	PHS UPL	Counting time (s)	Background position(s) relative to peak position	Concentration range *
RhKαC	F	LiF(220)	SC	0.6	1.5	200		
MoKα	F	LiF(200)	SC	0.7	1.7	160	−0.8 +0.65	0 - 5.2
NbKα	F	LiF(200)	SC	0.5	1.6	160		0 - 268
ZrKα	F	LiF(200)	SC	0.5	1.6	160		0 - 1210
YKα	F	LiF(200)	SC	0.5	1.6	160	−0.61 +0.54	0 - 143
SrKα	F	LiF(200)	SC	0.5	1.6	160	+0.60	0 - 440
U $L\alpha_1$	F	LiF(200)	SC	0.5	1.6	160		0 - 15
RbKα	F	LiF(200)	SC	0.5	1.6	160	+0.53	0 - 530
Th $L\alpha_1$	F	LiF(200)	SC	0.5	1.6	160		0 - 51
Pb $L\beta_1$	F	LiF(200)	SC	0.4	1.4	160	+1.27	0 - 40
ZnKα	F	LiF(220)	FS	20	80	200	−1.08 +4.24	0 - 235
CuKα	F	LiF(220)	FS	20	80	200	+4.44	0 - 227
NiKα	F	LiF(220)	FS	20	80	200	+2.52	0 - 630
CoKα	F	LiF(220)	FL	15	75	200	+1.00	0 - 116
MnKα	F	LiF(220)	FL	15	75	200	−2.30 +4.70	0 - 1700
CrKα	F	LiF(220)	FL	15	75	200	−4.10 +2.90	0 - 465
VKα	F	LiF(220)	FL	13	67	200	+3.40	0 - 640
Ba $L\alpha_1$	F	LiF(200)	FL	25	75	200	−5.20	0 - 2680
ScKα	F	LiF(200)	FL	25	75	200	−2.78	0 - 54

* = all concentrations expressed as part per million (ppm or $mg.kg^{-1}$)

The RhKα Compton peak is used to determine the mass absorption coefficients of the specimens at the RhKαC wavelength (Figure 5) and the calculated values are used to correct for absorption effects on the Mo, Nb, Zr, Y, Sr, U, Rb, Th, Pb, Zn, Cu and Ni analyte wavelengths. Primary and secondary mass absorption coefficients for the Co, Mn, Cr, V, Ba and Sc analyte wavelengths are calculated from major element compositions using the tables of Heinrich (1986). Mass absorption coefficient corrections are made to the net peak intensities, (gross peak intensities corrected for dead time losses, background and spectral overlap), to correct for absorption differences between standards and specimens. No corrections are made for enhancement, which could be small but significant ($< \sim 5\%$ relative) for the elements Cr, V, Ba and Sc in certain specimens, depending on their concentrations of Fe, Mn and Ti.

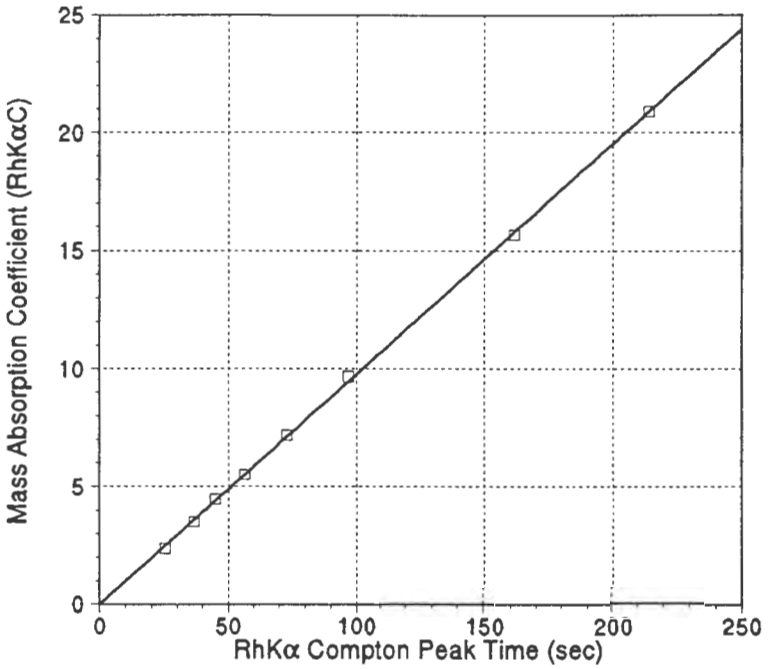

Figure VI.1 **Calibration line for determination of mass absorption coefficients at the RhKαC wavelength. RhKαC peak time is the time required to accumulate 400 000 counts on the RhKαC peak using the fixed count method.**

Measured intensity data are processed through the computer program TRACE to correct gross peak intensities for background and spectral overlap and to make mass absorption coefficient corrections according to the methods outlined in Duncan *et al.* (1984). First order calibration lines with zero intercept are calculated using six or more international rock standard reference materials (SRMs) for each element. The one standard deviation (1 σ) error due to counting statistics and the lower limit of detection is calculated for each element in each specimen.

Table 4 lists the given and calculated concentrations for selected elements in a number of rock SRMs, which gives an indication of the accuracy of the trace element data. Table 5 lists the one standard deviation counting error and lower limit of detection for each of the elements in an acidic (low Fe, Ca and Mg, high Si) rock and in a mafic (high Fe, Ca and Mg, low Si) rock. Because of the difference in mass absorption coefficients between the two types of specimen the counting error and lower limit of detection will be slightly higher in mafic rock specimens. The two examples given cover the range of mass absorption coefficients found in the majority of geological rock, soil and sediment specimens.

The counting error and lower limit of detection are calculated using the following formulae:

$$1\,\sigma \ error \ (in \ ppm) \ = \ Conc \times \frac{\sqrt{\frac{I_p}{T_p} + \frac{I_b}{T_b}}}{I_n}$$

and

$$LLD\ (in\ ppm) = \frac{6}{m}\sqrt{\frac{I_b}{T_{total}}}$$

whereConc = calculated concentration in ppm
m = net peak / concentration
I_p = gross peak count rate in cps
I_b = background count rate under the peak in cps
$I_n = I_p - I_b$ = true **net** peak count rate in cps
T_p = counting time for peak in seconds
T_b = total counting time for background in seconds
$T_{total} = T_p + T_b$

N.B. I_b is the calculated background *plus* any corrections for spectral interference, and is equal to $I_p - I_n$.

Table A VI.3 Given and calculated trace element data (all values in ppm) for some rock SRMs.

Element	QLO-1		BHVO-1		W-2		STM-1		BIR-1	
	Given	Calc	Given	Calc	Given	Calc	Given	Calc	Given	Calc
Mo	2.6	3.5	1.0	0.8	(0.6	0.5	5.2	3.1	(0.5	<0.8
Nb	10	11	19	19	7.9	7.4	268	267	0.6	0.9
Zr	185	190	179	181	94	95	1210	1220	16	19
Y	24	25	28	28	24	23	46	47	16	17
Sr	336	329	403	395	194	195	700	689	108	109
U	1.9	2.3	0.4	<1.6	0.5	<1.2	9.1	8.8	0.01	<1.2
Rb	74	71	11	9.7	20	20	118	114	0.3	<0.6
Th	4.5	4.0	1.1	1.8	2.2	2.7	31	31	0.03	<1.5
Pb	20	20	2.6	3.1	9.3	8.5	18	17	3	3.1
Zn	61	61	105	106	77	79	235	242	71	69
Cu	29	25	136	139	103	108	(4.6	2.1	126	132
Ni	(5.8	1.8	121	127	70	72	(3	1.7	166	170
Co	7.2	7.6	45	44	44	43	0.9	<1.9	51	52
Mn	720	690	1300	1290	1260	1240	1700	1600	1320	1280
Cr	(3.2	3.6	289	312	93	100	(4.3	3.2	382	404
V	54	44	317	314	262	257	(8.7	<1.6	313	306
Ba	1370	1430	139	138	182	191	560	589	7.0	10
Sc	8.9	10.3	31.8	33.9	35	36	0.6	0.5	44	39

(n.n = value given for information only

Table A VI.4 **Calculated trace element data, 1 σ counting error and lower limit of detection (all values in ppm) for two rock specimens having different mass absorption coefficients.**

Element	JR-2			JB-1a		
	Calc	1 σ	LLD	Calc	1 σ	LLD
Mo	4.1	0.2	0.6	1.8	0.3	0.7
Nb	19	0.1	0.4	28	0.2	0.5
Zr	87	0.1	0.3	152	0.2	0.4
Y	51	0.2	0.6	24	0.2	0.6
Sr	8.2	0.1	0.4	444	0.3	0.5
U	11	0.3	0.9	2.3	0.4	1.2
Rb	303	0.2	0.4	39	0.2	0.6
Th	34	0.4	1.1	9.8	0.5	1.4
Pb	24	0.5	1.3	7.5	0.6	1.8
Zn	28	0.2	0.6	84	0.4	0.9
Cu	1.1	0.3	0.8	55	0.5	1.1
Ni	1.3	0.3	0.8	139	0.7	1.3
Co	< 1.2	0.4	1.2	37	0.9	2.3
Mn	878	1.7	1.2	1100	2.0	1.8
Cr	1.6	0.4	1.3	406	1.5	2.0
V	1.7	0.4	1.2	193	1.4	3.0
Ba	28	0.6	1.5	523	1.8	3.3
Sc	6.0	0.2	0.5	26	0.4	0.9

Appendix VII

Water quality guidelines

A summary of the target water quality ranges as specified by the South African Department of Water Affairs and Forestry (DWAF,1996).

Table A VII.1 Water quality guidelines for elements and ions.

Element or ion	Target water quality range (mg/ℓ)
pH	6.0 - 9.0
TDS	0.0 - 450
SO_4^{2-}	0.0 - 200
Cl^-	0.0 - 250
NO_3^- as N	0.0 - 6.0
F^-	0.0 - 1.0
Na	0.0 - 100
K	0.0 - 50
Ca	0.0 - 32
Mg	0.0 - 70
Fe	0.0 - 0.1
Al	0.0 - 0.15
Mn	0.0 - 0.05
Zn	0.0 - 3.0
Cu	0.0 - 1.0
Pb	0.0 - 0.01

Appendix VIII

A note on the high lead concentrations in the Blesbokspruit waters

A discussion on the high lead concentrations of the Blesbokspruit waters.

The high lead concentration (>0.95 mg/l) in both the AMD and the fresh waters (W20, W21) of the Blesbokspruit can indicate analytical error in the ICP analysis of the water samples.

However, Blesbokspruit sediments do contain elevated concentrations of lead, suggesting the precipitation of lead sulphate ($PbSO_4$) in these sulphate rich waters. The presence of lead containing minerals could not be confirmed by XRD spectroscopy.